HYDRODYNAMICS OF ULTRA-RELATIVISTIC HEAVY-ION COLLISIONS

Thesis by

Ming-chung Chu

In Partial Fulfillment of the Requirements

for the Degree of

Doctor of Philosophy

California Institute of Technology

Pasadena, California

1987

(Submitted May 12, 1987)

ACKNOWLEDGMENTS

I was "brought up" in the world of physics by Professor Steven Koonin, who taught me physics and gave me much useful advice. Two of my favorite quotes from him: "Don't work too hard, Ming!", and "Cheer up, it's not that bad!"

I was also helped by useful discussions with Drs. Harald Friedrich, Peter Koch, Berndt Müller, Philip Siemens, Andreas Schäfer, Michael Strayer, Cheuk-yin Wong, and Sait Ulmer. I gratefully acknowledge the hospitality of Oak Ridge National Laboratory and the University of Frankfurt, where parts of my work presented here were finished.

And my officemates. I owe them thanks not only for teaching me physics and English, but also for making our office such a lively and comfortable place to "live". They would even share delicious chocolate bars! Also, I truly enjoy being a member of the "family" of Kellogg Radiation Laboratory.

Last but not least, I thank my parents and my friends. Together they provide a huge heat bath of help and support, making it a lot easier to live in this complex world.

Numerical computations for this work were done on either a VAX-750 of the W. K. Kellogg Radiation Laboratory or the Oak Ridge array processor (FPS 164). This thesis was typeset in D. E. Knuth's "TEX," and the graphs were prepared with the graphics package "Topdrawer" from the Stanford Linear Accelerator Center. This work was supported by the National Science Foundation.

ABSTRACT

Relativistic hydrodynamic calculations are presented to describe the dynamics of ultra-relativistic heavy-ion collisions. In contrast to the "standard picture" of the field, our calculations do not assume scaling symmetry, and in fact we find large scaling violations near the fragmentation regions. In our 1+1-dimensional calculations, we find that while the hydrodynamic evolution is very sensitive to the formation and thermalization time and to the models of the source terms, the effects of changing the viscosity and the equation of state are small. Our 2+1-dimensional calculations show that transverse expansion is not important in the central rapidity region. We also present a brief review of the proposed signatures of the formation of quark-gluon plasma in high energy heavy-ion collisions, as examples of applications of hydrodynamics.

TABLE OF CONTENTS

CHAPTER I

Introduction

In recent years, there has been considerable interest in high-energy heavy-ion collisions, a major reason being that it may be possible to create an extended region of extremely high energy density in such a process [Sh80, Sa81, Ja82, Lu84, Ka85, Mu85]. In fact, the energy density achievable may be high enough to carry matter through the deconfinement phase transition, thus forming a quark-gluon plasma [Qn80, Ka82, Mc82, Bj83]. Such an exotic state of matter is believed to simulate the conditions in the early universe and possibly in the interior of gravitationally collapsing astrophysical objects. The physics of quark-gluon plasma, therefore, is of interest not only to nuclear and particle physicists, but also to astrophysicists.

Why are ultra-relativistic heavy-ion collisions (URHIC) good tools to produce an extended region of high energy density? There are basically two reasons. First, by accelerating a heavy ion to ultra-relativistic speed (kinetic energy much greater than rest mass), we have localized all its nucleons in a small volume in the lab frame because of Lorentz contraction. In particular, for beam energies per nucleon, E, exceeding $m\sqrt{4R^2-1}$, where $m \approx 1\text{GeV}$ is the nucleon mass and $R \approx 1.2A^{\frac{1}{3}}$ is the radius of the heavy ion (with atomic number A) in fm, nucleons in a beam ion occupy a spatial extent less than about 1 fm along the beam axis as seen in the lab frame. For collisions of uranium ions, this happens at about 14 GeV/A. Secondly, we get hundreds of nucleon-nucleon collisions in each heavy-ion collision. These elementary collisions occur in a small space-time volume, thereby producing

a high energy density region. As will be shown in Chapter IV, the energy density reached in a central collision of uranium ions at tens of GeV/A will probably be about ten to fifty times as high as nuclear matter density (0.17 GeVfm^{-3}).

We currently know very little about matter at extremely high energy density. A striking feature of Quantum Chromodynamics (QCD), which is believed to be the theory of the strong interaction, is that at short distance scales, interactions between quarks will become weak [Po74]. Lattice gauge calculations indeed suggest that at energy density about 2 GeVfm^{-3} , the quarks and gluons inside hadrons should be deconfined to form a quark-gluon plasma [En82, Mo82]. It is therefore very tempting to conclude that quark-gluon plasma can be produced in URHIC.

However, the situation is not clear yet. Recently, Polonyi proposed that the degrees of freedom in a high density QCD matter may actually be interpreted as chromomagnetic monopoles, and not as quarks and gluons [Po87]. It is then not correct to view such matter as governed by perturbative QCD, ignoring nonperturbative effects. Much of the following (with the exception of Chapter VIII) does not depend on the exact interpretation of the degrees of freedom in the high energy density region created in heavy-ion collisions. For convenience though, we will occasionally refer to the energy density as a quark-gluon plasma, and picture it as a collection of weakly interacting quarks and gluons.

If we indeed create an extended deconfined region of matter in high energy heavy-ion collisions, it will then be important to know what signatures are left behind by the quark-gluon plasma. Many possible candidates have been proposed, but none seems to be decisive so far. We shall briefly discuss three possible signa-

tures of the quark-gluon plasma in Chapter VIII: strangeness production, dilepton production, and transverse momentum distribution. Since the plasma will be a rapidly evolving system, it is important that estimates of these signatures be done in a dynamical framework. Our position here is that relativistic hydrodynamics is to good approximation an appropriate basis for a theoretical description of high energy heavy-ion collisions.

Hydrodynamics is a good model of a many-particle system if the quanta in the system come into local thermal equilibrium. Estimates of the mean free path and relaxation time suggest that they are small compared to the characteristic scales in a hot quark-gluon plasma [Bj83]. It is therefore plausible that throughout most of the history of a quark-gluon plasma, deviation from local equilibrium is small. In Chapter V and VI, we will also consider first-order corrections to local equilibrium, and hence study the effects of the transport coefficients. At the present, it is not clear whether hydrodynamics remain valid for the system at the formation stage and the hadronization stage. It is possible that violent fluctuations in the energy density are generated near the deconfinement phase transition making a mean-field description invalid. We shall however confine ourselves to the framework of relativistic hydrodynamics in this paper.

This thesis is organised as follows. We will first present the 'standard' scaling picture of URHIC in Chapter II. We then derive the equations of relativistic hydrodynamics in Chapter III. Chapter IV is devoted to a study of the source terms and the initial conditions in two extreme models - the inside-outside cascade model and the multiple-collision model, and Chapter V summarizes what little knowledge we

have of the transport coefficients. A detailed study of the one-dimensional hydrodynamics is then presented in Chapter VI, which is then extended to the cylindrical geometry in Chapter VII. Chapter VIII is a brief survey of some of the proposed signatures for quark-gluon plasma. We then summarize and conclude in Chapter IX.

CHAPTER II

Inside-Outside Cascade and the Scaling Picture of URHIC

A 'standard' space-time picture of URHIC has emerged during the past few years with the inside-outside cascade model (IOC) [Ko74, Bj75] and Bjorken's scaling picture [Bj83]. We shall summarize this standard picture in this chapter. In the following, we shall consider only central collisions of two heavy ions.

II.1 Nuclear Transparency

A key ingredient of IOC is nuclear transparency at high collision energy. To understand this, picture a nucleon-nucleus collision. After the nucleon strikes another nucleon in the target nucleus, it takes some characteristic proper time, $\tau_c \approx$ 1 fm, governed by the energy-time uncertainty principle, before the beam nucleon can interact again (or so to say, 'materializes'). If the speed of the beam nucleon is high enough, the time it takes the nucleon to pass through the thickness of the target nucleus, $2R$, will be less than τ_c. The projectile nucleon therefore, after its first collision, will pass through the target nucleus without further interaction. This transparency effect sets in for beam energies $E \geq 2mR/\tau_o$, where m is the nucleon mass. For nucleon-^{238}U collisions, this translates to a critical beam energy of about 14 GeV/A. This then also serves as a definition for what we mean by ultra-relativistic collisions (Fig. II.1).

II.2 Kinematic regions

Due to nuclear transparency, at high enough energies, two nuclei in a central collision will pass through each other, producing particles in three regions of phase space: the target fragmentation region (TFR), the projectile fragmentation region (PFR), and the central rapidity region (CRR). The highly Lorentz-contracted TFR and PFR contain most of the net baryon number of the system and continue receding away from each other near the speed of light after the collision. Between the TFR and PFR is the CRR with almost zero net baryon number but very high energy density. The fragmentation regions contain very rich information about nuclear matter at high temperature and pressure, but they are much more difficult to understand theoretically than the CRR. For the rest of this chapter, we shall focus on the CRR.

II.3 The central rapidity region: one-dimensional scaling

Bjorken has given a rough sketch of the space-time evolution of the CRR [Bj83] (see Fig. II.2): immediately after the collision, particles will only be weakly interacting and so undergo free streaming. Local thermal equilibrium will be established by a later proper time $\tau_o \approx 1$ fm/c. The system then undergoes hydrodynamic expansion, which lowers the energy density until hadronization occurs. The evolution of the plasma is then determined by the initial conditions specified at $\tau \equiv (t^2 - z^2)^{1/2} = \tau_o$ and the laws of hydrodynamics. Furthermore, motivated by the central plateau structure in the inclusive rapidity spectrum in nucleon-nucleon collisions at CERN SPS energies [Th77, Al81] (see Fig. II.3), we assume the ex-

istence of a similar central plateau in the inclusive rapidity spectrum in URHIC. This then implies that the space-time evolution of the system looks essentially the same in all reference frames related to the center-of-momentum (CM) frame by a Lorentz boost not exceeding the extent of the central plateau. In particular, this means a constant initial local energy density under Lorentz boosts in the longitudinal (z) direction, $\epsilon_o(\tau = \tau_o, z) = \epsilon_o(\tau_o)$, and a scaling form of the initial z velocity, $v_z = z/t$.

Let us first ignore the transverse expansion for now, and only study the longitudinal expansion of the system in the CM frame during the hydrodynamic phase. The symmetry we asserted above on the initial conditions is also respected by the hydrodynamic equations. This leads to a particularly simple description of the system: in the CM frame, the fluid moves away from the center ($z = 0$) symmetrically, with the speed of the fluid at a longitudinal distance z from the center being $v_z = z/t$, where t is the time elapsed after the ions collided.

The local energy density, ϵ, will depend only on τ. The decrease of ϵ is due to the expansion of the fluid and the work done by the pressure. By conservation of energy, and imposing the scaling symmetry on the expansion of the fluid, we can derive the ideal, scaling hydrodynamic equations (We will come back to a more general derivation of the hydrodynamic equations in Chapter III):

$$\frac{d\epsilon}{d\tau} = -\frac{(\epsilon + P)}{\tau} \tag{II.1}$$

For an ideal relativistic fluid, $\epsilon = 3P$, and so Eq. II.1 implies

$$\epsilon(\tau) = \epsilon(\tau_o) \left(\frac{\tau_o}{\tau}\right)^{\frac{4}{3}} \quad , \tag{II.2}$$

where τ_o is the proper time when the system enters the hydrodynamic phase. A pure gluon gas has the Stefan-Boltzmann behavior $\epsilon \propto T^4$, where T is the temperature. Therefore, the temperature of the system drops slowly, as $\tau^{-1/3}$. More generally, since $\epsilon + P = Ts$, where s is the entropy density,

$$\frac{d\epsilon}{d\tau} = \frac{d\epsilon}{dP}\frac{dP}{dT}\frac{dT}{d\tau} = -\frac{Ts}{\tau} \quad . \tag{II.3}$$

But $dP/dT = s$, and $d\epsilon/dP = \frac{1}{v_s^2}$, where v_s is the sound velocity, we have

$$\frac{1}{T}\frac{dT}{d\tau} = -\frac{v_s^2}{\tau} \quad .$$

The ideal gas equation of state gives $v_s^2 = 1/3$.

We now assume that the net baryon number, n_B, is zero in CRR. Then we can set the baryon chemical potential, μ_B, to zero. We have thus the following thermodynamic relations:

$$d\epsilon = Tds \quad , \quad dP = sdT \quad . \tag{II.4}$$

We can then also look at the time dependence of the entropy density by putting Eq. (II.4) into (II.3):

$$\frac{ds}{d\tau} = -\frac{s}{\tau} \quad , \tag{II.5}$$

which gives $s(\tau) = s(\tau_o)\tau_o/\tau$. Since the volume of the fluid increases as τ in scaling hydrodynamic, Eq. (II.5) is just a restatement of conservation of entropy, which is the result of assuming ideal hydrodynamic flow.

II.4 The central rapidity region: two-dimensional scaling

The simple results we obtained for one-dimensional scaling hydrodynamics are modified by the transverse flow. We shall now, in the framework of scaling hydrodynamics, consider cylindrical expansion of the plasma [Ba83], which is the correct geometry for central collisions.

We first write down the conservation of entropy, $\partial_\mu(su^\mu)$, where $u^\mu = (\gamma, \gamma\vec{v})$, in cylindrical coordinates:

$$\frac{\partial}{\partial t}(s\gamma) + \frac{1}{r}\frac{\partial}{\partial r}(rs\gamma v_r) + \frac{\partial}{\partial z}(s\gamma v_z) = 0 \ . \tag{II.6}$$

Our scaling hypothesis implies that the behavior of the system at z is related to that at $z = 0$ by a Lorentz boost. In particular, the transverse expansion of a slice of the fluid at z is related simply to that at the central slice at $z = 0$. The four-velocity must therefore have the Lorentz- invariant form,

$$u^\mu = f(\tau, r)(t, z, g(\tau, r), 0) \ .$$

We have $v_z = z/t$ and $v_r(z, r, t) = g(\tau, r)/t$, which implies

$$v_r(z, r, t) = v_r(0, r, \tau)\frac{\tau}{t} \ . \tag{II.7}$$

Therefore, we only need to solve II.6 in the $z = 0$ slice, and the solution at $z \neq 0$ will be obtained by use of (II.7). At $z = 0$, with $v_z = z/t$, (II.6) becomes

$$\frac{\partial}{\partial t}(s\gamma) + \frac{\partial}{\partial r}(s\gamma v_r) + s\gamma\left(\frac{v_r}{r} + \frac{1}{t}\right) = 0 \ . \tag{II.8}$$

If we write $v_r \equiv \tanh\alpha$, (II.8) can be recasted in the simple form

$$\frac{\partial}{\partial t}(rts\cosh\alpha) + \frac{\partial}{\partial r}(rts\sinh\alpha) = 0. \tag{II.9a}$$

From the conservation of energy and the thermodynamic relations (II.4), we get a similar equation for T,

$$\frac{\partial}{\partial t}(T\sinh\alpha) + \frac{\partial}{\partial r}(T\cosh\alpha) = 0 \ . \qquad \text{(II.9b)}$$

Together with the equation of state,

$$v_s^2 = \frac{\partial P}{\partial \epsilon} = \frac{s}{T}\frac{\partial T}{\partial s} \ , \qquad \text{(II.9c)}$$

equations (II.9a) and (II.9b) can be solved numerically. The results for ^{238}U collisions, obtained by Baym *et al.* [Ba83], are shown in Figs. II.4 to II.6. We see that it takes about 10 fm/c for the temperature to drop to half of its initial value, T_o. In Chapter IV, we shall present some estimates of the initial conditions, and we shall see that T_o is likely to be in the range of 200-300 MeV. The transverse expansion is not significant compared to the much faster longitudinal expansion, which probably cools the plasma down to the critical temperature of deconfinement transition before much of the plasma "feels" the transverse degree of freedom. Also note that (see Fig. II.6) in the scaling picture, the temperature is always increasing towards larger z, or the "ends" of the plasma tube.

The scaling picture is a simple and convenient framework to study the hydrodynamics of URHIC. However, there are a list of shortfalls in this "standard picture" the importance of which we must examine before we adopt this as a dynamical framework of URHIC.

The model should be closer to the truth for small z, but probably breaks down for large z due to the finite size of the plasma tube and the presence of the fragmentation regions. The scaling picture is a good approximation if the extent

of the CRR is long compared with the fragmentation regions. We therefore expect that scaling hydrodynamics becomes a better approximation for heavy-ion collisions of higher energies. But for beam energies available now or in the near future, we have to know where and when the scaling hypothesis breaks down.

The validity of the assumption that the plasma tube is created all at once and then undergoes hydrodynamic expansion is questionable. If the time duration at which collisions take place is not too small compared to the characteristic time scales of the expansion, we must view plasma creation as a continuous process occurring throughout much of the hydrodynamic phase. A consistent treatment of plasma creation and expansion can be achieved by putting source terms in the hydrodynamic equations [Ka83]. The addition of source terms allow us to model the physics of plasma creation or energy deposition in URHIC. It also alleviates us from the common practice of considering only the dynamics in the CRR as if it is separated from the fragmentation regions.

It is also not clear whether local thermal equilibrium can be established quickly enough that non-equilibrium effects can be ignored. While this question cannot be answered fully in the framework of hydrodynamics, we can incorporate to first order off-equilibrium effects and get a feeling of their importance by putting transport terms in the hydrodynamic equations.

We shall try to improve on the scaling model, and look at more realistic hydrodynamic solution. We shall incorporate the fragmentation regions in our description, investigate the effects of the transports coefficients, use more realistic equation of state, and model the initial conditions and source terms. Before we present our

hydrodynamic model in Chapter VI and VII though, we shall first go back to a more detailed discussion of the hydrodynamic equations (Chapter III), the initial conditions (Chapter IV), and the transport coefficients (Chapter V).

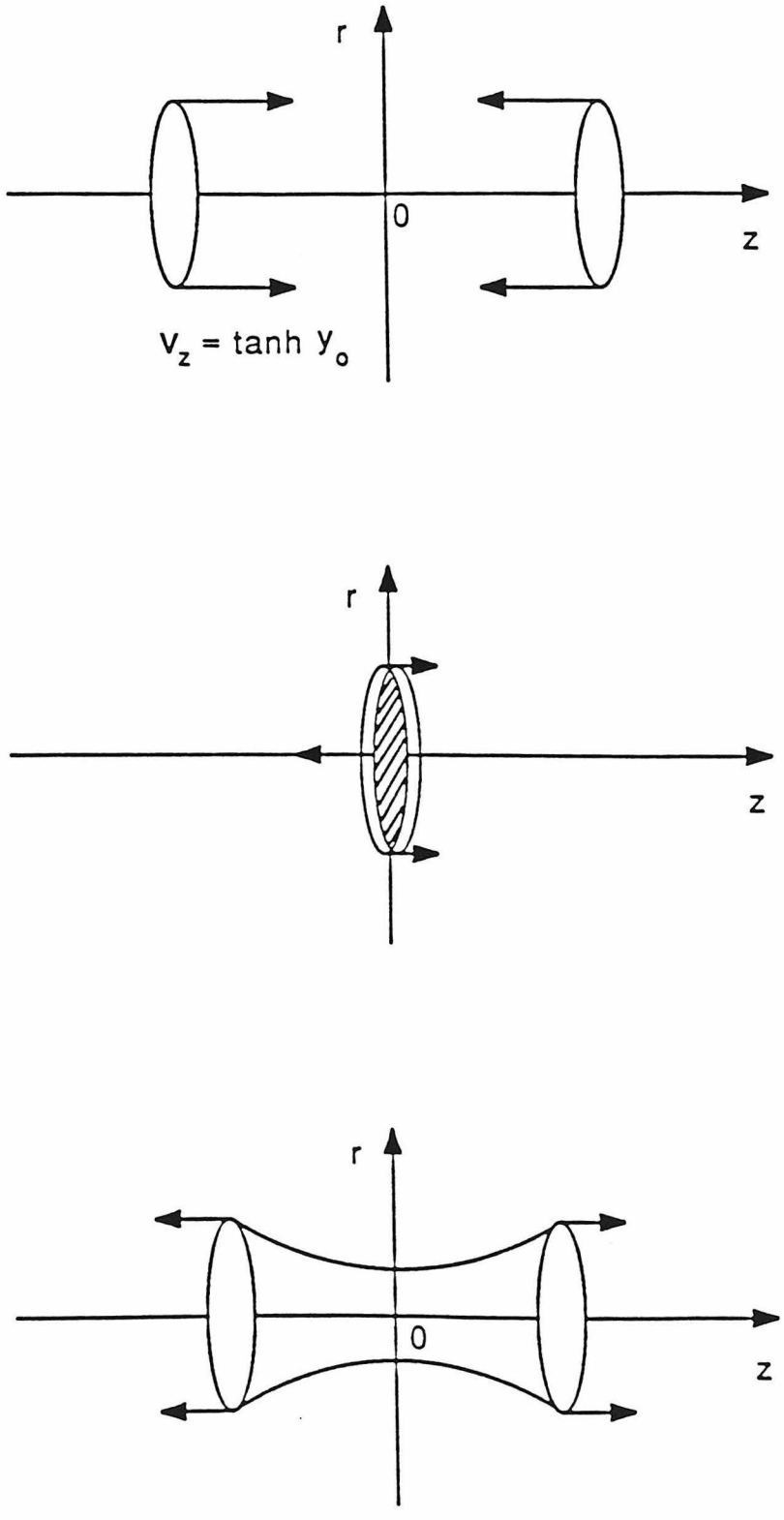

FIG. II.1 Central collision of identical heavy-ions in the center-of-mass frame.

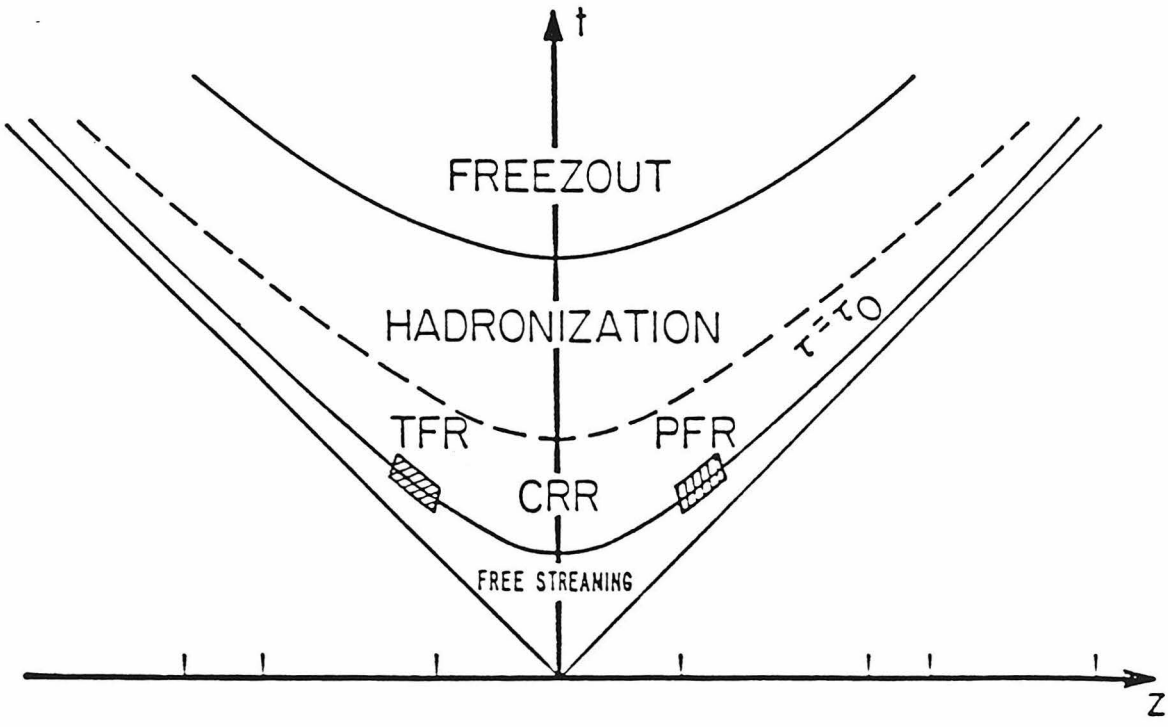

FIG. II.2 Space-time picture of the evolution of a quark-gluon plasma in ultra-relativistic heavy-ion collision.

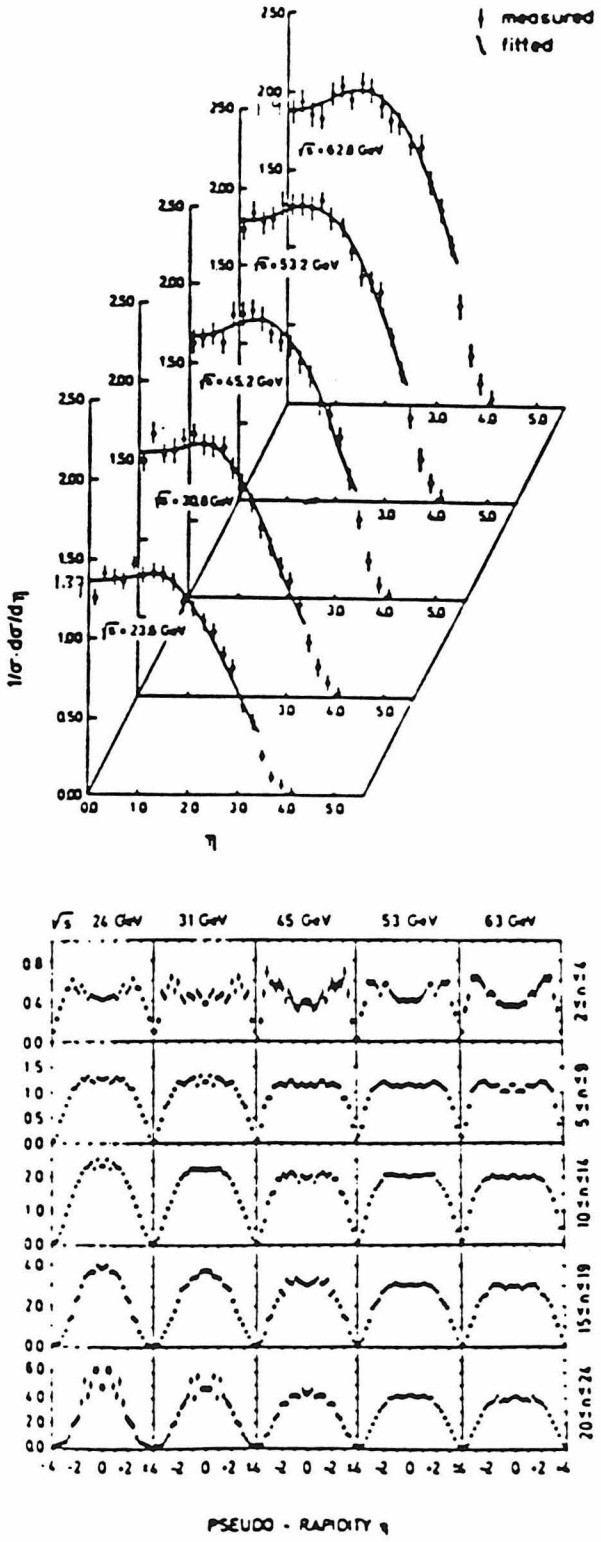

FIG. II.3 Pseudo-rapidity distributions in the center-of-mass frame for different energies [Th77].

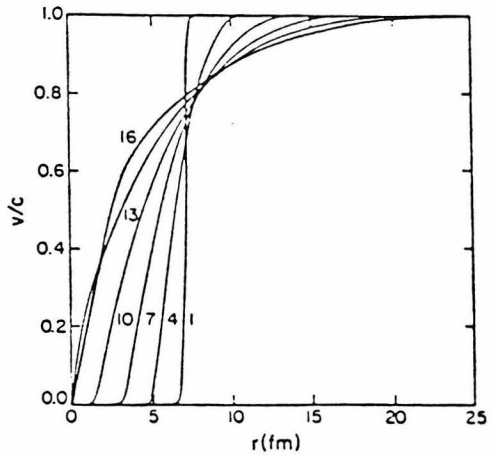

FIG. II.4 Velocity distributions for cylindrical expansion in the scaling picture. Curves are labelled by the time (fm) elapsed since the first collisions. Hydrodynamics commences at $\tau_o = 1$ fm [Ba83].

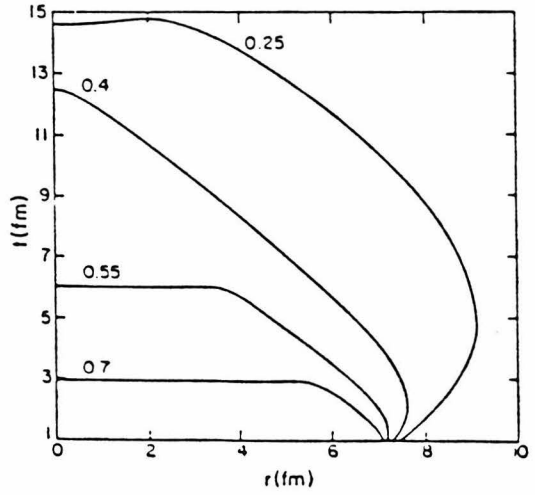

FIG. II.5 Isotherms in the $r - t$ plane for cylindrical expansion in the scaling picture. Curves are labelled by T/T_o, T_o being the initial temperature. $\tau_o = 1$ fm [Ba83].

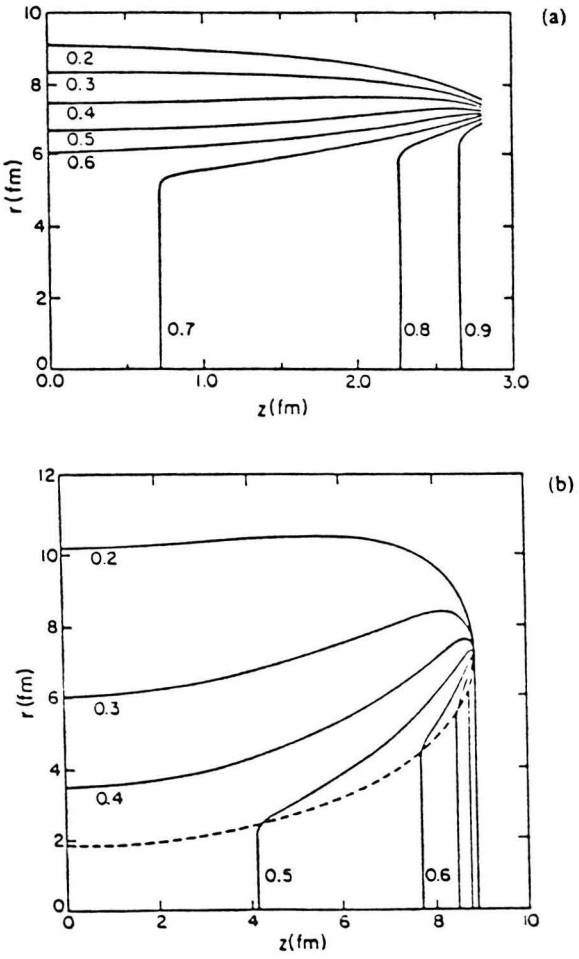

FIG. II.6 Isotherms in the $z-r$ plane at a) t=3 fm, and b) t=9 fm. Curves are labelled by T/T_o. The dashed curve in b) shows the rarefaction front [BaS3].

CHAPTER III

The Hydrodynamic Equations

The laws of hydrodynamics are equivalent to the statements of conservation of energy-momentum, which governs how the energy density and the momentum density evolve in space-time, and the conservation of net baryon number, which tells us how the net baryon number current flows. After a discussion of the energy-momentum tensor (section III.1), we shall derive the ideal hydrodynamic equations (section III.2). We then turn our attention to the modifications of these equations due to transport phenomena (section III.3) and the source terms (section III.4). We shall use the convention that the Greek affixes, α, β, γ, ..., take values 0,1,2,3 for the time and space indices, whereas the Latin affixes, i, j, k, ..., take values 1,2,3 for space indices. We shall also use the metric $g_{ii} = 1 = -g_{00}$.

III.1 The energy-momentum tensor

Recall what the different components of the energy-momentum tensor (sometimes called the stress-energy tensor) $T_{\mu\nu}$ mean [La59, Mi70]: T_{ij} is the i^{th} component of the force going through a surface perpendicular to the j^{th} direction, or equivalently the i^{th} component of the momentum flux in the j^{th} direction. T_{00} is the proper mass-energy density, and T_{0i} gives the density of momentum in the i^{th} direction, or equivalently the i^{th} component of energy flux. $T_{\mu\nu}$ is by definition symmetric with respect to the interchange of its indices. In the rest frame of a

fluid element, the momentum density is zero. Also, the pressure in the fluid elements P must be equal in all directions and perpendicular to the surface it acts on. Therefore, the energy-momentum tensor in the proper frame of a fluid element must be

$$T_{\mu\nu} = \begin{pmatrix} \epsilon & 0 & 0 & 0 \\ 0 & P & 0 & 0 \\ 0 & 0 & P & 0 \\ 0 & 0 & 0 & P \end{pmatrix} \qquad \text{(III.1)}$$

In an arbitrary reference frame, $T_{\mu\nu}$ must be a linear combination of $u_\mu u_\nu$ and $g_{\mu\nu}$, just from the tensor structure. It also has to reduce to the form (III.1) in the fluid rest frame. We therefore conclude that in an arbitrary reference frame,

$$T_{\mu\nu} = (\epsilon + P)u_\mu u_\nu + P g_{\mu\nu} \quad . \qquad \text{(III.2)}$$

III.2 Equations of ideal relativistic hydrodynamics

Conservation of energy-momentum implies

$$\partial_\mu T^{\mu\nu} = 0 \quad . \qquad \text{(III.3a)}$$

This then also gives the equations of ideal hydrodynamics, which tell us how the energy density, momentum density, and velocity fields evolve in space- time. If there is net baryon number in the system, we supplement (III.3a) with the law of conservation of net baryon number,

$$\partial_\mu J_B^\mu = 0 \quad , \qquad \text{(III.3b)}$$

where $J_B^\mu \equiv n_B u^\mu$ is the net baryon number current, with n_B being the proper net baryon number density. Equations III.3 then completely describe the hydrodynamics of a fluid.

Let us now consider several geometries of the system and write out (III.3a) in coordinate form. First we imagine the longitudinal (z) expansion of the plasma, ignoring transverse flow. The energy-momentum tensor in this geometry reads

$$T^{00} = w\gamma^2 - P \ , \ T^{01} = T^{10} = w\gamma^2 v_z \ , \ T^{11} = w\gamma^2 v_z^2 + P \ .$$

Here, $w = \epsilon + P$ is the enthalpy, v_z the fluid velocity along z direction, and $\gamma^2 = 1/(1 - v_z^2)$. Equation III.3a then becomes

$$\partial_t\left[w\gamma^2 - P\right] + \partial_z\left[w\gamma^2 v_z\right] = 0 \ , \tag{III.4a}$$

$$\partial_t\left[w\gamma^2 v_z\right] + \partial_z\left[w\gamma^2 v_z^2 + P\right] = 0 \ , \tag{III.4b}$$

whereas (III.3b) gives

$$\partial_t(n_B\gamma) = 0 \ . \tag{III.4c}$$

For one dimensional relativistic hydrodynamics, a more natural set of variables to use is

$$s \equiv \ln\frac{\tau}{\tau_o} \ , y \equiv \frac{1}{2}\ln\frac{t+z}{t-z} \ , \tag{III.5}$$

which has simple Lorentz transformation properties. Taking $\cosh y \times$ (III.4a) - $\sinh y \times$ (III.4b) we get

$$\partial_2\epsilon + w\partial_1\theta = 0 \ , \tag{III.6a}$$

whereas cosh $y \times$ (III.4b) - sinh $y \times$ (III.4a) gives

$$\partial_1 P + w\partial_2\theta = 0 \ . \tag{III.6b}$$

The baryon number equation becomes

$$\partial_2 n_B + n_B\partial_1\theta = 0 \ . \tag{III.6c}$$

Here,

$$\partial_1 \equiv \alpha\partial_s + \beta\partial_y \;\; ; \;\; \partial_2 \equiv \beta\partial_s + \alpha\partial_y \;\; ; \tag{III.7}$$

$$\alpha \equiv \sinh(\theta - y) \;\; , \;\; \beta \equiv \cosh(\theta - y) \;\; ,$$

and $\theta \equiv \tanh^{-1} v_z$ is the fluid rapidity. Note that if scaling holds, $\theta = y$, and so $\partial_1 = \partial_y$ and $\partial_2 = \partial_s$. Then (III.6) reduce to

$$\partial_s \epsilon + w = 0 \;\; , \tag{III.8a}$$

$$\partial_y P = 0 \;\; , \tag{III.8b}$$

$$\partial_s n_B + n_B = 0 \;\; . \tag{III.8c}$$

Equation (III.8a) is equivalent to Eq. (II.1), and for ideal gas equation of state, $\epsilon = 3P$, (III.8b) is just a restatement of the fact that ϵ depends only on τ.

Next we consider cylindrical flow. In this case, Equations (III.3a) and (III.3b) give

$$\frac{\partial}{\partial t}\left[w\gamma^2 - P\right] + \frac{1}{r}\frac{\partial}{\partial r}\left[rw\gamma^2 v_r\right] + \frac{\partial}{\partial z}\left[w\gamma^2 v_z\right] = 0 \;\; , \tag{III.9a}$$

$$\frac{\partial}{\partial t}\left[w\gamma^2 v_z\right] + \frac{1}{r}\frac{\partial}{\partial r}\left[rw\gamma^2 v_r v_z\right] + \frac{\partial}{\partial z}\left[w\gamma^2 v_z^2 + P\right] = 0 \;\; , \tag{III.9b}$$

$$\frac{\partial}{\partial t}\left[w\gamma^2 v_r\right] + \frac{1}{r}\frac{\partial}{\partial r}\left\{r[w\gamma^2 v_r^2 + P]\right\} + \frac{\partial}{\partial z}\left[w\gamma^2 v_r v_z\right] = 0 \;\; . \tag{III.9c}$$

Here, v_r (v_z) is the flow velocity perpendicular (parallel) to the collision axis. The coordinate origin is put at the center of the collision, and therefore we have reflection symmetry with respect to the $z = 0$ plane. Equation (III.9a) expresses energy conservation, while Eqs. (III.9b) and (III.9c) describe momentum conservation in the z and r directions, respectively.

III.3 Transport phenomena

The ideal energy-momentum tensor in (III.2) will be modified in the presence of dissipative processes. Another way to think of this is that small deviations of the distribution function from the equilibrium give rise to small corrections to (III.2),

$$T^{\mu\nu} = wu^{\mu}u^{\nu} + Pg^{\mu\nu} + T_d^{\mu\nu} \quad , \tag{III.10a}$$

where $T_d^{\mu\nu}$ represents the dissipative part of the energy-momentum tensor [La59]. Similarly, the net baryon number current is affected by heat transport,

$$J_B^{\mu} = n_B u^{\mu} + \nu^{\mu} \quad . \tag{III.10b}$$

In nonrelativistic mechanics, we normally think of the rest frame as one in which the particles are stationary, or where the mass flux density vanishes. In relativistic mechanics though, there can be several different definitions of the rest frame that agree in the nonrelativistic limit. Of the more common used are the Landau-Lifshitz definition and the Eckart definition [Ec40]. In the Landau-Lifshitz definition, the rest frame of a fluid element is the one in which "the momentum of the element is zero, and its energy is expressible in terms of the other thermodynamic quantities by the same formulae as when the dissipative processes are absent." [La59] In other words, u_{μ} is defined so that

$$u_{\mu}T_d^{\mu\nu} = 0 \quad . \tag{III.11a}$$

Similarly,

$$\nu^{\mu}u_{\mu} = 0 \quad . \tag{III.11b}$$

The Eckart definition requires that the baryon three-current vanish in the rest frame. That is, the Eckart baryon current has the form $J_B^{\mu} = (n_B, 0)$, whereas the

Landau-Lifshitz baryon current is $J_B^\mu = (n_B, \vec{\nu})$. It is clear therefore that the two definitions are related by a Lorentz boost of velocity $\vec{v}_{L\to E} = \vec{\nu}/n_B$. We shall use the Landau-Lifshitz definition in the following.

We confine our attention to the first order terms (in gradients) in $T_d^{\mu\nu}$ and ν^μ. The entropy density current for a system defined by (III.10a) and (III.10b) is now

$$s^\alpha = su^\alpha - \nu^\alpha \frac{\mu_B}{T} \quad , \tag{III.12}$$

where $\mu_B = (w - Ts)/n_B$ is the baryon chemical potential, and s is the entropy density. The requirement that entropy increases with time, $\partial_\alpha s^\alpha \geq 0$, together with (III.11a) and (III.11b) uniquely determine the form of $T_d^{\mu\nu}$ and ν^μ:

$$T_d^{\mu\nu} = -\eta\left[\partial^\mu u^\nu + \partial^\nu u^\mu + u^\mu u^\alpha \partial_\alpha u^\nu + u^\nu u^\alpha \partial_\alpha u^\mu\right] - \left(\xi - \frac{2}{3}\eta\right)(g^{\mu\nu} + u^\mu u^\nu)\partial_\rho u^\rho \tag{III.13a}$$

$$\nu^\mu = -\kappa\left[\frac{n_B T}{w}\right]^2 (\partial^\mu + u^\mu u^\nu \partial_\nu)\left(\frac{\mu}{T}\right) \quad , \tag{III.13b}$$

where η and ξ are the coefficients of shear and bulk viscosity and κ the thermal conductivity. We shall discuss some estimates of the transport coefficients in Chapter V.

The one-dimensional hydrodynamic equations III.3 become

$$\partial_2 \epsilon + w\partial_1 \theta = \frac{\chi}{\tau}(\partial_1 \theta)^2 \quad , \tag{III.14a}$$

$$\partial_1 P + w\partial_2 \theta = \frac{\chi}{\tau}\left[\partial_1^2 \theta + \partial_1\theta\partial_2\theta - \alpha\partial_1\theta\right] + \frac{1}{\tau}\partial_1\theta\partial_1\chi \quad , \tag{III.14b}$$

$$\partial_2 n_B + n_B\partial_1\theta = \kappa\left[\partial_1\left[\frac{c}{\tau}\partial_1\left(\frac{\mu}{T}\right)\right] + \frac{c}{\tau}\partial_1\left(\frac{\mu}{T}\right)\partial_2\theta\right] \quad , \tag{III.14c}$$

where

$$\chi \equiv \xi + \frac{4}{3}\eta \quad ,$$

and

$$c \equiv \left[\frac{n_B T}{w}\right]^2 \quad .$$

In the scaling limit, (III.14a) reduces to

$$\frac{\partial \epsilon}{\partial \tau} + \frac{w}{\tau} = \frac{\chi}{\tau^2} \quad . \tag{III.15}$$

We see explicitly that the simple scaling solution (II.2) is broken by dissipative effects.

III.4 Source terms

In URHIC, the time scale of plasma creation is probably not too small compared to that of the hydrodynamic expansion. Therefore, the picture that a plasma tube is formed and then undergoes hydrodynamic expansion may not be correct. Most authors also like to consider the plasma in the CRR separately and independent of the fragmentation regions. For the dynamic evolution of the system, this may oversimplify the problem since the outgoing fragments are probably connected to the plasma in the CRR, and thus impose very different boundary conditions than if they are disconnected. We shall therefore put source terms in our hydrodynamic equations so as to incorporate the fragmentation regions in our calculations. Another additional advantage of doing so is that we can now model physics in the source terms and investigate the effects of different models on the dynamical evolution of the quark-gluon plasma.

Denoting the energy-momentum and net baryon number source terms by Σ^ν and σ respectively, we have,

$$\partial_\mu T^{\mu\nu} = \Sigma^\nu \quad , \tag{III.16a}$$

$$\partial_\mu n_B^\mu = \sigma \quad . \tag{III.16b}$$

The one dimensional hydrodynamic equations (III.6) thus become [Ch86]

$$\partial_2 \epsilon + w\partial_1 \theta = \frac{\chi}{\tau}\left(\partial_1 \theta\right)^2 + \tau S_1 \quad , \tag{III.17a}$$

$$\partial_1 P + w\partial_2 \theta = \frac{\chi}{\tau}\left[\partial_1^2 \theta + \partial_1\theta\partial_2\theta - \alpha\partial_1\theta\right] + \frac{1}{\tau}\partial_1\theta\partial_1\chi + \tau S_2 \quad , \tag{III.17b}$$

$$\partial_2 n_B + n_B\partial_1\theta = \kappa\left[\partial_1\left[\frac{c}{\tau}\partial_1\left(\frac{\mu}{T}\right)\right] + \frac{c}{\tau}\partial_1\left(\frac{\mu}{T}\right)\partial_2\theta\right] + \tau\sigma \quad , \tag{III.17c}$$

where $S_1 \equiv \Sigma^0 \cosh y - \Sigma^1 \sinh y$ and $S_2 \equiv \Sigma^1 \cosh y - \Sigma^0 \sinh y$. Note that now both the viscosity and the source terms tend to break the scaling solution. We shall study in detail the solution of (III.17) in Chapter VI, and the extension to cylindrical geometry in Chapter VII.

CHAPTER IV

Initial Conditions and Source Terms in URHIC

An understanding of the initial conditions of the QGP flow is very important. For example, we want to know whether the energy density immediately after the two heavy ions pass through each other is high enough to deconfine the quarks and gluons. The initial velocity of the plasma may also affect significantly the evolution at later time. We shall in the first two sections of this chapter study some simple estimates of the initial conditions. As argued in Chapter III, it is probably more sensible to talk about the source terms in such a rapidly evolving system. We shall therefore turn our attention to a study of the source terms in the last two sections of this chapter.

IV.1 Bjorken's Model

Bjorken's space-time picture of URHIC allows us to make some simple estimates of the initial conditions of the plasma flow in the CRR [Bj83, Gy84]. We shall briefly summarize his arguments here.

According to the IOC, at the energies we consider, each nucleon in the colliding nuclei collides once only. We can therefore think of a central collision of two identical heavy ions (with A nucleons each) as A nucleon-nucleon collisions. From SPS data [Th77, Al81] we know that for proton-proton collisions at center-of-mass energies of tens of GeV/A, the number of charged particle produced (mostly pions) per unit

rapidity, dN_{ch}/dy, is about 3. For every two charged particles detected, we estimate there is a neutral particle undetected. Therefore, assuming that each produced particle carries in average about 400 MeV, we have the average energy per rapidity, $d\langle E\rangle/dy \approx 3 \times 0.4 \times 1.5 \approx 1.8\text{GeV}$. We can now estimate the initial energy density in a thin slab at $z = 0$ (see Fig. IV.1) in an URHIC. Assuming that the effects of all A nucleon-nucleon collisions are simply additive, we have the energy contained within that slab being,

$$E = A\frac{d\langle E\rangle}{dy}\Delta y \quad , \tag{IV.1}$$

where Δy is the width in rapidity space of the slab. Now the scaling picture implies that $\Delta y \approx 2d/\tau_o$ for small d, where $2d$ is the thickness of the slab along z-direction, and τ_o is the proper time elapsed after the heavy-ion collision. Therefore,

$$\epsilon_o = A\frac{d\langle E\rangle}{dy}\frac{2d}{\tau_o}\frac{1}{\mathcal{A}d} \approx \frac{A^{\frac{1}{3}}}{4.5\text{fm}^2}\frac{d\langle E\rangle}{dy}\frac{2}{\tau_o} \quad , \tag{IV.2}$$

with $\mathcal{A}$ being the transverse area of the reaction region. For ^{238}U collisions, assuming $\tau_o \approx 1$ fm, (IV.2) gives $\epsilon_o \approx 5$ GeVfm^{-3} . By the scaling picture, this will be the energy density throughout the plasma tube in CRR at $\tau_0 \approx 1$ fm after the heavy ions pass through each other, when the system enters the hydrodynamic phase. In this picture, since the produced particles in the CRR undergo free-streaming for $\tau \leq \tau_o$, the velocity distribution at τ_o will have the form $v_z = z/t$. Notice that while the full additivity of produced energy is probably an overestimate (we shall correct this in section IV.3), the assumption of a single collision only may be an underestimate. Also, there still are no reliable estimates of τ_o. Therefore, the value of ϵ_o obtained above should be taken as only an order-of-magnitude estimate. What

we have learned is that it is plausible that $\epsilon \approx 1 - 10$ GeVfm^{-3} can be reached in URHIC, and therefore the creation of a QGP.

IV.2 Multiple Collision Model (MCM)

Pairwise single nucleon-nucleon collisions is the essential feature of the IOC, which is the basis of Bjorken's estimate of ϵ_o. At the other extreme, which recent nucleon-nucleus data seem to suggest as being more realistic, there are the multiple collision models (MCM). In this section, we shall use a Glauber type of MCM [Gl59, Bl81, Wo84, 85] to estimate ϵ_o.

We define a normalized thickness function for heavy-ion collisions at impact parameter $\vec{b}$,

$$T(\vec{b}) = \int\int \rho_B(\vec{b}_B, z_B)\rho_C(\vec{b}_C, z_C)t(\vec{b} - \vec{b}_B - \vec{b}_C)d\vec{b}_B dz_B d\vec{b}_C dz_C \quad . \qquad \text{(IV.3)}$$

Here, $\rho_B(\vec{b}_B, z_B)$ $(\rho_C(\vec{b}_C, z_C))$ is the normalized density distribution for nucleus $B(C)$ at longitudinal and transverse coordinates $z_B(z_C)$ and $\vec{b}_B(\vec{b}_C)$ respectively, with the origin at the center of $B(C)$ (see Fig. IV.2). The normalized nucleon-nucleon thickness function, t, gives the probability of having a nucleon-nucleon $(N - N)$ collision when multiplied by the $N - N$ cross section. Therefore, in a central collision of two identical heavy ions of A nucleons each, the probability for the occurence of n inelastic $N - N$ collisions is [Wo83, 84]

$$P(n) = N\binom{A^2}{n}\left[T(0)\sigma_{\text{in}}\right]^n\left[1 - T(0)\sigma_{\text{in}}\right]^{A^2-n} \quad , \qquad \text{(IV.4)}$$

where

$$N = \frac{1}{1 - \left[1 - T(0)\sigma_{\text{in}}\right]^{A^2}}$$

is a normalization factor so as to make

$$\sum_{n=1}^{A^2} P(n) = 1 \quad .$$

We can now take the average of n weighted by $P(n)$ to get

$$\langle n \rangle = NA^2 T(0) \sigma_{\text{in}} \quad . \tag{IV.5}$$

For heavy ions, we can parametrize the density distribution with a Woods-Saxon form,

$$\rho_B(\vec{b}_B, z_B) = \frac{\rho_o}{\left[1 + \exp\left[\sqrt{b_B^2 + z_B^2} - R_A\right]/a\right]} \quad , \tag{IV.6}$$

with $R_A = r_o A^{1/3}$ being the radius of the nucleus. Here, $r_o \approx 1.2$ fm , $a \approx 0.5$ fm being the diffuseness parameter, ρ_o is a normalization constant adjusted to make $\int \rho_B(\vec{b}_B, z_B) dz_B d\vec{b}_B = 1$. Taking a delta function for the nucleon thickness function, $t(\vec{b}) = \delta(\vec{b})$, which just says that two (point) nucleons can collide only if they are at the same transverse coordinates, we can calculate $T(0)$ numerically using (IV.6). For a rough estimate, we can just take a step function form of the density, $\rho_A(\vec{b}_A, z_A) \propto \theta(|\vec{b}_B| - R_A)\theta(z_B - R_A)$, and then we can evaluate (IV.5) analytically, giving

$$T(0) = \frac{9}{8\pi R_A^2} \quad .$$

Each collision in general will degrade the momentum of a nucleon, and we should change the cross section accordingly. In an approximate manner, we shall take the momentum degradation into account by enlarging the effective radii of the nuclei. r_o is made a free parameter, which is fitted to the experimental multiplicity data.

For ^{238}U collisions at tens of GeV/A, $\sigma_{\rm in} \approx 30$mb, and $\langle n \rangle \approx 800$, or each nucleon undergoes on average 3-4 collisions.

Now we can estimate the initial energy density in URHIC using MCM. Again we look at a thin slab at $z = 0$ (see Fig. IV.2); its energy content is now

$$E = \bar{m} \frac{dN^{BC}}{dy} \frac{2d}{\tau_o} \quad , \tag{IV.7}$$

where $dN^{BC}/dy = n \times dN^{nn}/dy$ is the number of produced particle per unit rapidity in URHIC. We have therefore

$$\epsilon_o = NA^2 \sigma_{\rm in} T(0) \frac{dN^{nn}}{dy} \frac{2\bar{m}}{\mathcal{A}\tau_o} \quad , \tag{IV.8}$$

which gives $\epsilon_o \approx 10$ GeVfm^{-3} for ^{238}U collisions at 30 GeV/A, assuming $\tau_o = 1$ fm.

In the transverse direction, the initial energy density won't be uniform. We can use this same model to map out the dependence of ϵ on the transverse coordinates $\vec{r}$. The result is, not surprisingly, a Gaussian-like energy density distribution in $\vec{r}$ [Wo83] (Fig. IV.3). This model can also allow us to investigate impact parameter dependence and also collisions between unequal nuclei. We shall come back to this model in next section when we derive the source terms. There we shall be more careful in handling the summation of energy production as well as the question of momentum degradation in MCM.

IV.3 One-dimensional Source Terms

We now take the viewpoint that plasma creation is a dynamical process continuing throughout much of the hydrodynamic phase. It is therefore necessary to work with the source terms in the hydrodynamic equations.

Again, we shall assume that heavy-ion collisions are made up of $N-N$ collisions. And for $N-N$ collisions, the produced particles can be treated as a collection of classical particles undergoing free-streaming. Therefore, their energy-momentum tensor and the net baryon number current can be written as [Ka83]

$$T_n^{\mu\nu}(z,t) = \sum_{\mathrm{i}=\pi,\mathrm{N},\ldots} \bar{m}_i \frac{dN_i^{\mathrm{nn}}}{dy}(y) \frac{1}{\mathcal{A}(z)\tau} \theta(\tau-\tau_o) u^\mu u^\nu \quad , \tag{IV.9a}$$

$$J_B^\mu(z,t) = \frac{dN_B^{\mathrm{nn}}}{dy}(y) \frac{1}{\mathcal{A}(z)\tau} \theta(\tau-\tau_o) u^{mu} \quad , \tag{IV.9b}$$

where $u^\mu = x^\mu/\tau$, $\mathcal{A}(z)$is the transverse area of the colliding ions at z, $\bar{m}_i$ the transverse mass and $\rho_i(y)$ is the rapidity density of particles of type $i = \pi, N, \ldots$. With the help of

$$\partial_\mu \tau = u_\mu \ , \ \partial_\mu u^\nu = \frac{1}{\tau}(g_\mu^\nu + u_\mu u^\nu) \ , \ u^\mu \partial_\mu = \partial_\tau \quad ,$$

we get

$$\partial_\mu T^{\mu\nu} = \sum_i \bar{m}_i \frac{dN_i^{\mathrm{nn}}}{dy} \frac{x^\mu}{\mathcal{A}\tau_o^2} \delta(\tau-\tau_o) \quad , \tag{IV.10a}$$

$$\partial_\mu J_B^\mu = \frac{1}{\mathcal{A}\tau_o} \frac{dN_B^{\mathrm{nn}}}{dy} \delta(\tau-\tau_o) \quad . \tag{IV.10b}$$

Therefore, summing over the effects of all $N-N$ collisions, we have for heavy-ion collisions,

$$\Sigma^\mu = \sum_{\text{collisions}} \sum_i \frac{m_i}{\mathcal{A}} \frac{x^\mu}{\tau_o^2} \frac{dN_i^{\mathrm{nn}}}{dy} \delta(\tau-\tau_o) \quad , \tag{IV.11a}$$

$$\sigma_B = \sum_{\text{collisions}} \frac{1}{\mathcal{A}\tau_o} \frac{dN_B^{\mathrm{nn}}}{dy} \delta(\tau-\tau_o) \quad . \tag{IV.11b}$$

In the IOC model with single pairwise collisions, the number of $N-N$ collisions equals the number of nucleons in each colliding heavy-ion. Therefore, the

summation over all collisions can be replaced by a summation over the number of nucleons entering the collision region. Assuming uniform density distribution we have,

$$\sum_{\text{collisions}} \approx n_o \sinh y_o \int \mathcal{A} dt$$

in the center-of-mass frame, with y_o being the rapidity and n_o the average proper density of each colliding ion. The source terms thus obtained are [Ch86],

$$\Sigma^o(y,s) = n_o \sinh y_o \sum_i \frac{m_i}{\tau_o} \frac{dN_i^{nn}}{dy}(y')\Theta(y,s) \quad , \tag{IV.12a}$$

$$\sigma_B(y,s) = \frac{n_o \sinh y_o}{\tau_o} \frac{dN_B^{nn}}{dy}(y') \frac{1}{\sqrt{e^{2s}\sinh^2 y + 1}} \Theta(y,s) \quad , \tag{IV.12b}$$

and

$$\Sigma^1(y,s) = \frac{e^s \sinh y}{\sqrt{e^{2s}\sinh^2 y + 1}} \Sigma^0(y,s) \quad . \tag{IV.12c}$$

Here, $y' \equiv \sinh^{-1}[e^s \sinh(y)]$, and Θ is a step function representing the source region[3] (discussed below).

At the other extreme is the multiple-collision model (MCM) [Gl59, Bl81, Wo84, Wo85, Ka83a]. In this model, most of τ_o is due to a thermalization time, during which the produced particles interact but have not yet established local thermal equilibrium. A nucleon in the beam can therefore make many collisions within the volume of the target nucleus. The probability of making a collision at transverse coordinate $\vec{b}$ is $P_B(\vec{b}) = T_B(\vec{b})\sigma_{\text{tot}}$, where σ_{tot} is the total nucleon-nucleon cross section $\approx$30 mb, and $T_B(\vec{b})$ is the normalized thickness function[14] for a nucleus [Wo84,85],

$$T_B(\vec{b}) = \int \rho(\vec{b}, z_B) dz_B \quad ,$$

with $\rho(\vec{b}, z_B)$ being the density (normalized to unity) at transverse and longitudinal coordinates $\vec{b}$ and z_B respectively, with the origin at the center of the nucleus. We shall use a Woods-Saxon form for ρ with a diffuseness of 0.5 fm and radius R=7 fm for ^{238}U.

We formulate our version of the MCM in the target's rest frame where the beam ion is very much Lorentz-contracted (see Fig. IV.4). It is therefore reasonable to make the approximation that all collisions between a nucleon in the target and the tube of beam nucleons at the same transverse coordinates occur at the same time and same place, which correspond to the overlap of the coordinates of the center of the projectile tube with those of the target nucleon. In the system of coordinates defined in Fig. IV.4, $z_C = t_C \tanh y_o$, where z_C, t_C are the space, time coordinates where the collisions occur. The average probability for a nucleon in a strip of the target of length Δz_C to make n collisions with the projectile nucleons is then

$$\Delta P^{(n)}(z_C) = \Delta z_C \binom{A}{n} \int d\vec{b}\ \rho(\vec{b}, z_C)[P_B(\vec{b})]^n [1 - P_B(\vec{b})]^{A-n} \quad ,$$

where A is the total number of nucleons in each colliding nucleus.

From the observation that a nucleon is scattered into the entire range of possible Feynman x [Ta76] with approximately uniform distribution, Wong obtained the rapidity distribution of target baryons after n collisions [Wo84a]:

$$D_t^{(n)}(y) = \frac{e^{y_o - y}}{2\sinh y_o} \frac{1}{(n-1)!} \left[\ln\left(\frac{2\sinh y_o}{e^{y_o - y} - e^{-y_o}} \right) \right]^{(n-1)} \theta(2y_o - y)\theta(y) \ ; \quad n \geq 1$$

$$D_t^{(0)}(y) = \delta(y) \quad . \tag{IV.13}$$

We can then sum $D_t^{(n)}(y)$ weighted by $\Delta P^{(n)}$ over n to obtain the contributions of

the slab at z_C to the target net baryon rapidity density:

$$\Delta\frac{dN_B^{\rm slab}}{dy} = A\sum_{n=0}^{A} D_t^{(n)}(y')\Delta P^{(n)}(z_C) \quad . \tag{IV.14}$$

Eq. (IV.14) is then summed over all slabs in the target to get the contributions of the target to the baryon number current source term,

$$\sigma_B^t = \sum_{\rm slabs} \Delta\frac{dN_B^{\rm slab}}{dy}\frac{1}{\tau_o \mathcal{A}(z_C)}\delta(\tau-\tau_o) \quad ,$$

with $\mathcal{A}(z_C) = \pi[2R|z_C| - {z_C}^2]$ being the transverse area of the target nucleus at z_C. We can now go back to the center-of-mass frame and add together the contributions from the target and the projectile nucleus, the latter being just the mirror image of the former with respect to $y = 0$. The result is:

$$\sigma_B(y,s) = \frac{\sinh y_o}{\tau_o}\sum_{n=0}^{A} D^{(n)}(y')G^{(n)}(z_C = at_o)\frac{\Theta(y,s)}{\sqrt{e^{2s}\sinh^2 y + 1}} \tag{IV.15a}$$

where

$$G^{(n)}(z_C) = \binom{A}{n}\int d\vec{b}\;\rho(\vec{b})\left[T_B(\vec{b})\sigma_{\rm tot}\right]^n\left[1 - T_B(\vec{b})\sigma_{\rm tot}\right]^{A-n}\frac{A}{\mathcal{A}(z_C)} \quad , \tag{IV.16}$$

with $t_o = \tau_o \cosh y_o\left[e^s \cosh y - \sqrt{e^{2s}\sinh^2 y + 1}\;\right]$ is the time at which collisions occur (in the rest frame of the target, but expressed in center-of-mass y), and

$$D^{(n)}(y) = \frac{\theta(y_o+y)\theta(y_o-y)}{2\sinh y_o (n-1)!}\left\{e^y\left[\ln\left(\frac{2\sinh y_o}{e^y - e^{-y_o}}\right)\right]^{(n-1)} + e^{-y}\left[\ln\left(\frac{2\sinh y_o}{e^{-y} - e^{-y_o}}\right)\right]^{(n-1)}\right\} \; ; \; n \geq 1$$

$$D^{(0)}(y) = \frac{1}{\sqrt{2\pi}\sigma_x}\left\{\exp\left[\frac{-[\exp(-y+y_o)-1]^2}{2{\sigma_x}^2}\right]\exp(y-y_o) + \exp\left[\frac{-[\exp(-y-y_o)-1]^2}{2{\sigma_x}^2}\right]\exp(-y-y_o)\right\} \quad .$$

Note that we have smeared out $D^{(0)}(y)$ with $\sigma_x \approx 0.1$ because of Fermi motion, which has only a small effect on $n \neq 0$ terms. If uniform density distribution in each of the colliding ^{238}U ions is assumed, this model predicts that a nucleon in either ions will suffer 3.5 collisions in average.

The treatment of the produced pions is only slightly different. In this case, we have to sum up contributions from all collisions:

$$\Delta \frac{dN_\pi^{\rm slab}}{dy} = \sum_{n=1}^{A} G_{in}^{(n)}(z_C)\Delta z_C \rho_\pi^{(n)} \quad ,$$

with

$$\rho_\pi^{(n)} \equiv \sum_{j=1}^{n} \frac{dN_\pi^{nn}}{dy}(\sqrt{s_j}, y') \quad .$$

Here $\sqrt{s_j} = m_N \cosh(y_o - j + 1)$ is the center-of-mass energy of a nucleon just before its $j^{\rm th}$ collision, and the elastic term ($n = 0$) is excluded. Note that Eq. (IV.13) implies that a nucleon in the beam losses in average one unit of rapidity per collision [Wo84a] (except for the first one, which just smears out the rapidity distribution), and we have downgraded its energy accordingly. $G_{\rm in}^{(n)}$ is the same as $G^{(n)}$ except that the inelastic cross section $\sigma_{\rm in}$ should be used in place of $\sigma_{\rm tot}$ in Eq. (IV.16). We thus have in the center-of-mass frame

$$\Sigma^0(y,s) = \frac{\sinh y_o}{\tau_o}\left[m_\pi \sum_{n=1}^{A} G_{in}^{(n)}(at_o)\rho_\pi^{(n)}(\sqrt{s_j}, y') + m_N \sum_{n=0}^{A} D^{(n)}(y')G^{(n)}(at_o)\right]\Theta(y,s) \quad , \tag{IV.15b}$$

and

$$\Sigma^1(y,s) = \frac{e^s \sinh y}{\sqrt{e^{2s}\sinh^2 y + 1}}\Sigma^0(y,s) \quad . \tag{IV.15c}$$

The source region has boundaries in space-time due to kinematic restrictions [Ka83]. First, we cannot have any contribution before the products of the first collisions thermalized, $s \leq 0$, nor after the thermalization of the products of the last collisions, $(t - d_t)^2 - z^2 \geq 1$, or

$$s \leq \ln\left[\frac{d_t}{\tau_o}\cosh y + \sqrt{\left(\frac{d_t}{\tau_o}\right)^2 \sinh^2 y + 1}\right] \ ,$$

with $d_t \geq 2R/\sinh y_o$ being the time it takes the two colliding ions to pass through each other. The source region also effectively cuts off when all the momentum of a nucleon is lost, $|z| = \tau_o \sinh y_o$, or

$$|y| \geq \sinh^{-1}\left(e^{-s}\sinh y_o\right) \ .$$

The source region in the $y - s$ plane is sketched in Fig. IV.5. It is seen that while energy is deposited in a short duration in the CRR, $d_t = 2R/\sinh y_o$, the process is much slower in the fragmentation regions, taking about $\Delta\tau \approx 2R^{\frac{1}{2}}$ fm. For ^{238}U collisions at 30 GeV/A, $d_t \approx 0.5$ fm and $\Delta\tau \approx 7.5$ fm.

IV.4 The source terms in cylindrical geometry

It is straigtforward to extend the source terms obtained in last section to cylindrical coordinates. However, we shall be interested in the source energy-momentum tensor $S^{\mu\nu}$ and net baryon current σ_B^μ instead, where $S^{\mu\nu}$ and σ_B^μ are defined by

$$\partial_\mu\left(T^{\mu\nu} - S^{\mu\nu}\right) = 0$$

and

$$\partial_\mu\left(J_B^\mu - \sigma_B^\mu\right) = 0 \ .$$

An easy extension of (IV.9) to cylindrical coordinates gives

$$S^{\mu\nu}(r,z,t) = \sum_{\text{collisions}} \sum_{\text{i}=\pi,\text{N}} \bar{m}_i \frac{dN_i^{\text{nn}}}{dy} \frac{1}{\mathcal{A}\tau} \theta(\tau - \tau_o) u^\mu u^\nu \rho(R-r) \quad , \qquad \text{(IV.16a)}$$

and

$$\sigma_B^\mu(r,z,t) = \sum_{\text{collisions}} \frac{dN_N^{\text{nn}}}{dy} \frac{1}{\mathcal{A}\tau} \theta(\tau - \tau_o) u^\mu \rho(R-r) \quad . \qquad \text{(IV.16b)}$$

We use a Woods-Saxon form for the density distribution in the transverse direction,

$$\rho(R-r) = \frac{\rho_o}{1 + e^{(r-R)/a}} \quad .$$

It is reasonable to assume that initially after the URHIC, produced particles follow free-streaming in the longitudinal directions, and have $u^r = 0$, $u^z = z/\tau$. Therefore the only non-vanishing components of $S^{\mu\nu}$ are

$$S^{tt} = n_s \int_0^{d_t} dt' \mathcal{M} \frac{(t-t')^2}{\left[(t-t')^2 - z^2\right]^{\frac{3}{2}}} \quad , \qquad \text{(IV.17a)}$$

$$S^{tz} = n_s \int_0^{d_t} dt' \mathcal{M} \frac{(t-t')z}{\left[(t-t')^2 - z^2\right]^{\frac{3}{2}}} \quad , \qquad \text{(IV.17b)}$$

$$S^{zz} = n_s \int_0^{d_t} dt' \mathcal{M} \frac{z^2}{\left[(t-t')^2 - z^2\right]^{\frac{3}{2}}} \quad , \qquad \text{(IV.17c)}$$

where

$$\mathcal{M} = \theta\left[(t-t')^2 - z^2 - \tau_o^2\right] \sum_{\text{i}=\pi,\text{N}} \bar{m}_i \rho_i(y) \rho(R-r) \quad .$$

Similarly,

$$\sigma_B^t = n_s \int_0^{d_t} dt' \mathcal{M}'(t-t') \quad , \qquad \text{(IV.18a)}$$

$$\sigma_B^z = n_s \int_0^{d_t} dt' \mathcal{M}' z \quad , \qquad \text{(IV.18b)}$$

with

$$\mathcal{M}' = \frac{\theta\left(\sqrt{(t-t')^2 - z^2} - \tau_o\right)}{(t-t')^2 - z^2} \; \frac{dN_N^{\rm nn}}{dy}\left(y = \frac{1}{2}\ln\frac{t-t'+z}{t-t'-z}\right)\rho(R-r) \quad ,$$

and $n_s = n_o \sinh y_o$. We have again made use of IOC to change the summation over all collisions to $n_s \int_0^{d_t} dt' \mathcal{A}$. Some of the integrals in (IV.17) can be done analytically, but it is easy enough to do all of them numerically.

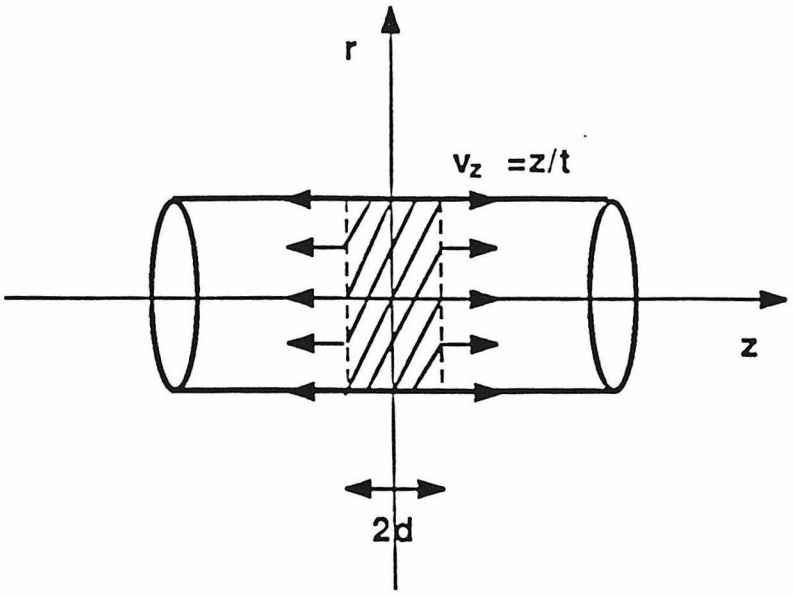

FIG. IV.1 The central region in ultra-relativistic heavy-ion collisions.

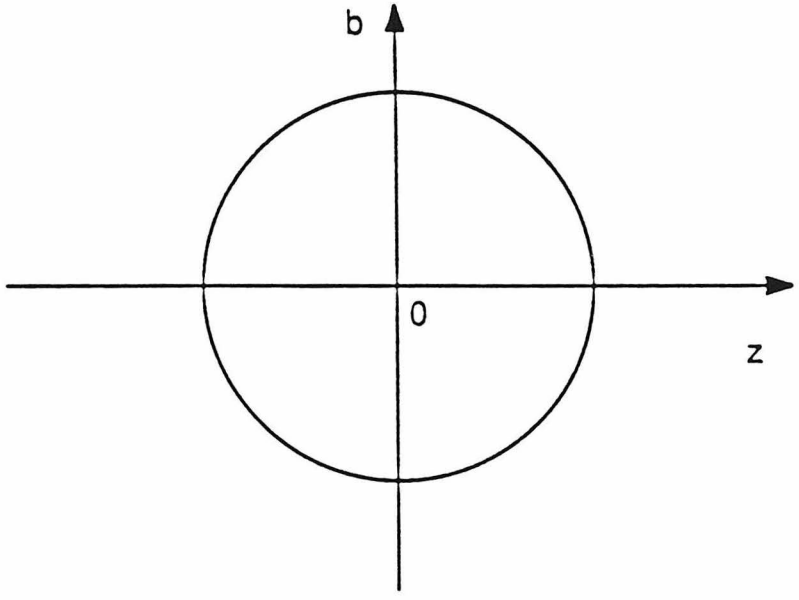

FIG. IV.2 Coordinates in a spherical heavy-ion.

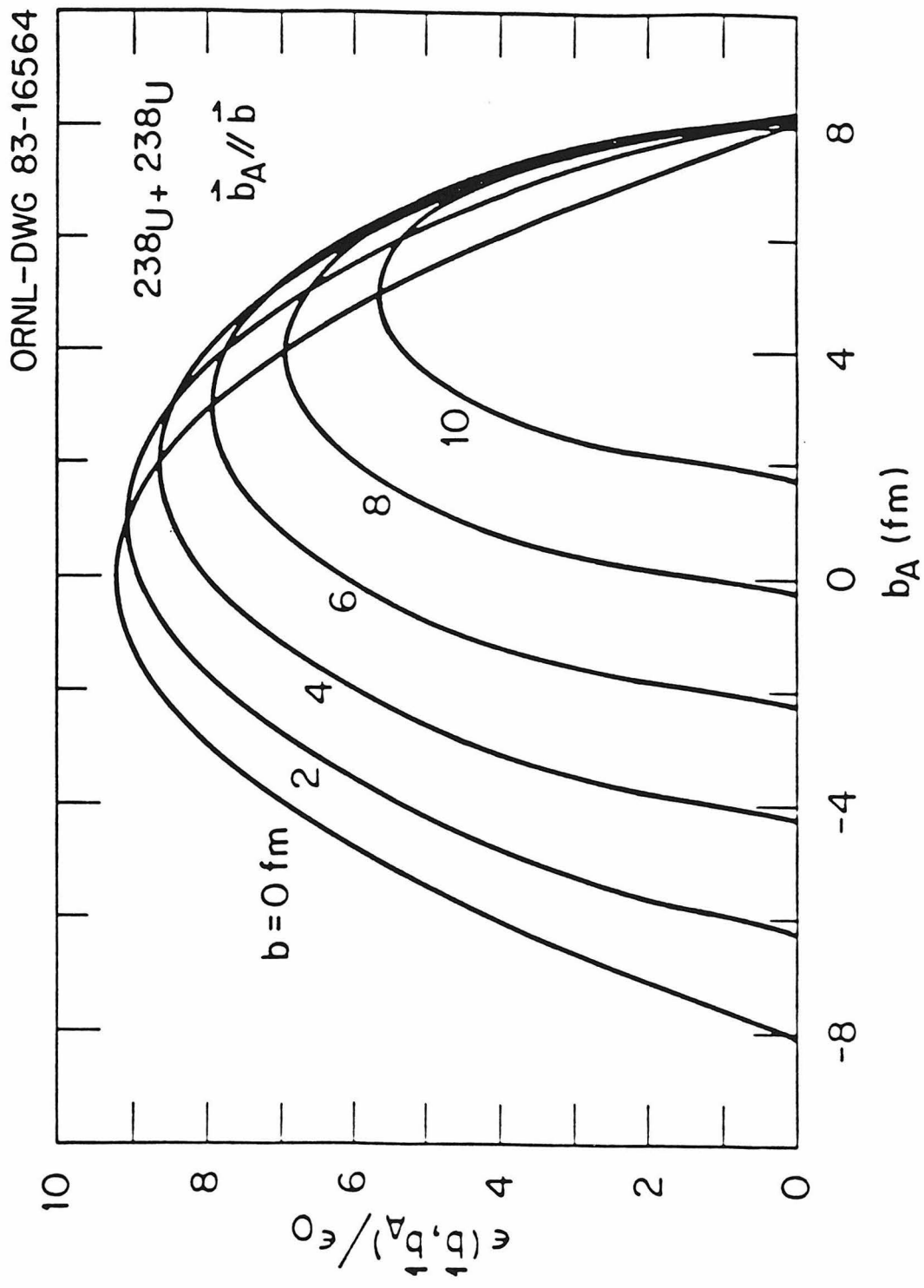

FIG. IV.3 Initial energy density profile in the transverse direction in collisions of Uranium ions [Wo83].

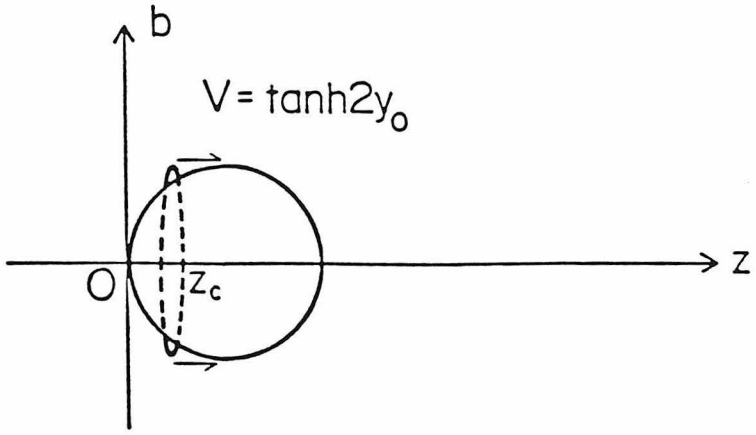

FIG. IV.4 Central collision of two identical heavy-ions in the target's rest frame.

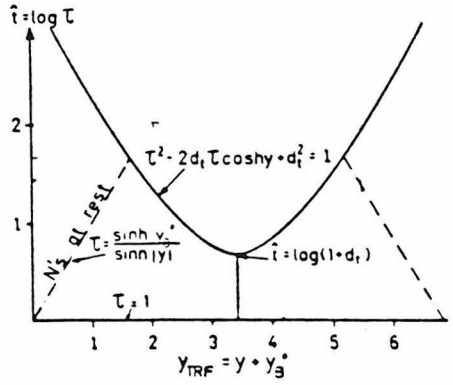

FIG. IV.5 The source region in the $y - s$ plane in the target's rest frame. The transformation to the center-of-mass frame preserves the shape of the region; only the origin of the y-axis is shifted [KaS3].

CHAPTER V

Transport Coefficients

In this chapter, we shall follow Gavin's work [Ga85] closely and give some estimates of the transport coefficients for the QGP: the shear and bulk viscosities, η and ξ respectively, and thermal conductivity κ. We start from a kinetic theory description of the system (Sec. V.1) and extract the transport coefficients in the collision time approximation from the first order deviations of the distribution function from equilibrium (Secs. V.2-4). In the case of a pion fluid, it is possible to estimate the collision time from experimental pion-pion scattering amplitudes. Section V.5 is a brief summary of results on the pion fluid. We then conclude this chapter with a short discussion of an alternative calculation of the transport coefficients [Da85].

V.1 Kinetic Theory

We shall use the Boltzmann-like equation,

$$\frac{\partial}{\partial t} f_p + \vec{v}_p \cdot \vec{\nabla} f_p \;=\; I[f_p] \quad , \tag{V.1}$$

which just says that the time rate of change of the proper distribution function $f_p(\vec{x}, \vec{p})$ is due to the spatial divergence of distribution, $\vec{v}_p \cdot \vec{\nabla} f_p$, where $\vec{v}_p = \vec{p}/\epsilon_p$ is the single-particle velocity, and a collision term $I[f_p]$. For a system of bosons (fermions) with zero net baryon chemical potential at local thermal equilibrium, the distribution function takes the Bose-Einstein (Fermi-Dirac) form

$$f_p^o = \frac{1}{e^{(\epsilon_p - \vec{p}\cdot\vec{u})/T} \mp 1} \quad , \tag{V.2}$$

where ϵ_p is the single particle energy, $\vec{p}$ the momentum, $\vec{u}$ the spatial part of the fluid four-velocity and T the temperature. By definition, $I[f_p^o]$ vanishes. We shall consider the case when $\delta f_p = f_p - f_p^o$ is small compared to f_p. The energy-momentum tensor has components

$$T^{00} = \int d\Gamma \epsilon_p f_p \tag{V.3a}$$

$$T^{0i} = \int d\Gamma p^i f_p \ , \tag{V.3b}$$

$$T^{ij} = \int d\Gamma p^i v_p^j f_p \ , \tag{V.3c}$$

where $d\Gamma = g d^3p/(2\pi)^3$, and g is the degeneracy. We impose the conditions that

$$T^{00} = \int d\Gamma \epsilon_p f_p^o \ , \ T^{0i} = \int d\Gamma p^i f_p^o \ , \tag{V.4}$$

even for systems slightly off local equilibrium. Equation (V.4) then defines the temperature and velocity for the non-equilibrium system.

It is now possible to derive the hydrodynamic equations by considering the moments of f and using (V.1). In particular, let's look at a one-dimensional scaling picture as discussed in Chapter II. Then (V.1) takes the form

$$\frac{\partial}{\partial t} f_p(\vec{p}, z, t) + v_{p_z} \frac{\partial f_p(\vec{p}, z, t)}{\partial z} \ = \ I\big[f_p(\vec{p}, z, t)\big] \ . \tag{V.5}$$

The scaling hypothesis says that f_p is unchanged under a Lorentz boost [Ba84],

$$f_p(p_\perp, p_z, z, t) = f_p(p_\perp, p_z', \tau) \ . \tag{V.6}$$

Here $p_z' = \gamma(p_z - \epsilon_p v_z)$, ϵ_p being the time component of p^μ, p_z and $p_\perp$ are the longitudinal and transverse single-particle momenta, and $v_z = z/t$, $\gamma = t/\tau$. Then

$$\begin{aligned} v_{p_z} \frac{\partial f_p}{\partial z} &= \frac{\partial p_z'}{\partial z} \frac{\partial f_p}{\partial p_z'} + \frac{\partial \tau}{\partial z} \frac{\partial f_p}{\partial \tau} \\ &= -v_{p_z} \Big(\gamma \frac{\epsilon_p}{t} \frac{\partial f_p}{\partial p_z'} + \frac{z}{\tau} \frac{\partial f_p}{\partial \tau} \Big) \ . \end{aligned}$$

In particular, at $z = 0$,

$$v_{p_z} \frac{\partial f_p}{\partial z} = -\left(\frac{p_z}{t}\right) \frac{\partial f_p}{\partial p_z} \quad . \tag{V.7}$$

By comparing (V.3) and (V.4), we also know that the energy moment of I vanishes. We have therefore, taking the energy moment of (V.5),

$$\int d\Gamma \epsilon_p \frac{\partial}{\partial t} f_p(p_\perp, p_z, z, t) + \int d\Gamma \epsilon_p v_{p_z} \frac{\partial}{\partial z} f_p(p_\perp, p_z, z, t) \; = \; 0 \quad . \tag{V.8}$$

Plugging (V.7) into (V.8) we obtain at $z = 0$

$$\int \frac{\partial}{\partial t}(\epsilon_p f_p) = \int d\Gamma \epsilon_p \left(\frac{p_z}{t} \frac{\partial f_p}{\partial p_z}\right) \quad . \tag{V.9}$$

But from (V.3), the fluid local energy density and longitudinal pressure are:

$$\epsilon(z,t) = \int d\Gamma \epsilon_p f_p \quad , \tag{V.10}$$

$$P_L(z,t) = \int d\Gamma \frac{p_z^2}{\epsilon_p} f_p \quad . \tag{V.11}$$

Therefore integrating the right hand side of (V.9) by parts and using (V.10,11), we get

$$\frac{\partial \epsilon}{\partial t} + \frac{1}{t}(\epsilon + P_L) = 0 \quad , \text{ at } z = 0 \quad , \tag{V.12}$$

which is just a special case of Eq. (II.1).

It is also possible to add other degrees of freedom into (V.1). In particular, for the QGP, the color degree of freedom should be considered. We can then look explicitly into the evolution of the system in color space. This relativistic kinetic theory for QGP with non-Abelian gauge interactions has been the subject of active research in the past few years [He85, Ka85a, Pl85, El86, He87]. However, owing to its complexity, there have not been any numerical results to date. We shall in this

thesis stick to the framework of hydrodynamics, and in this chapter, we employ the kinetic theory only as a mean to obtain estimates of the transport coefficients.

V.2 The coefficient of shear viscosity

We now use the collision time approximation [Ba84, Ga85],

$$I[f_p] \approx -\frac{(f_p - f_p^o)}{\tau_c} \quad , \tag{V.13}$$

where τ_c is the collision time, taken to be independent of the energy. This approximation designates τ_c to be the characteristic time scale in which the distribution function changes due to collisions, and approximates the change of f_p during this time interval linearly. Eq. (V.13) should therefore be a good estimate of the collision term if only one time scale dominates the collision process, and that f_p does not change too abruptly. Then (V.1) becomes

$$\delta f_p \equiv f_p - f_p^o = -\tau_c\left(\frac{\partial}{\partial t} f_p^o + \vec{v}_p \cdot \vec{\nabla} f_p^o\right) \quad . \tag{V.14}$$

But expanding (V.3c) to first order, we have

$$T^{ij} = T_o^{ij} + \int d\Gamma p^i v_p^j \delta f_p \quad , \tag{V.15}$$

with T_o^{ij} the ideal part (as discussed in Sec. III.1). Therefore, for a steady flow of the form $u^i = \big(u^x(y), 0, 0\big)$, with uniform temperature,

$$T_d^{xy} \equiv T^{xy} - T_o^{xy} = -\tau_c \int d\Gamma \Big(\frac{p_x p_y}{\epsilon_p}\Big) \frac{p_y}{\epsilon_p} \frac{\partial f_p^o}{\partial y} \quad . \tag{V.16}$$

For f_p^o of the form (V.2),

$$\frac{\partial f_p^o}{\partial y} = -p_x \frac{\partial u_x}{\partial y} \frac{\partial f_p^o}{\partial \epsilon_p} \quad . \tag{V.17}$$

Putting (V.17) into (V.16), we have

$$T_d^{xy} = \tau_c \int d\Gamma \Big(\frac{p_x p_y}{\epsilon_p}\Big)^2 \frac{\partial f_p^o}{\partial \epsilon_p} \frac{\partial u_x}{\partial y} \quad . \tag{V.18}$$

From Sec. II.3, Eq. (II.11a), we know that in general

$$T_d^{ij} = \eta\Big(\frac{\partial u^i}{\partial x^j} + \frac{\partial u^j}{\partial x^i}\Big) - \Big(\xi - \frac{2}{3}\eta\Big)\vec{\nabla} \cdot \vec{u}\delta^{ij} \quad , \tag{V.19}$$

which in this case reduces to

$$T_d^{xy} = -\eta \frac{\partial u_x}{\partial y} \quad . \tag{V.20}$$

Therefore, comparing (V.20) with (V.18), we have

$$\eta = -\frac{\tau_c}{15} \int d\Gamma \frac{p^4}{\epsilon_p^2} \frac{\partial f_p^o}{\partial \epsilon_p} \quad . \tag{V.21}$$

For a massless Bose fluid, (V.21) simplifies to

$$\eta_{SB} = \frac{4\tau_G}{15}\epsilon(T) \quad ,$$

where $\epsilon(T) = \frac{g}{30}\pi^2 T^4$ is the Stefan-Boltzmann relation, and τ_G is the collision time in the gluon fluid.

If we have a quark-anti-quark $(q - \bar{q})$ gas with quark chemical potential $\mu_q = \mu_B/3 = -\mu_{\bar{q}}$,

$$f_{p\pm}^o = \frac{1}{e^{(\epsilon_p - \vec{p}\cdot\vec{u} \mp \mu_q)/T} + 1} \quad ,$$

and (V.21) is modified to

$$\eta_Q = -\frac{\tau_Q}{15} \int d\Gamma \frac{p^4}{\epsilon_p^2} \left[\frac{\partial f_{p+}^o}{\partial \epsilon_p} + \frac{\partial f_{p-}^o}{\partial \epsilon_p}\right] \quad , \tag{V.22}$$

where τ_Q is the collision time in the $q - \bar{q}$ gas. Equation (V.22) can be evaluated numerically for arbitrary quark mass. In the limit of massless quarks with zero baryon chemical potential, (V.22) reduces to

$$\eta_Q(m = 0, \mu_B = 0) = \frac{7\pi^2 g}{450}\tau_Q T^4 \quad . \tag{V.23}$$

For an interacting quark-gluon plasma, we have to include quark-gluon scatterings in the calculation as well. In general, this involves solving three coupled Boltzmann equations. But if the collision times corresponding to the quark-quark, quark-gluon, gluon-quark, and gluon-gluon scatterings (τ_{QQ} , τ_{QG} , τ_{GQ} , τ_{GG}) are all small compared to the characteristic time scales of the evolution of the different components in the system, η can be obtained simply by replacing τ_Q by $\left(\tau_{QG}^{-1} + \tau_{QQ}^{-1}\right)^{-1}$ and τ_G by $\left(\tau_{GQ}^{-1} + \tau_{GG}^{-1}\right)^{-1}$. In summary, the coefficient of shear viscosity for a QGP is

$$\eta = \eta_G + \eta_Q = \frac{32}{225}\tau_G \pi^2 T^4 + \frac{-\tau_Q}{15}\int d\Gamma \frac{p^4}{\epsilon_p^2}\left[\frac{\partial f^o_{p+}}{\partial \epsilon_p} + \frac{\partial f^o_{p-}}{\partial \epsilon_p}\right] \quad , \tag{V.24}$$

where the degeneracy factor for a gluon liquid has been taken to be $g = 16$. The numerical result of evaluating (V.24) are shown in Fig. V.1. The calculations of the collision times involve non-perturbative QCD and are not done to date. We shall treat them as parameters with values around the typical QCD scale, 1 fm/c.

V.3 The coefficient of bulk viscosity

In both the non-relativistic and the ultra-relativistic limits, a gas with a conserved number of particles has zero bulk viscosity [Ho83]. However, a QGP can dissipate energy as it is compressed uniformly by creating $q - \bar{q}$ pairs, say, from

the vacuum giving rise to finite bulk viscosity. We estimate the coefficient of bulk viscosity, ξ, using a similar treatment as for η.

First we take the trace of the spatial part of the dissipative energy-momentum tensor, (II.11a),

$$T_d^{ii} = -3\xi\vec{\nabla}\cdot\vec{u} \ . \tag{V.25}$$

On the other hand (V.14) and (V.15) give

$$T_d^{ii} = -\tau_c \int d\Gamma \Big(\frac{\partial}{\partial t} f_p^o + \vec{v}_p \cdot \nabla f_p^o\Big)\frac{p^2}{\epsilon_p} \ . \tag{V.26}$$

Taking the Fermi-Dirac or Bose-Einstein distribution for f_p^o, we have

$$\frac{\partial f_p^o}{\partial t} = \frac{\partial f_p^o}{\partial \epsilon_p}\frac{1}{T}\left[T\frac{\partial}{\partial t}(-\vec{p}\cdot\vec{u}) - (\epsilon_p - \vec{p}\cdot\vec{u})\frac{\partial T}{\partial t}\right] \ . \tag{V.27}$$

But

$$\frac{\partial T}{\partial t} = \frac{\partial \epsilon}{\partial t}\frac{\partial T}{\partial \epsilon} = \frac{-w}{C_v}\vec{\nabla}\cdot\vec{u} \ , \quad C_v \equiv \frac{\partial \epsilon}{\partial T} \ , \tag{V.28}$$

where in the last step, the ideal hydrodynamic equation (II.1) was used, along with (III.6b),

$$-T\vec{p}\cdot\frac{\partial \vec{u}}{\partial t} = -T\frac{\vec{p}}{w}\cdot\vec{\nabla}P \ . \tag{V.29}$$

In the local rest frame ($\vec{u} = 0$), we have therefore reduced (V.27) to

$$\frac{\partial f_p^o}{\partial t} = \frac{\partial f_p^o}{\partial \epsilon_p}\Big[-\frac{\vec{p}}{w}\cdot\vec{\nabla}P + \epsilon_p\frac{w}{C_v T}\vec{\nabla}\cdot\vec{u}\Big] \ . \tag{V.30}$$

Similarly,

$$\vec{v}_p\cdot\vec{\nabla}f_p^o = T\frac{\partial f_p^o}{\partial \epsilon_p}\Big[\frac{\vec{p}}{T\epsilon_p}\cdot\vec{\nabla}(-\vec{p}\cdot\vec{u}) - \frac{(\epsilon_p - \vec{p}\cdot\vec{u})}{\epsilon_p T}\vec{p}\cdot\vec{\nabla}T\Big] \ . \tag{V.31}$$

But since $\vec{\nabla}T/T = -\vec{\nabla}P/w$, (V.31) becomes (in the rest frame),

$$\vec{v}_p \cdot \vec{\nabla} f_p^o = \frac{\partial f_p^o}{\partial \epsilon_p}\Big[-\vec{v}_p \cdot \vec{\nabla}(\vec{p}\cdot\vec{u}) + T\frac{\vec{p}}{w}\cdot\vec{\nabla}P\Big] \quad . \tag{V.32}$$

Putting (V.32) and (V.30) into (V.26) we get,

$$T_d^{ii} = -\tau_c \int d\Gamma \frac{\partial f_p^o}{\partial \epsilon_p}\Big[\frac{\epsilon_p w}{C_v T}\vec{\nabla}\cdot\vec{u} - (\vec{v}_p\cdot\vec{\nabla})(\vec{p}\cdot\vec{u})\Big]\frac{p^2}{\epsilon_p} \quad . \tag{V.33}$$

Comparing (V.33) with (V.25), we find that

$$\xi = \frac{1}{3}\tau_c \int d\Gamma \frac{p^2}{\epsilon_p}\frac{\partial f_p^o}{\partial \epsilon_p}\Big[\frac{\epsilon_p w}{C_v T} - \frac{p^2}{\epsilon_p}\Big] \quad . \tag{V.34}$$

If the mass of the particles in the fluid is small, we can expand the result in m/T,

$$\xi = \frac{g\tau_c}{72\pi} m^3 T\big(1 - 0.1627\frac{m}{T} + ...\big) \quad .$$

If we have a $q - \bar{q}$ gas, or finite chemical potential, the above result is slightly modified because now ϵ also depends on the net baryon number density, n_B. The result is $\xi_Q = \xi_{Q_+} + \xi_{Q_-}$, with

$$\xi_{Q_\pm} = -\tau_c \int d\Gamma \frac{\partial f_{p\pm}^o}{\partial \epsilon_p}\Big[\epsilon_p\Big(\frac{\partial P}{\partial \epsilon}\Big)_{n_B} \pm \Big(\frac{\partial P}{\partial n_B}\Big)_{\epsilon} - \frac{1}{3}pv_p\Big]^2 \quad , \tag{V.35}$$

which must be evaluated numerically. The total contribution to ξ in a QGP is therefore $\xi = \xi_G + \xi_Q$, where ξ_G is just the massless case of (V.34). As expected (see Fig. V.1), ξ is small compared to η.

V.4 Heat transport

If the system has finite net baryon current, we have to consider heat conduction as a dissipative process as well. In terms of the distribution functions, the net baryon number density and current are

$$n_B = \int d\Gamma (f_{p+} - f_{p-}) \ , \tag{V.36}$$

$$J_B^i = \int d\Gamma (f_{p+} - f_{p-}) v_p^i \ . \tag{V.37}$$

The heat current is the flow of the energy relative to the baryon enthalpy,

$$I^i = T^{0i} - \frac{w}{n_B} J_B^i \ . \tag{V.38}$$

Putting (V.4), (V.36) and (V.37) together we get

$$I^i = \int d\Gamma \frac{p^i}{\epsilon_p} \Big\{ \Big[\epsilon_p - \frac{w}{n_B} \Big] \delta f_{p+} + \Big[\epsilon_p + \frac{w}{n_B} \Big] \delta f_{p-} \Big\} \ . \tag{V.39}$$

In a static system, $\delta f_{p\pm} = -\tau_c \vec{v}_p \cdot \vec{\nabla} f^o_{p\pm}$ (cf. (V.14)). Taking the Fermi-Dirac distribution, we have

$$\vec{\nabla} f^o_{p\pm} = \frac{\partial f^o_{p\pm}}{\partial \epsilon_p} \Big[\frac{\epsilon_p}{T} \vec{\nabla} T \mp T \vec{\nabla} \Big(\frac{\mu_B}{T} \Big) \Big] \ . \tag{V.40}$$

But the Gibbs-Duhem relation implies $w dT/T = -n_B T d(\mu_B/T)$ for a system in steady state. Therefore,

$$\delta f_{p\pm} = \tau_c \frac{\partial f^o_{p\pm}}{\partial \epsilon_p} \frac{1}{T} \Big(\epsilon_p \mp \frac{w}{n_B} \Big) \vec{v}_p \cdot \vec{\nabla} T \ . \tag{V.41}$$

After putting (V.41) into (V.39) and comparing with the definition $I^i = -\kappa \nabla^i T$, we find

$$\kappa_Q = -\frac{\tau_c}{3T} \int d\Gamma \Big(\frac{p}{\epsilon_p} \Big)^2 \Big\{ \frac{\partial f^o_{p+}}{\partial \epsilon_p} \Big(\epsilon_p - \frac{w}{n_B} \Big)^2 + \frac{\partial f^o_{p-}}{\partial \epsilon_p} \Big(\epsilon_p + \frac{w}{n_B} \Big)^2 \Big\} \ . \tag{V.42}$$

The numerical results evaluating (V.42) are shown in Fig. V.1 . In the zero quark mass limit, (V.42) becomes

$$\kappa_Q(m=0) = \frac{\tau_c w C_v}{9n_B^2}\Big(\frac{\partial n_B}{\partial \mu_B}\Big)_T \ ,$$

with the heat capacity

$$C_v = \frac{3\Big[w\Big(\frac{\partial n_B}{\partial \mu_B}\Big)_T - 3n_B^2\Big]}{T}\Big(\frac{\partial n_B}{\partial \mu_B}\Big)_T \ .$$

Note that κ_Q diverges as $1/n_B^2$ as $n_B \to 0$. This is no cause of concern as only κn_B^2 enters the equation of motion, which remains finite in the zero baryon chemical potential limit. On the other hand, had we used the Eckart definition of the rest frame [Ec40], heat conduction would enter the energy-momentum tensor giving rise to a correction to the energy flux

$$T_E^{0i} = \kappa\Big[\frac{n_B T^2}{\epsilon} + P\Big]\nabla^i\Big(\frac{\mu}{T}\Big) \ ,$$

which would diverge as $1/n_B$ in the $n_B \to 0$ limit. For zero baryon chemical potential problems such as in the CRR of a QGP, it is clearly preferable to use the Landau-Lifshitz choice of the rest frame.

V.5 Pion fluid

When the hydrodynamic expansion of the QGP cools it down to the critical temperature of the confinement transition, the system hadronizes to a soup of mesons and baryons. By far the most abundant final state particles are the pions, and we can treat the final stage of URHIC approximately as consisting of a pion fluid. We shall briefly consider the collision time in this system.

The dominant reaction in a pion fluid is low-energy pion-pion scattering. Also, number-changing processes such as $4\pi \rightleftharpoons 2\pi$ are either very slow or absent. We shall use a variational method to estimate the collision time [Ga85]. First we write

$$f_p = f_p^o + \frac{\partial f_p^o}{\partial \epsilon_p}\phi_p \quad ,$$

where ϕ_p is a small variational trial function. We can then calculate the entropy production to lowest order in ϕ_p due to the collision term $I[\phi_p]$ describing the process $p_1^\mu + p_2^\mu \rightarrow p_3^\mu + p_4^\mu$,

$$\begin{aligned} \dot{S} &= \int d\Gamma \phi_p I[\phi_p] \\ &= \frac{1}{4T^2}\int \prod_{i=1}^{4} \frac{d\Gamma_i}{\epsilon_i} f_1^o f_2^o (1+f_3^o)(1+f_4^o) s\sigma(s_1 \cos\theta)\delta^4(\Delta p^\mu)\left[\Delta\phi_p\right]^2 \quad , \end{aligned} \tag{V.43}$$

where we have abbreviated $\Delta p^\mu = p_3^\mu + p_4^\mu - p_1^\mu - p_2^\mu$, and similarly for $\Delta\phi_p$. In (V.43), s is the square of the center-of-mass energy of the collision, and $f_1^o f_2^o (1+f_3^o)(1+f_4^o)$ is the appropriate phase space factors for bosons. The transport coefficients are related to $\dot{S}$ by

$$\eta = \frac{\left(T_d^{xy}\right)^2}{T\dot{S}} \quad , \tag{V.44}$$

$$\kappa = \frac{I^2}{T^2\dot{S}} \quad , \tag{V.45}$$

and we can therefore use some trial function ϕ_p to get an upper bound on $\dot{S}$, or equivalently, lower bounds on η and κ. The results of such a calculation are shown in Fig. V.2 . Notice that both η and κ are small in the pion phase compared to the QGP phase.

V.6 Alternative calculations

We based our discussion above on the collison time appoximation of Gavin [Ga85]. Here we briefly report another calculation.

Danielewicz and Gyulassy reported some bounds on η due to constraints on the mean free path λ in a QGP [Da85]. First the uncertainty principle requires $\lambda_i \geq \langle p \rangle_i^{-1}$, where $\langle p \rangle_i$ is some characteristic momentum transported by particle i in the plasma. Second, λ cannot be shorter than the interparticle distance, $\lambda_i \geq n_i^{-1/3}$, where n_i is the local density of particle i. Since kinetic theory arguments give [Re65]

$$\eta \simeq \frac{1}{3} \sum_i (n \langle p \rangle \lambda)_i \quad , \tag{V.46}$$

we therefore conclude that $\eta \geq 2T^3$. The authors also gave an estimate of η using QCD phenomenology. They first calculated the cross section for the dominant t-channel gluon-exchange by generalizing the perturbative result:

$$\sigma_\eta = - \int_{-s}^{0} dt \frac{\pi}{2t^2} \frac{4t}{s} \left[1 + \frac{t}{s} \right] \alpha_T^2 \left[\frac{t}{t - m_E^2} + \frac{t}{t - m_M^2} \right]^2 \quad ,$$

with $\alpha_T = \alpha_s(t = -17T^2)$, the running strong coupling constant, m_E and m_M being effective color-electric and color-magnetic masses for N_c colors and N_f flavors with flavor chemical potential μ_f [Na83]:

$$m_E^2 \approx \alpha_s(t) \left[4\pi \left(N_c + \frac{N_f}{2} \right) \frac{T^2}{3} + \left(\frac{2}{\pi} \sum_{f=1}^{N_f} \mu_f^2 \right) \right] \quad ,$$

$$m_M^2 \approx \alpha_s^2(t) T^2 [4\pi(0.27)] \quad .$$

Then η is related to the cross section using (V.43). Their result is (Fig. V.3)

$$\eta = \frac{T}{\sigma_\eta} \left[\frac{n_g}{\frac{9}{4} n_g + n_q} + \frac{n_q}{\frac{4}{9} n_q + n_g} \right] \quad . \tag{V.47}$$

The bulk viscosity arising from the variation of the sound velocity in the mixed phase was estimated by considering the pressure at small deviation from equilibrium,

$$P(\epsilon, f) \approx P_{\rm eq} + \delta f \left(\frac{\partial P}{\partial f}\right)_{\epsilon} \quad , \tag{V.48}$$

where $P_{\rm eq}$ is the pressure at equilibrium, and f is the fraction of volume occupied by the plasma phase, which at equilibrium is

$$f_{\rm eq}(\epsilon) = \frac{\epsilon - \epsilon_H}{\epsilon_Q - \epsilon_H} \quad .$$

We have put the phase boundaries at $\epsilon = \epsilon_Q$ for the plasma and $\epsilon = \epsilon_H$ for hadrons (ie. pure plasma for $\epsilon \geq \epsilon_Q$ and pure hadrons for $\epsilon \leq \epsilon_H$). Now we use the relaxation time approximation,

$$\frac{df}{d\tau} = -\frac{1}{\tau_r}(f - f_{\rm eq}) \quad . \tag{V.49}$$

Therefore,

$$\delta f = -\tau_r \frac{df_{\rm eq}}{d\tau} = -\frac{\tau_f}{\Delta\epsilon}\frac{d\epsilon}{d\tau} = \frac{\tau_f}{\Delta\epsilon}(\epsilon + P)\vec{\nabla}\cdot\vec{u} \quad , \tag{V.50}$$

where the ideal hydrodynamic equation (III.6a) was used, and $\Delta\epsilon \equiv \epsilon_Q - \epsilon_H$. Putting (V.50) into (V.48) we then get

$$P = P_{\rm eq} - \tau_r C_f^2 (\epsilon + P)\vec{\nabla}\cdot\vec{u} \quad , \tag{V.51}$$

where $C_f^2 = (\partial P/\partial\epsilon)_{f_{\rm eq}}$ is the speed of sound squared in the system with the fraction of volume in plasma held fixed. We can therefore, by comparing (V.51) with (III.8a), identify $\xi = \tau_r C_f^2(\epsilon + P_{\rm eq})$. Near $\epsilon \approx \epsilon_Q$, taking $C_f^2 \approx 1/3$ (for ideal relativistic gas), $\xi \approx 1$ GeVfm^{-3} , which is comparable to η.

Because of the non-perturbative nature of transport phenomena in QGP at the temperature we are interested in, a rigorous calculation from QCD is possible only

with lattice calculations using Kubo formulae [Ho84]. Otherwise, we either sweep all detailed physics into a collision time and express all transport coefficients in terms of it, or go through some phenomenological estimates. We cannot even compare the results obtained by the two methods because the collision time and its possible temperature dependence are unknown. We shall take Gavin's results and adjust τ_c to investigate the importance of transport phenomena in the hydrodynamics of QGP.

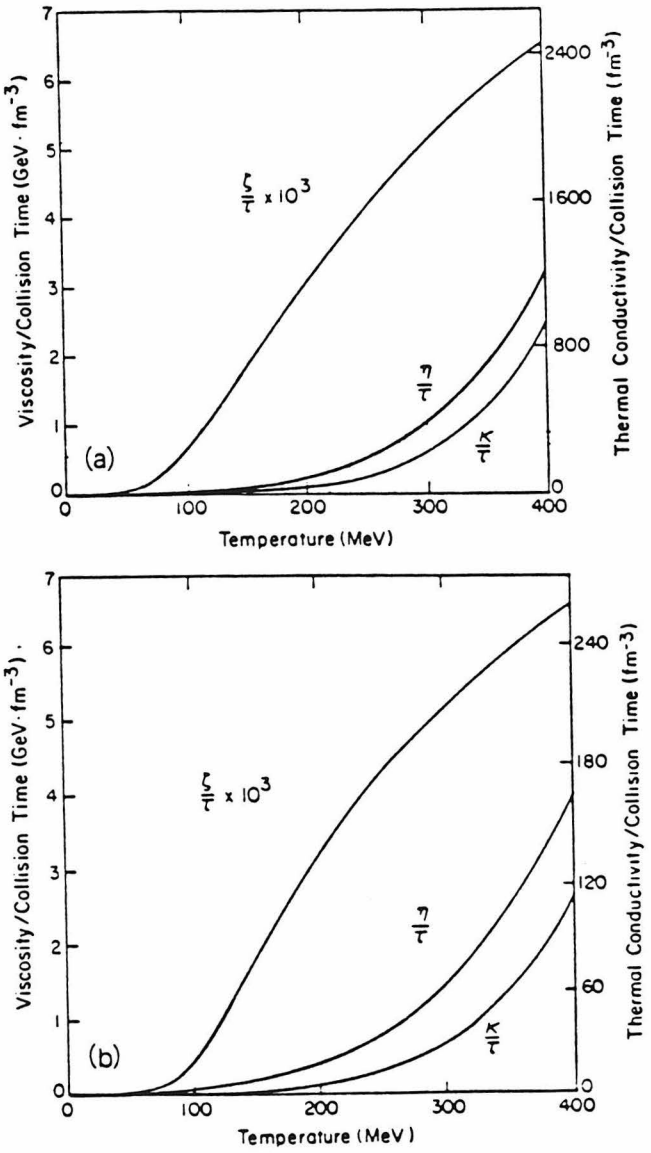

FIG. V.1 The coefficients of shear and bulk viscosity (η, ξ) and heat transport (κ) relative to the collision time for a massive quark-anti-quark fluid as a function of temperature (MeV). The baryon chemical potential, μ_B, is assumed to be a) 100 MeV, b) 300 MeV. Note that the values of ξ are shown multiplied by 10^3. The dependence on μ_B is weak for η and ξ in this temperature range. Results taking the contributions of the gluons into account change these curves by very little [GaS5].

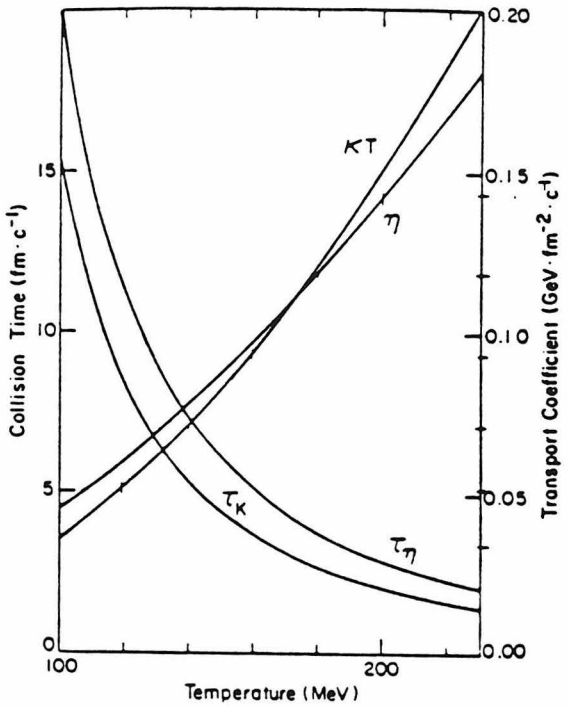

FIG. V.2 Relaxation times for the shear viscosity, τ_η, and heat conduction, τ_κ, as a function of temperature for a pion gas. The corresponding transport coefficients are also shown [Ga85].

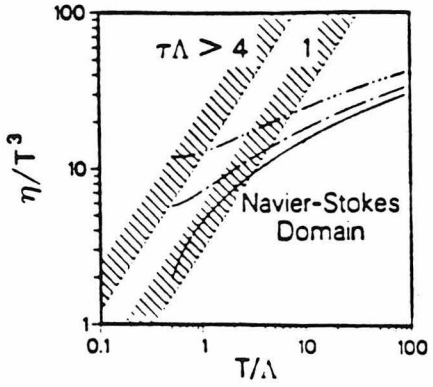

FIG. V.3 The coefficient of shear viscosity η divided by T^3 as a function of T/Λ, estimated with QCD phenomenology described in section V.6. The three curves correspond to different magnetic mass parameters. The shaded regions show the boundaries of Navier-Stokes domains. At high temperature, Navier-Stokes equation is valid. Non-perturbative effects become important at low temperatures [Da85].

CHAPTER VI

One-dimensional Hydrodynamics of URHIC

As we have argued in the introduction, an important ingredient in a theory of URHIC is the understanding of the dynamics of the process, and hydrodynamics serves as both a plausible and a convenient framework for such a description. We have shown in Chapter II Bjorken's pioneer work on one dimensional scaling hydrodynamics [Bj83], which gives a simple picture for the process. Since then, we have acquired some more knowledge of the initial conditions and the source terms (Ch. IV) as well as the transport coefficients. Despite the fact that most workers in the field have adopted the scaling hydrodynamics as the standard, we believe it is now time to build a more realistic hydrodynamic model [Ba84a,85,86, Bl87, Ch85,86, Cl85, Ga87, Gy86, Ka83].

A major modification to the scaling model we are interested in is the incorporation of source terms in the hydrodynamic equations. Following Kajantie [Ka83], we have discussed the importance of a consistent treatment of the source terms. Moreover, recent studies suggest that nuclei seem not to be as transparent as they were once thought [Bu84]. This may indicate deviations from the inside-outside cascade model [Ko74, Bj75], which was used by most of the earlier hydrodynamic calculations. We have therefore developed the source terms based on two "benchmark" models - the inside-outside cascade (IOC) and the multiple-collision model (MCM), and we shall investigate their effects on the hydrodynamics.

It is also important to investigate the sensitivity of the hydrodynamics to vis-

cosity, the equation of state, and the formation and thermalization time τ_o of the plasma, not only because these parameters are essential ingredients in a study of the properties of quark-gluon plasma, but also because the very existence of the plasma in heavy-ion collisions may depend on the actual values of these parameters.

In this chapter we present a one-dimensional, viscid, relativistic hydrodynamic model of high energy heavy-ion collisions. Our purpose is two-fold: we want to make what we believe to be necessary modifications to the earlier calculations, and to probe the importance of several other uncertain parameters.

VI.1 Methods of solution

We want to solve equations (III.17), which describe the hydrodynamics of a central collision along the z-axis in the center-of-mass frame with time t ($t = 0$ when the first collisions occur). We shall also restrict our calculations to collisions of identical nuclei, so that the system is symmetric with respect to the $z = 0$ plane. In a plasma with zero baryon chemical potential, the heat-transport term (see Eq. (III.13)), ν^μ, vanishes becauses it involves transport of heat with respect to the baryons [Ba83a, Ga85]. In the bulk of a quark-gluon plasma created in heavy-ion collisions at energies considered here, the baryon chemical potential and the net baryon density are both small; therefore it is safe to ignore ν^μ . After all, the heat transport term represents a small correction to the baryon-number current, which we shall treat approximately only (by considering equations of state not depending on the baryon chemical potential). We shall therefore set κ to zero in Eq. (III.17c). We derived (III.17) in the coordinate system $(\vec{e}_s, \vec{e}_y)$, where $\vec{e}_s$

and $\vec{e}_y$ are the unit vectors along the $s = \ln(\tau/\tau_o)$, $\tau \equiv \sqrt{t^2 - z^2}$ being the proper time, and $y \equiv \frac{1}{2}\ln((t+z)/(t-z))$ axes. Before we discretize (III.15), we shall first transform them to a new set of coordinates $\hat{\mathbf{u}}, \hat{\mathbf{v}}$ defined as:

$$\hat{\mathbf{u}} \equiv \frac{1}{a}(\alpha \mathbf{e_s} + \beta \mathbf{e_y}) \ ,$$

$$\hat{\mathbf{v}} \equiv \frac{1}{a}(\beta \mathbf{e_s} + \alpha \mathbf{e_y}) \ , \qquad \text{(VI.1)}$$

in terms of which the hydrodynamic equations are simplified. Here $\alpha \equiv \sinh(\theta - y)$, $\beta \equiv \cosh(\theta - y)$, $\theta = \cosh^{-1}\gamma$ being the local fluid rapidity, and $a \equiv \sqrt{\alpha^2 + \beta^2}$. The set of curves along $\hat{\mathbf{u}}$ and $\hat{\mathbf{v}}$ directions are similar to the characteristics of the flow, except that we use the fluid velocity as seen from a scaling frame, $\tanh(\theta - y)$, instead of the velocity of signal propagation [Co76, Ka83]. Note that if scaling holds, $\theta = y$, then the $\hat{\mathbf{u}}$ and $\hat{\mathbf{v}}$ axes coincide with the y, s axes. The directional derivatives along $\hat{\mathbf{u}}$ and $\hat{\mathbf{v}}$ are

$$\partial_u = \frac{1}{a}[\alpha\partial_s + \beta\partial_y] \equiv \frac{1}{a}\partial_1 \qquad \text{(VI.2a)}$$

and

$$\partial_v = \frac{1}{a}[\beta\partial_s + \alpha\partial_y] \equiv \frac{1}{a}\partial_2 \ . \qquad \text{(VI.2b)}$$

The hydrodynamic equations thus become

$$\partial_v \epsilon + (\epsilon + P)\partial_u \theta = \frac{1}{t_d}\chi(\partial_u\theta)^2 + t_d S_1 \ , \qquad \text{(VI.3a)}$$

$$\partial_u P + (\epsilon + P)\partial_v\theta = \frac{1}{t_d}\left\{\chi\left[\frac{2\alpha\beta}{a^2}\partial_u\theta + \partial_v\theta - \frac{\alpha}{a}\left(2\frac{\beta^2}{a^2} + 1\right)\right]\partial_u\theta + \chi{\partial_u}^2\theta + \partial_u\chi\right\} + t_d S_2 \ , \qquad \text{(VI.3b)}$$

with $S_1 = \Sigma^0 \cosh\theta - \Sigma^1 \sinh\theta$, $S_2 = \Sigma^1 \cosh\theta - \Sigma^0 \sinh\theta$, Σ^0 and Σ^1 being the source terms as described in detail in Chapter IV, and

$$\partial_v n_B + n_B \partial_u \theta = t_d \sigma_B \quad . \tag{VI.3c}$$

Here, $\chi \equiv \xi + \frac{4}{3}\eta$, and $t_d \equiv \tau/a$.

We also need an equation of state to supplement (VI.3). We shall only consider cases where $P = P(\epsilon)$, and investigate the sensitivity of the hydrodynamic evolution to the existence of a phase transition.

For the numerical calculations presented below, we assume central collisions of ^{238}U ions with $R = 7$ fm and $n_o = 0.166$ fm^{-3}. We will use the following parametrization of experimental nucleon-nucleon data [Th77, Al81, Ka83]:

$$\frac{dN_\pi^{nn}}{dy}(y, \sqrt{s_j}) = (0.83 \ \ln\sqrt{s_j} - 0.39)\left[1 - \frac{m_\pi}{\sqrt{s_j}}\cosh y\right]^3 \tag{VI.4a}$$

$$\frac{dN_B^{nn}}{dy}(y) = \frac{\cosh y}{\sinh y_o} \tag{VI.4b}$$

We will also take the transverse pion mass $m_\pi = 0.5$ GeV and nucleon mass $m_N = 1$ GeV.

The system of equations (VI.3a)-(VI.3c) with the source terms given by (IV.12) for IOC and (IV.15) for MCM using (VI.4a)-(VI.4b) can be solved by straightforward discretization of the $(\hat{\mathbf{u}}, \hat{\mathbf{v}})$ plane, which is related to the (y, s) plane through (VI.2). The initial conditions, ie. $n_B = 0$, $\epsilon = P = 0$, and $\theta = y$ are implemented on the $s = 0$ axis, which coincides with $\hat{\mathbf{v}} = \mathbf{0}$. The finite difference equation corresponding to (VI.3a) is then used to evolve ϵ in the $\hat{\mathbf{v}}$ direction, while that corresponding to (VI.3b) evolves θ. We use a simple forward scheme to calculate

finite differences in the $\hat{\mathbf{v}}$ direction while centering all finite differences in the $\hat{\mathbf{u}}$ direction. These difference equations are given in Appendix A. We first solve (VI.3a) and (VI.3b) for ϵ and θ, and then feed θ into (VI.3c) to obtain n_B at each iteration in $\hat{\mathbf{v}}$. Typical step size used is $\Delta u = 0.02$ and $\Delta v = 0.002$. At beam energy of 14 GeV/A, assuming $\tau_o = 1$ fm, pion plateau height of 2.4, and with the viscosity turned off, our results agree with those in [Ka83].

VI.2 Results and discussion

Samples of the results of our calculations are shown in Figs. VI.1 to VI.9 We now discuss the dependence of the hydrodynamic evolution on τ_o, the viscosity, the equation of state, beam energy, and the model of source terms:

i) dependence on τ_o

The initial time of the hydrodynamic phase, τ_o, is a poorly known parameter, because an estimate of it involves non-perturbative QCD. There are rough estimates and bounds on the values of τ_o, based on phenomenological and plausibility arguments. The common consensus seems to be that $\tau_o \approx 1$ fm (characteristic scale in QCD). We shall take values of τ_o ranging from 0.5 fm to 2 fm and consider the effects of changing τ_o. As shown in Figs. VI.1a, 2a and 3, the maximum energy density reached, ϵ_m is strongly affected by τ_o. Bjorken's estimation for the τ_o dependence of the initial energy density, $\epsilon_m \sim 1/\tau_o$ is slightly modified. As a result of the difference in energy density, the proper life-time of the plasma, τ_l, also changes as a function of τ_o, although not as fast as ϵ_m. Assuming IOC, if τ_o is as long as 2 fm, this study shows that even at 100 GeV/A, the energy density created in

heavy-ion collision won't be high enough to reach the pure quark-gluon phase ($\epsilon \geq$ 2 GeV/fm^3), while if τ_o is only 0.5 fm, 30 GeV/A is sufficient. Both ϵ_m and τ_l given here are lower than earlier estimates; this reflects the diluting effect of hydrodynamics when the source term is effective for finite duration. Figs. VI.1b, 2b and 4 also shows that the degradation of the rapidity of the outgoing fragments in IOC increases as τ_o decreases. This can be understood as the following: the baryons lose some of their momenta when thermalized with the slower moving plasma; if τ_o is smaller, the baryons materialize at smaller y in average, and thus they suffer more rapidity degradation. This additional rapidity loss of the fragmentation region in heavy-ion collisions when compared to that of nucleon-nucleon data, can be regard as a signature of collective effects. Unfortunately, this effect is swamped by the much larger rapidity downshifting inherent in MCM.

Another feature associated with a smaller τ_o is the increase in sharpness of the baryon peak. This is obviously a result of the smaller space-time region in which the baryons materialize if τ_o is small.

One last remark on τ_o: scaling is violated more severely for smaller τ_o. Scaling is exact in the limit of an infinitely long plasma tube. The smaller τ_o is, the shorter the plasma tube is, and hence the larger deviations from scaling. This, together with the opening up of low baryon number region, makes Bjorken's scaling picture a better approximation for large τ_o.

ii) dependence on viscosity

We have studied the coefficients of viscosity of the QGP with a collision time method in Chapter V. The uncertainty in the results are still very large because

of the assumption that the collision time is independent of temperature, T. Also, near the phase transition temperature, the coefficients of viscosity may be greatly suppressed due to large non-perturbative effects. We shall use the results from [Ga85] with a relaxation time of 1 fm, which gives values of $\eta \approx 1.1$ GeVfm^{-2} at $T = 300$ MeV, decreasing to $\eta \approx 0.2$ GeVfm^{-2} at $T = 200$ MeV. Assuming a characteristic length of 10 fm, the classical Reynold number of the system is typically about 40.

We have done calculations using coefficients from both [Ga85] and [Da85], and found no significant difference in the results. We have also tried two values of τ_r (0.5 fm, 1.0 fm), again we have found that the results are little affected. The coefficient of bulk viscosity, ξ, is very small in the plasma phase, but may become comparable to η in the mixed and the hadronic phase [Da85]. We show in Fig. VI.5 results of our calculations assuming $\xi = \eta$ for $\epsilon \leq 2$ GeV/fm^3. Comparing with Fig. VI.1, we find that the hydrodynamic behavior for $\xi = 0$ and for $\xi = \eta$ does not differ very much. The only effect of the viscosity we observe is a slight increase of τ_l ($\approx 10\%$ for the case shown in Figs. VI.1 and 5) and ϵ_m (just a few per cent) if larger coefficients of viscosity are used. This is simply explained in terms of a slower flow rate when the fluid is more viscous. The effects of the viscosity on the life-time of the plasma as measured in the center-of-mass frame will be even smaller due to the fact that slower plasma flow means less time dilation, which compensates the small gain in proper life-time. Overall, viscosity does not seem to be an important ingredient of the (one-dimensional) hydrodynamics of high-energy heavy-ion collisions.

iii) equation of state

Lattice gauge calculations [En82, Mo82] show that a pure gluon plasma behaves like an ideal Stefan-Boltzmann gas for temperatures not too close to the critical point of the deconfinement transition. We therefore use two extreme equations of state in this calculation: that of an ideal relativistic gas 1) with no phase transition, $P = \epsilon/3$, and 2) with a first order phase transition motivated by the bag model [Ch74, De75]:

$$P = \begin{cases} \epsilon/3, & 0 \leq \epsilon \leq \epsilon_H \ ; \\ \epsilon_H/3, & \epsilon_H \leq \epsilon \leq \epsilon_Q; \\ (\epsilon - \epsilon_Q + \epsilon_H)/3, & \epsilon \geq \epsilon_Q. \end{cases} \tag{VI.5}$$

Here, ϵ_H and ϵ_Q are the lower and upper boundaries of the mixed phase, chosen to be 0.8 GeVfm^{-3} and 2 GeVfm^{-3}, respectively, for the results presented here. Changing the numerical values of ϵ_H and ϵ_Q, or using a pion gas equation of state with finite pion mass for the hadronic phase does not change the results significantly.

A comparison of the results for the two equations of state used shows that while the lifetime of the plasma is longer for a bag model equation of state (by about 15% for the case shown in Figs. VI.1 and 6), most other features of the hydrodynamic flow are insensitive to the equation of state (cf. Figs. VI.1,6). This is in accord with the findings of Wehrberger and Weiner [We85] for Landau hydrodynamics. The small difference in the plasma lifetime can be explained by the fact that at the mixed phase region the speed of sound becomes zero, and therefore the expansion is slower than if there were no phase transitions. We should remark that we have treated the first order phase transition within the framework of mean-field theory (and for numerical reason, we have also introduced a small smearing of the equation of state so that the slope is not discontinuous at ϵ_H and ϵ_Q). It is quite possible that we miss some drastic phenomena [Gy84a] due to the phase transition.

iv) dependence on beam energies

Since the pion plateau height in nucleon-nucleon collisions increases as $\ln E$ for increasing collision energy E up to 100 GeV/A [Th77, Al81], we expect that the maximum energy density achieved in heavy-ion collisions also goes as $\epsilon_m = c \ln E + d$, c and d being constants. In Fig. VI.7a we show this fit to our results for energies up to 100 GeV/A. In both models of the source, the lifetime of the plasma, however, does not increase significantly as we raise E from 30 GeV/A to 100 GeV/A (see Fig. VI.7b). While collisions with higher energies create plasma with higher energy density, the speed of the hydrodynamic flow is also higher. The duration it takes the plasma to cool down to the critical temperature is thus quite insensitive to the collision energy (cf. Figs. VI.1,8). Another feature associated with increasing E is the opening-up of the low baryon number region in the IOC. The MCM on the other hand does not give such a gap in the range of energies considered here.

v) source terms

The two models of source terms we use here are very different, and indeed they lead to drastically different results (cf. Figs. VI.1,9). As expected, the baryons in the MCM dissipate more energies and momenta than in IOC. Therefore, in the MCM the maximum energy density is higher, while the baryon rapidity is lower than in IOC. Consequently, the plasma lifetime in MCM is longer than that in IOC. Another obvious signature of the MCM as compared to the IOC is the large rapidity smearing of the baryon peaks. In fact, for the MCM, our calculations show that the net baryon number is distributed almost uniformly in the final states.

VI.3 Summary

From the calculations presented above, we can draw the following conclusions:

1. Viscosity is not essential for a qualitative understanding of the hydrodynamics of ultra-relativistic heavy-ion collision.
2. Neither is the equation of state.
3. The hadronization time, τ_o, is an important parameter. Before pinning down this parameter more accurately, we cannot even say at what beam energies quark-gluon plasma should be produced. In the IOC, the rapidity loss of the baryon peaks may provide a clue to the magnitude of τ_o (smaller rapidity loss for larger τ_o).
4. The maximum energy density created in an ultra-relativistic heavy-ion collision increases only as the logarithm of the beam energy.
5. Results for the MCM and the IOC differ so much that one cannot with confidence say that either approximates reality well. But we do expect that reality lies somewhere between these two models.

It is clear, then, that a better understanding of τ_o and the source terms is urgently needed for further theoretical investigation of the physics of ultra-relativistic heavy-ion collisions.

Figure Captions

FIG. VI.1 Contour plots for a) energy density in GeV/fm^3, and b) net baryon number density in fm^{-3} for a central collision of ^{238}U ions at 50 GeV/A each. An inside-outside cascade is assumed, with τ_o=1 fm. The coefficient of shear viscosity, η, is taken from [Ga85], assuming a relaxation time of 1 fm, and the coefficient of bulk viscosity, ξ, is ignored here. The bag model equation of state is used (Eq. VI.5 in text). Contours are drawn in steps of a)0.4 GeV/fm^3, from 0.4 GeV/fm^3 to 2.8 GeV/fm^3, and b)0.05 fm^{-3}, from 0.05 fm^{-3} to 0.35 fm^{-3}.

FIG. VI.2 Same as FIG. VI.1 except that τ_o= 0.5 fm. Contours are drawn in steps of a) 0.8 GeV/fm^3, from 0.8 GeV/fm^3 to 4.4 GeV/fm^3, and b) 0.05 fm^{-3}, from 0.05 fm^{-3} to 0.55 fm^{-3}.

FIG. VI.3 τ_o dependence of a) maximum energy density, ϵ_m, and b) plasma life time, τ_l. Collisions of 30 and 100 GeV/A (pluses with holes and crosses respectively) are shown for the inside-outside cascade model (IOC), and 50 GeV/A for both IOC (squares) and the multiple collision model (MCM, circles). In a) the dashed lines correspond to the boundaries of the mixed phase for the bag model equation of state used. In b), the plasma life time is defined as the proper time duration for which the energy density at z=0 is higher than 0.8 GeV/fm^3. The solid lines are drawn to guide the eyes.

FIG. VI.4 τ_o dependence of the baryon peak rapidity in IOC, shown for E=30 (pluses), 50 (squares), 70 (diamonds), and 100 (crosses) GeV/A. The solid lines are drawn to guide the eyes.

FIG. VI.5 Same as FIG. VI.1 except that ξ is equal to η when the energy density

falls to below 2 GeV/fm^3. Contours are drawn in steps of a) 0.4 GeV/fm^3, from 0.4 GeV/fm^3 to 2.8 GeV/fm^3, and b) 0.05 fm^{-3}, from 0.05 fm^{-3} to 0.3 fm^{-3}.

FIG. VI.6 Same as FIG. VI.1 except that the ideal gas equation of state with no phase transition, $P = \epsilon/3$ is used. Contours are drawn in steps of a) 0.4 GeV/fm^3, from 0.4 GeV/fm^3 to 2.4 GeV/fm^3, and b) 0.05 fm^{-3}, from 0.05 fm^{-3} to 0.35 fm^{-3}.

FIG. VI.7 Beam energy (in center-of-mass frame) dependence of a) maximum energy density, and b) plasma life time. τ_o = 0.5 and 2 fm are shown for IOC (crosses and squares), and τ_o = 1 fm is shown for both IOC (circles) and MCM (pluses). In a) the dashed lines correspond to the boundaries of the mixed phase for the bag model equation of state used. The solid lines are fits to $\epsilon_m = c\ \ln E + d$, c and d being constants. In b) the solid lines are drawn to guide the eyes.

FIG. VI.8 Same as FIG. VI.1 except that the collision energy is 100 GeV/A for each ion. Contours are drawn in steps of a) 0.4 GeV/fm^3, from 0.4 GeV/fm^3 to 3.6 GeV/fm^3, and b) 0.05 fm^{-3}, from 0.05 fm^{-3} to 0.3 fm^{-3}.

FIG. VI.9 Same as FIG. VI.1 except that the MCM is assumed. Contours are drawn in steps of a) 0.8 GeV/fm^3, from 0.8 GeV/fm^3 to 4.4 GeV/fm^3, and b) 0.05 fm^{-3}, from 0.05 fm^{-3} to 0.2 fm^{-3}.

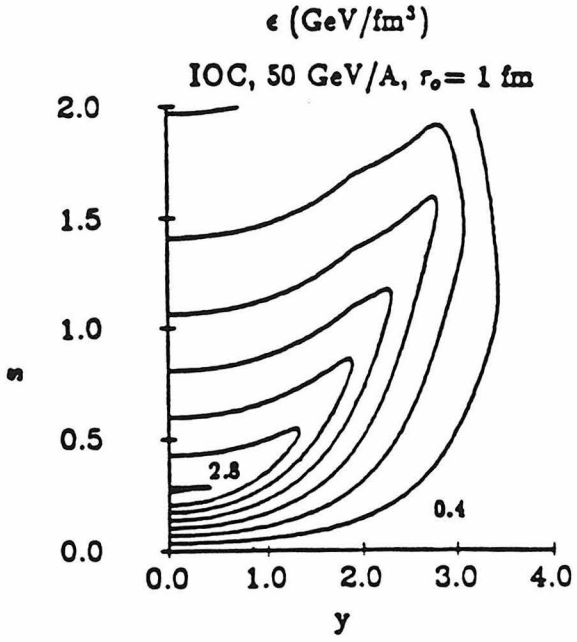

FIG. VI.1a

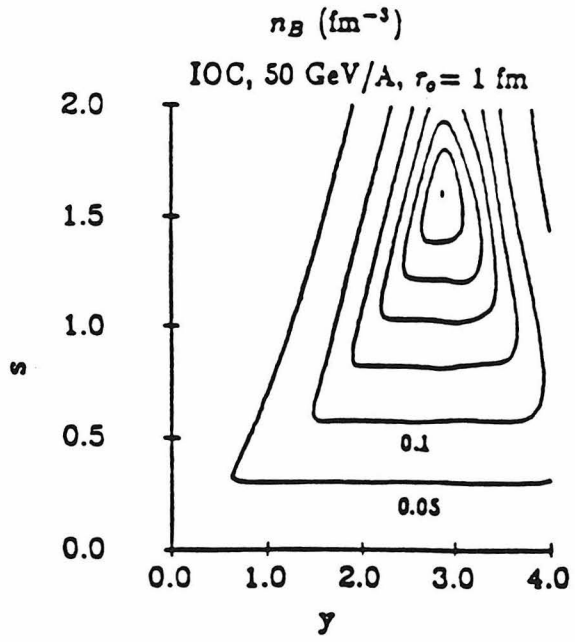

FIG. VI.1b

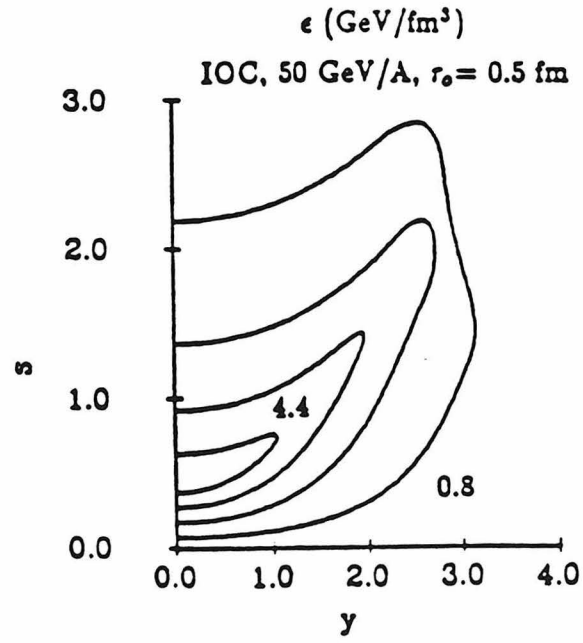

FIG. VI.2a

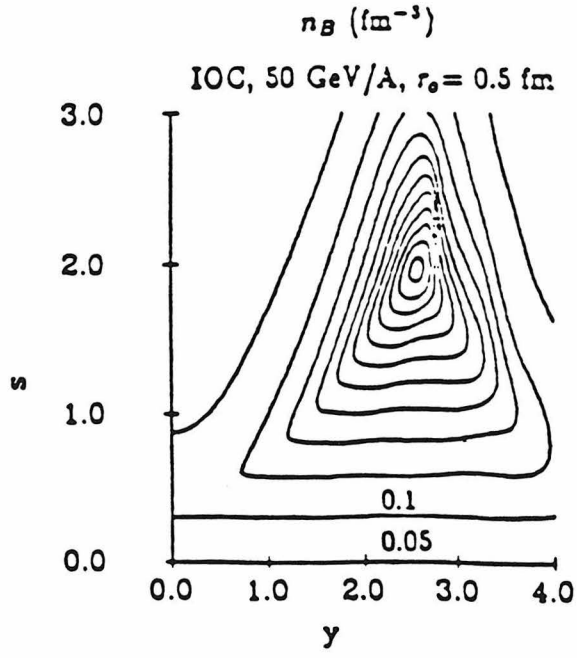

FIG. VI.2b

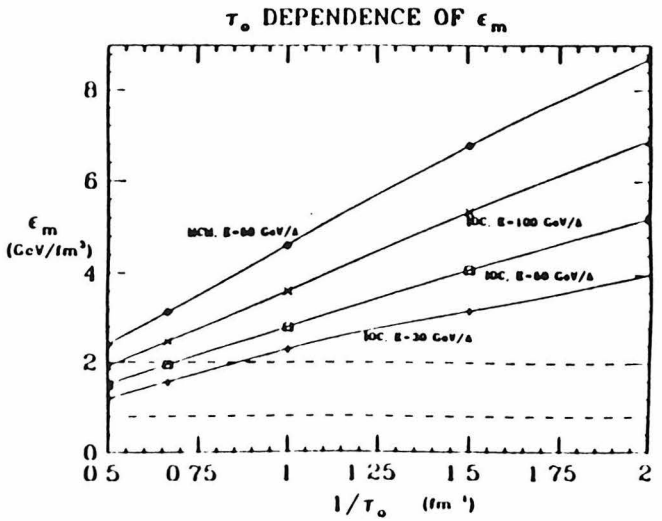

FIG. VI.3a

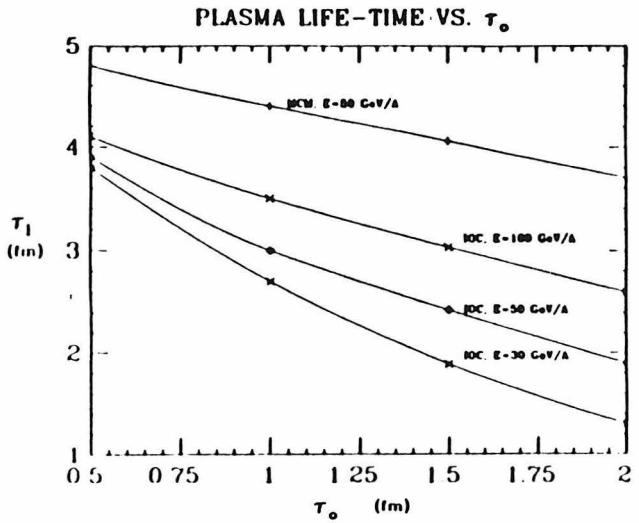

FIG. VI.3b

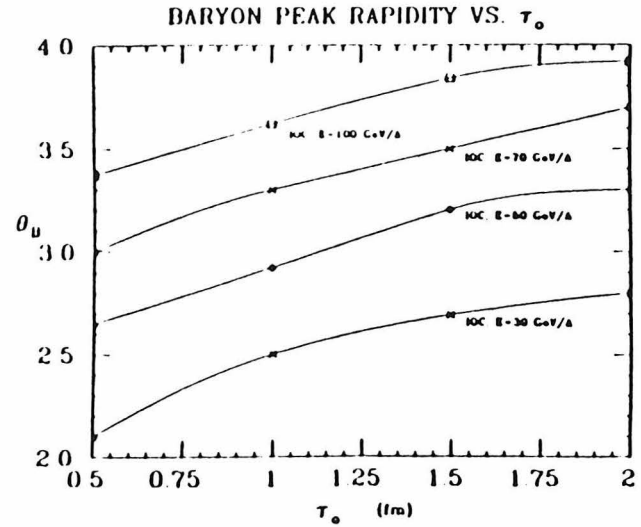

FIG. VI.4

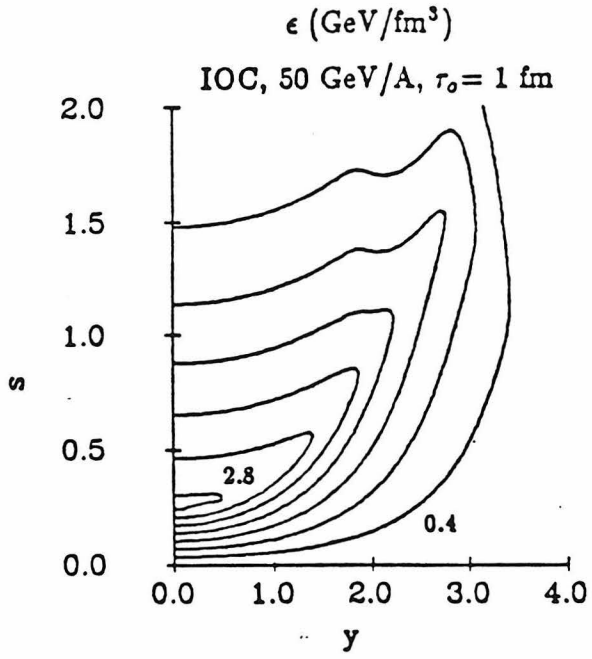

FIG. VI.5a

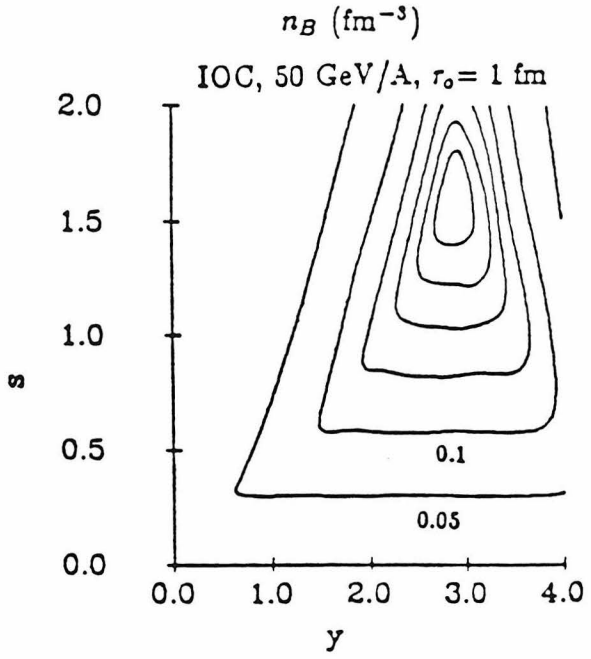

FIG. VI.5b

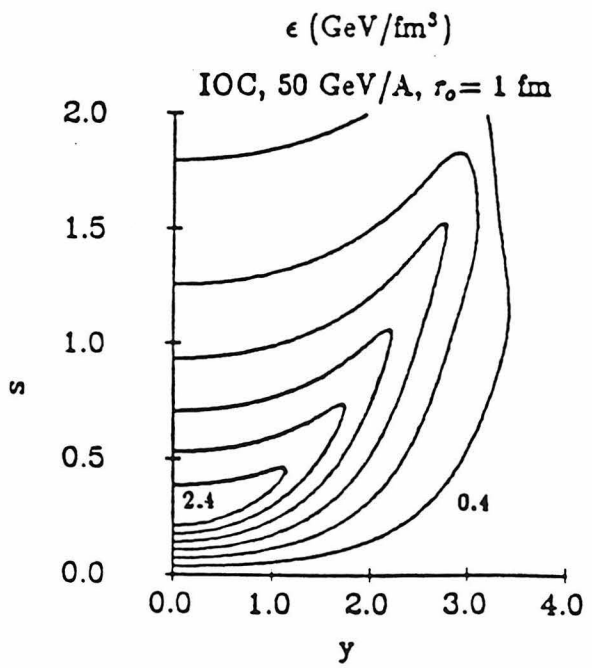

FIG. VI.6a

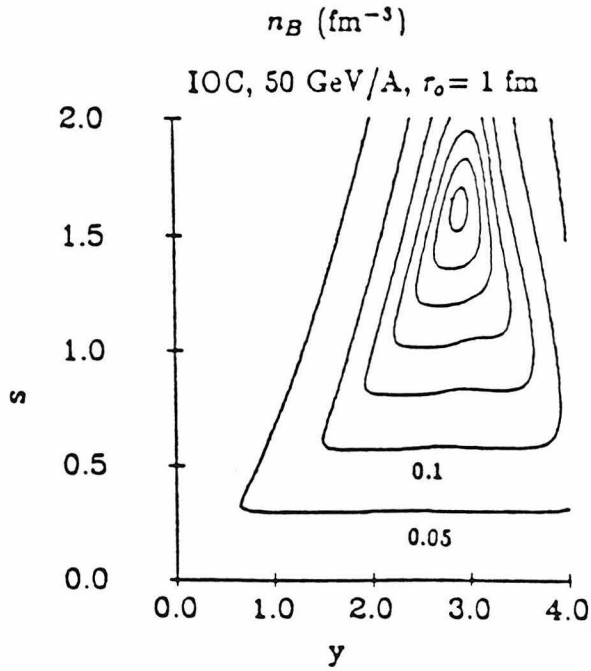

FIG. VI.6b

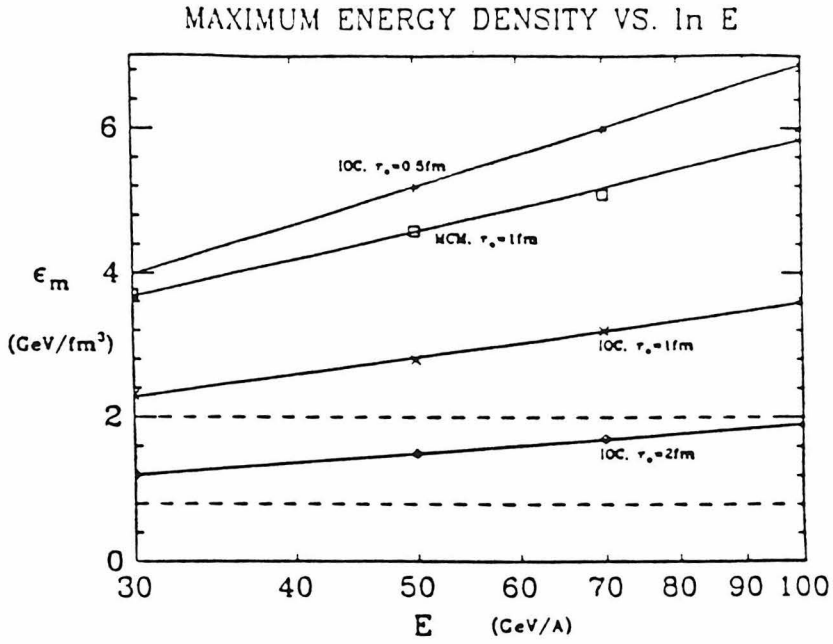

FIG. VI.7a

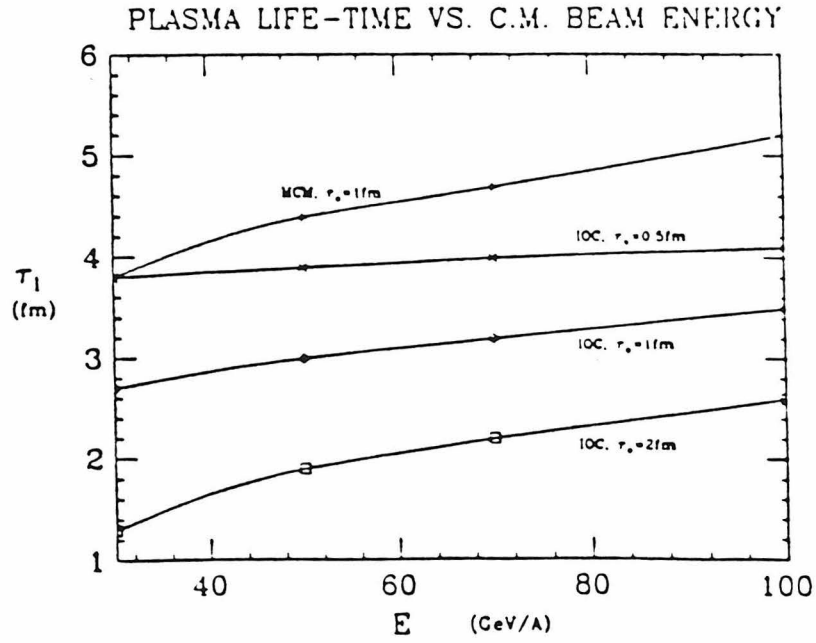

FIG. VI.7b

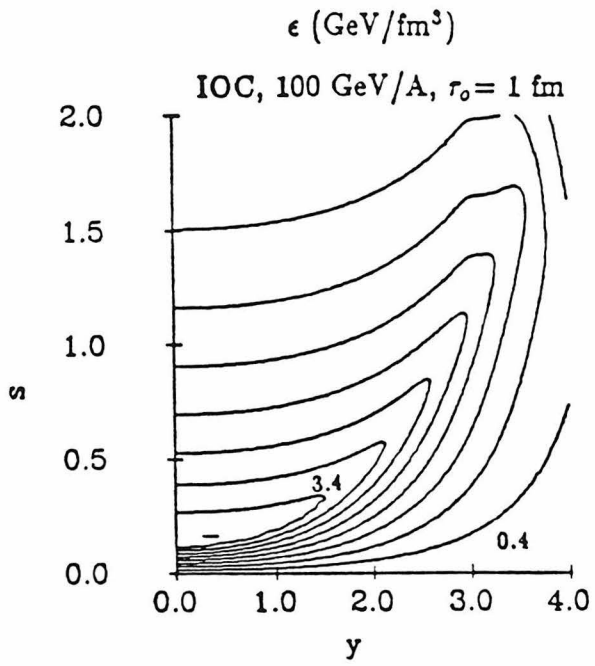

FIG. VI.8a

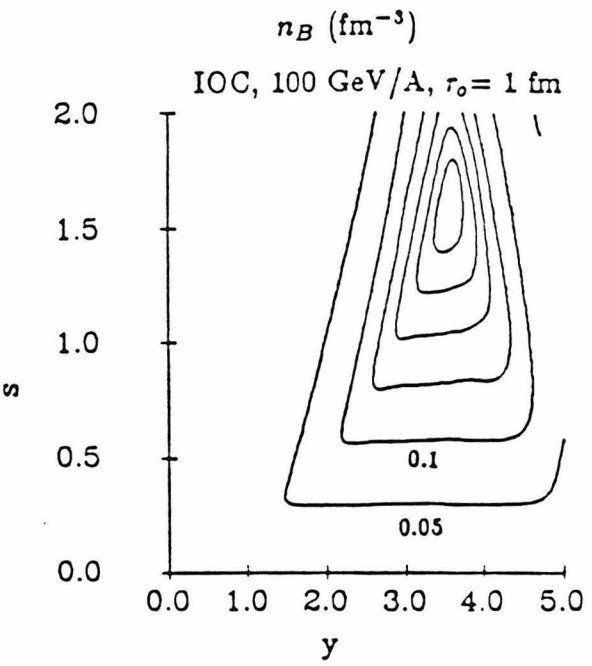

FIG. VI.8b

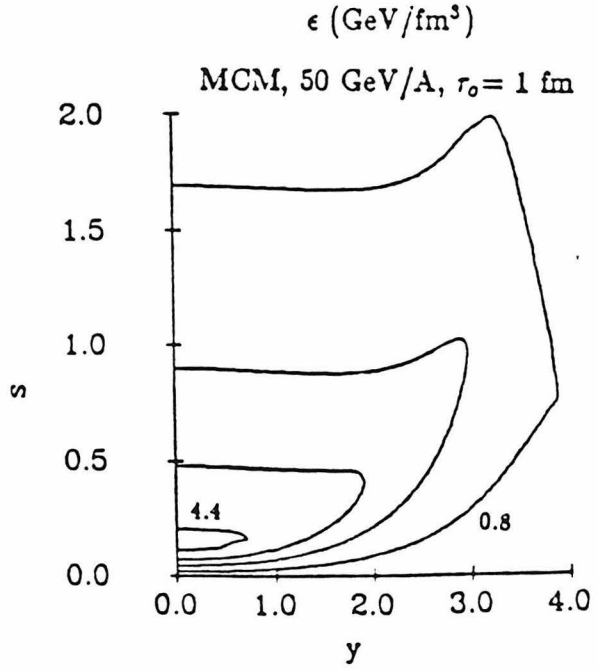

FIG. VI.9a

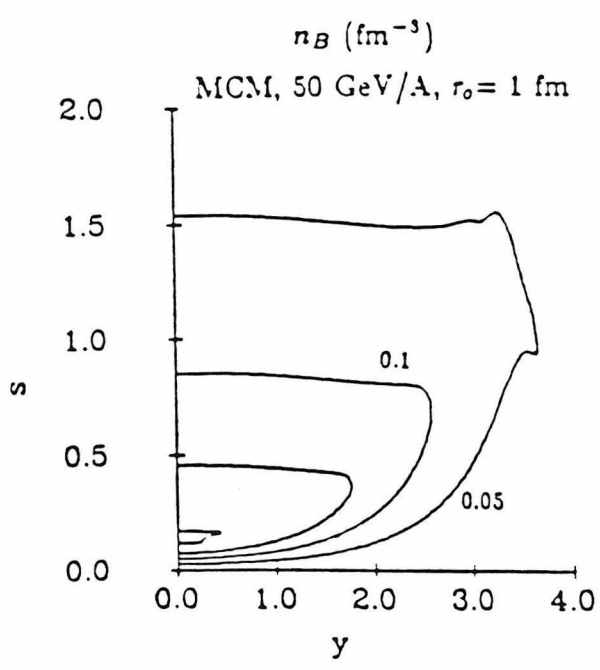

FIG. VI.9b

CHAPTER VII

Hydrodynamics of URHIC in Cylindrical Geometry

We have learned a lot of the essential dynamical features of URHIC from one-dimensional hydrodynamics. However, one possibly important piece of physics is missing- that of the transverse degree of freedom. The correct geometry of a central collision of identical heavy-ions is that of a cylinder, and while the longitudinal expansion is probably much more rapid compared to the transverse one at the longitudinal "ends" of the plasma, the two might be comparable in the center of the tube. One way to estimate the importance of the transverse expansion is to consider the time scale associated with it. The information that the plasma has a finite extent in the transverse direction is propagated from the transverse "edge" to the center of the plasma at the speed of sound, $v_s = (dP/d\epsilon)^{1/2}$, which is about 60% of the speed of light for an ideal relativistic gas ($P = \epsilon/3$). Therefore the characteristic time associated with the transverse expansion is $\tau_{\rm tr} \approx R/v_s$, with $R \approx 1.2A^{1/3}$ fm being the radius of the collision region. For ^{238}U, $\tau_{\rm tr}$ is about 10 fm/c, which is long compared to the time scale in the longitudinal expansion as indicated in Chapter VI. But if we consider collisions of ^{16}O, say, $\tau_{\rm tr}$ is only about 5 fm/c, and transverse expansion may be important.

Another motivation to study the transverse degree of freedom in URHIC comes from high energy cosmic ray data [Bu85]. There have been events observed with anomalously high transverse momentum. These events prompted speculations that a first order QCD phase transition may be reflected in the transverse momentum

spectrum [Sh79, Va82, Vo86,87]. We shall examine this possible signature of the QGP in more details in Chapter VIII.

In the scaling picture, the longitudinal expansion is slowest near the center of the plasma tube ($v_z = z/t$) [Bj83]. Therefore, we could expect the effects of the transverse expansion to be most important near $z = 0$. We shall therefore study first the cylindrical hydrodynamics for the central rapidity region. More specifically, we consider the expansion of a plasma tube with a finite length but ignoring the source terms. As mentioned in Chapter II, the standard scaling model is an approximation that becomes exact in the limit of an infinitely long plasma tube. Our model here therefore could be thought of as being another extreme in approximating the source terms.

We shall then in section VII.2 incorporate the source terms in cylindrical geometry in the hydrodynamic equations. Now we proceed in a spirit very similar to that in Chapter VI, the major difference being the neglect of viscosities in two dimensions. Although the effects of viscosities in one dimension were shown to be small, we have to caution that this does not by itself justify ignoring transport phenomena in two-dimenional hydrodynamics.

VII.1 Sourceless Case

We shall in this section study the solutions of Eqs. III.9, with the source terms set to zero:

$$\frac{\partial}{\partial t}\left[w\gamma^2 - P\right] + \frac{1}{r}\frac{\partial}{\partial r}\left[rw\gamma^2 v_r\right] + \frac{\partial}{\partial z}\left[w\gamma^2 v_z\right] = 0 \ , \qquad \text{(III.9a)}$$

$$\frac{\partial}{\partial t}\left[w\gamma^2 v_z\right] + \frac{1}{r}\frac{\partial}{\partial r}\left[rw\gamma^2 v_r v_z\right] + \frac{\partial}{\partial z}\left[w\gamma^2 v_z^2 + P\right] = 0 \ , \qquad \text{(III.9b)}$$

$$\frac{\partial}{\partial t}\left[w\gamma^2 v_r\right] \; + \; \frac{1}{r}\frac{\partial}{\partial r}\left\{r[w\gamma^2 v_r^2 + P]\right\} \; + \; \frac{\partial}{\partial z}\left[w\gamma^2 v_r v_z\right] \; = \; 0 \quad . \qquad \text{(III.9c)}$$

The initial energy density is not distributed uniformly in the plasma. At the time when the entire plasma is thermalized, $t_o = \left(\tau_o^2 + Z_m^2\right)^{1/2}$, where Z_m is the length of the cylindrical plasma, the energy density is lower near $z = 0$ because particles in that region thermalize the earliest and have undergone some cooling. This initial cooling takes the form [Bj83]

$$\epsilon(\tau) = \epsilon_o(\tau_o/\tau)^{4/3} \quad ,$$

assuming longitudinal scaling initial expansion of the plasma. However, we also know that the plasma region is finite in extent, and thus there must be a fall off of energy density at large z. We shall take the scaling form of the energy density,

$$\epsilon(z,t,r) = \epsilon(0,\tau,r) \quad ,$$

where r is the transverse coordinate, modified by a Woods-Saxon cutoff near $z = Z_m$. There must also be variations in the energy density in the transverse direction depending on the radii of the colliding ions. The energy density profile in the transverse direction is given in [Wo84], and for the central collision of two ^{238}U nuclei at 30 GeV center-of-mass energy per nucleon, a Gaussian of width $R_m = 7$ fm reproduces the profile reasonably accurately for $r \leq R_m$. We cut off the Gaussian tail by multiplying it with a Woods-Saxon function to approximate the energy density profile for $r \geq R_m$.

We shall use the equation of state for a relativistic ideal gas, $P = \epsilon/3$, which is shown by lattice Monte Carlo calculations to be a good approximation for a

pure gluon gas at temperatures above the critical temperature of the hadronization transition [En82, Mo82]. The Stefan-Boltzmann law relates ϵ to temperature, T,

$$\frac{\epsilon}{\epsilon_o} = \left[\frac{T}{T_o}\right]^4 \quad ,$$

where T_o is the initial temperature.

i) Methods of solution

We have considered two methods to solve Eqs. III.9. The first utilizes a finite element discretization in the $z - r$ plane, and propagates in time with a fourth-order predictor-corrector method. In the second method, we rewrite Eq. III.9, together with the equation of state, in a form resembling a Schrödinger equation, which is then solved with the Peaceman-Rachford method [Va62]. Both methods are stable to a time much later than when the temperature drops to below that for hadronization. All the calculations shown here are done with the first method because of its greater efficiency.

In the first method, the fields of interest (ϵ, v_z, v_r) are expanded in a set of finite element basis functions (or "tent" functions, see Fig. VII.1 for notation):

$$f(r,z,t) = \sum_{i,j} C_i(r) C_j(z) F_{ij}(t) \quad ,$$

with

$$\begin{aligned} C_i(r) &= \frac{1}{h_i}(r - r_{i-1}) \ \text{ if } r_{i-1} \le r \le r_i \quad , \\ &= \frac{1}{h_{i+1}}(r_{i+1} - r) \ \text{ if } r_i \le r \le r_{i+1} \quad , \\ &= 0 \ \text{ otherwise} \quad , \end{aligned}$$

and

$$C_j(z) = \frac{1}{k_j}(z - z_{j-1}) \text{ if } z_{j-1} \leq z \leq z_j \ ,$$
$$= \frac{1}{k_{j+1}}(z_{j+1} - z) \text{ if } z_j \leq z \leq z_{j+1} \ ,$$
$$= 0 \text{ otherwise .}$$

Here h_i and k_j are the grid sizes in the r and z directions, respectively,

$$h_i = r_i - r_{i-1} \ ; \quad k_j = z_j - z_{j-1} \ .$$

The expansion coefficients, $F_{ij}(t)$, coincide exactly with the function values at the grid points:

$$F_{ij}(t) = f(r_i, z_j, t) \ ,$$

so that the $\{F_{ij}\}$ form a discrete approximation to f.

Equation III.9 is then reduced to a set of ordinary differential equations in t relating the expansion coefficients of the various fields in the original partial differential equations. In this particular case, the ordinary differential equations have the form:

$$\frac{d}{dt}F(t) = BG(t) + H(t)C \ ,$$

where F, G and H are matrices of expansion coefficients, and B and C are constant matrices. We solve this equation with a standard fourth-order Adams integration [Ab65].

In the second method, we rewrite Eqs. III.9 as:

$$\frac{\partial}{\partial t}\rho = -\left[\frac{\partial}{\partial z}(\alpha v_z \rho) + \frac{\partial}{\partial r}(\alpha v_r \rho)\right] \ , \qquad \text{(VII.1a)}$$

$$\frac{\partial}{\partial t}M_z = -\left[\frac{\partial}{\partial z}(v_z M_z) + \frac{\partial}{\partial r}(v_r M_z) + S_z\right] \ , \qquad \text{(VII.1b)}$$

$$\frac{\partial}{\partial t}M_r = -\left[\frac{\partial}{\partial z}(v_z M_r) + \frac{\partial}{\partial r}(v_r M_r) + S_r\right] \quad , \qquad \text{(VII.1c)}$$

where

$$\rho = r\epsilon(\gamma^2 - 1/4),\ M_z = r\epsilon\gamma^2 v_z,\ M_r = r\epsilon\gamma^2 v_r \ ,$$

$$S_z = \frac{\partial}{\partial z}\left[\frac{\rho}{4\gamma^2 - 1}\right],\ S_r = \frac{\partial}{\partial r}\left[\frac{\rho}{4\gamma^2 - 1}\right] \quad ,$$

and

$$\alpha = \frac{\gamma^2}{\gamma^2 - 1/4} \quad .$$

Equation VII.1 now has the form of a Schrödinger equation in imaginary time

$$\frac{\partial}{\partial t}\phi = -H_o\phi + S \quad ,$$

with $\phi = \rho$, M_z, or M_r, and H_o is Hermitian. The Peaceman-Rachford method is very convenient to use in this case since H_o split up naturally into a "horizontal" piece, H, and a "vertical" piece, V, which act only along the z and the r directions, respectively. Also, both H and V are tridiagonal, allowing for efficient inversions. The time evolution operator can be approximated by

$$U = \left[\frac{1}{1 + \frac{\Delta t}{2}V}\right]\left[\frac{1 - \frac{\Delta t}{2}H}{1 + \frac{\Delta t}{2}H}\right]\left[1 - \frac{\Delta t}{2}V\right] \quad .$$

To propagate ρ from time t to $t + \Delta t$, we first evaluate $\bar{\phi} = U(t)\phi(t)$ at $t + \Delta t/2$, then calculate $U[t+(\Delta t/2)]$ with $\bar{\phi}$, and finally evaluate $\phi(t+\Delta t)$ with $U[t+(\Delta t/2)]$ acting on $\phi(t)$.

ii) Results

We consider the central collision of two ^{238}U nuclei at a center-of-mass energy of about 30 GeV per nucleon. At this energy, we take $\epsilon_o \approx (9/\tau_o)$ GeV/fm^3. The parameter τ_o remains highly uncertain; we present calculations for $\tau_o = 1$ and 2 fm/c for comparison.

The initial conditions imposed at t_o are summarized here:

$$\begin{aligned}\epsilon(z,t_o,r) =& \epsilon_o e^{-(r/R_m)^2}\left[\frac{\tau_o}{(t_o^2-z^2)^{1/2}}\right]^{4/3} \\ & \times\left(1+e^{(|z|-Z_m)/\delta_z}\right)^{-1} \\ & \times\left(1+e^{(r-R_m)/\delta_r}\right)^{-1} \quad ,\end{aligned}$$

$$v_r = 0 \quad ,$$

$$v_z = \frac{z}{t_o} \quad \text{if } r \le R_m,\ |z| \le Z_m \ ,$$

where δ_z and δ_r are some small artificial widths (0.15 and 0.2 fm, respectively) introduced to smooth out the initial boundaries. A time step of 0.05 fm/c is used although that of 0.1 fm/c gives essentially the same results. Typical grid sizes are 0.15 and 0.2 fm in the z and r directions, respectively. The total energy of the system is calculated at regular intervals, and the calculation is stopped if overall conservation is violated by more than 0.5% , which indicates that the plasma has expanded out to the boundaries of the gridded area (50×100 grid points). A calculation with 80 time iterations takes about three hours on a VAX 750, but only a few minutes with the Oak Ridge array processor (FPS 164).

Two sets of contour plots of the temperature distribution in the $z-r$ plane at consecutive time frames are shown in Fig. VII.2. for $\tau_o = 1$ and 2 fm/c. If we take

2 GeV/fm^3 as the critical energy density at which hadronization starts, then we see that in both cases, hadronization commences at just ≈ 1.5 fm/c after the onset of the hydrodynamic expansion. There is probably some degree of supercooling, and it also takes some finite time (of the order of τ_o) for hadronization to complete. But even taking all these into consideration, it is very unlikely that the plasma lives longer than a few fm/c.

At the $z = 0$ plane, our results agree with that of Baym *et al.* [Ba83]. However, the behavior of the system at $z \neq 0$ is very different in the present calculation because of the difference in the initial conditions assumed. Instead of the scaling behavior assumed in [Ba83], which leads to higher temperatures at larger z, we see that the expansion tends to wash out the initial nonuniformity in the temperature distribution. In fact, the temperature distribution becomes fairly uniform in the z direction within the plasma region in just 1-2 fm/c. We can understand this qualitative difference of the results obtained in this calculation and that in [Ba83] by the following reasonings. The longitudinal pressure gradient, and hence the rate of matter being pushed towards larger z, is much larger near a free end than a scaling end. It is therefore a lot harder to pile up matter near a free end, and we see a much more uniform cooling in the plasma than could be expected with a scaling initial condition.

Comparing Fig. VII.2a with Fig. VII.2b, we find that the rate of cooling is slower for larger τ_o. But since the initial energy density is higher for smaller τ_o, the time to reach hadronization is not very sensitive to this parameter.

The angular distribution of the energy density assuming $\tau_o = 1$ fm/c is shown

in Fig. VII.3. Here, θ is the angle between the velocity vector and the z axis:

$$\theta = \tan^{-1}\left[\frac{v_r}{v_z}\right] \quad .$$

The distribution is sharply peaked at $\theta = 0$, which reflects the one-dimensional character of the expansion. The dominance of the longitudinal expansion can be seen clearly in Figs. VII.4a and 4b, where the longitudinal rapidity ($y = \tanh^{-1} v_z$) and transverse velocity (v_r) distributions of energy are shown, respectively.

iii) Summary and discussions

We have studied the hydrodynamic evolution of a cylindrically symmetric quark-gluon plasma formed in ultrarelativistic heavy-ion collisions numerically. We found that for the central collisions of two ^{238}U nuclei at a c.m. energy of about 30 GeV per nucleon, the plasma cools to the hadronization temperature within 1.5 fm/c after the expansion starts. As a result, the transverse degrees of freedom do not affect the expansion significantly prior to hadronization. Because of the finite length of the plasma cylinder, the temperature distribution becomes fairly uniform towards the beginning of hadronization. The rate of cooling is slower for larger thermalization time, but the time to reach hadronization is little affected.

We have made the implicit assumption that the plasma decoupled from the nuclear "pancakes" after the collision. While Fig. IV.4a shows that while this assumption remains consistent with the conditions of the bulk of the plasma (rapidity less than that of the outgoing nuclei), it may not be valid near the boundaries between the fragmentation regions and the CRR. A source term will have to be added to the hydrodynamic equations if the coupling between the plasma and the

outgoing heavy ions is considered, and that is exactly what we are going to do in the next section.

VII.2 Cylindrical Hydrodynamics with Source Terms

The major defect of our "toy" model in last section is the ignorance of the source terms. We now study Eq. III.16 in cylindrical coordinates:

$$\partial_t \left[r \left(w\gamma^2 - P - S^{tt} \right) \right] + \partial_z \left[r \left(w\gamma^2 v_z - S^{zt} \right) \right] + \partial_r \left[r \left(w\gamma^2 v_r - S^{rt} \right) \right] = 0 \quad , \tag{VII.2a}$$

$$\partial_t \left[r \left(w\gamma^2 v_z - S^{tz} \right) \right] + \partial_z \left[r \left(w\gamma^2 v_z^2 + P - S^{zz} \right) \right] + \partial_r \left[r \left(w\gamma^2 v_r v_z - S^{rz} \right) \right] = 0 \quad , \tag{VII.2b}$$

$$\partial_t \left[r \left(w\gamma^2 v_r - S^{tr} \right) \right] + \partial_z \left[r \left(w\gamma^2 v_r v_z - S^{zr} \right) \right] + \partial_r \left[r \left(w\gamma^2 v_r^2 + P - S^{rr} \right) \right] = 0 \quad , \tag{VII.2c}$$

$$\partial_\mu \left(J_B^\mu - \sigma_B^\mu \right) = 0 \quad , \tag{VII.2d}$$

with the inside-outside cascade model source terms (IV.17) as discussed in Chapter IV.

i) Method of solution

Eqs. VII.2 can be written in the conservation-law form

$$\partial_t U + \partial_z F(U) + \partial_r G(U) = 0 \quad ,$$

where U, F and G can be thought of as column vectors containing the quantities in square brackets in Eq. (VII.2). For example,

$$U_1 = \left[r \left(w\gamma^2 - P - S^{tt} \right) \right] \quad ,$$

etc. We shall use the two-step Lax-Wendroff method to solve this system [La60, Ri67]. Essentially we first propagate the fields at time step n to time step $n+\frac{1}{2}$ using centered-spatial and forward-time differencing. Then U at time step $n+1$ is obtained from U at time step n through difference operators at time step $n+\frac{1}{2}$. This method, even though stable for linear problems if [Ri67]

$$(|\vec{v}|+v_s)\frac{\Delta t}{\Delta x} < \frac{1}{\sqrt{2}} \quad ,$$

gives rise to instabilities in the present (highly non-linear) system. We cure this by using artificial viscosity; the detailed scheme is presented in Appendix B.

When the equation of state is not in simple closed form, such as $P=\epsilon/3$, we have to employ an iterative scheme to obtain $F(U)$ and $G(U)$ from U. We first calculate

$$a_1 \equiv U_1 + rS^{tt} = r\left(w\gamma^2 - P\right) \quad ,$$

$$a_2 \equiv U_2 + rS^{tz} = rw\gamma^2 v_z \quad ,$$

$$a_3 \equiv U_3 + rS^{tr} = rw\gamma^2 v_r \quad .$$

We then make an initial guess for the pressure, P_i. A convenient choice is $P_i=\epsilon/3$, with ϵ taken from the previous time step. We can then calculate the velocities:

$$v_r = a_3/\left(a_1 + rP_i\right) \quad ; \quad v_z = v_r a_2/a_3 \quad . \tag{VII.3}$$

With this set of initial guess, we can calculate all other variables. In particular, we can calculate

$$w = \frac{\left(a_1 + rP_i\right)}{r\gamma^2} \quad , \tag{VII.4}$$

and therefore P from the input equation of state. If P does not agree with the initial guess, P_i, to within some tolerance, we replace P_i by P and iterate (VII.3) and (VII.4) until convergence.

Notice that we are solving the hydrodynamic equations in (t, z, r) instead of going into some rapidity-proper-time space such as what we did in the one-dimensional case. The reason is that such a transformation is much more complicated in two dimensions due to the additional degree of freedom.

ii) Results

Results of solving Eq. (VII.2) are shown for collisions of ^{238}U at 15 GeV/A in Fig. VII.5, ^{16}O at 15 GeV/A in Fig. VII.6 and at 100 GeV/A in Fig. VII.7. Contour plots of energy density and net baryon number density are shown in consecutive time frames. We use the bag model equation of state, Eq. (VI.5), and the IOC source terms (IV.17,18) in the calculations, assuming $\tau_o = 1$ fm/c. The initial conditions are:

$$\epsilon = 0 \ , \ n_B = 0 \ , \ v_r = 0 \ , \ v_z = z/t \ \text{ at } t = \tau_o \ .$$

Typical step sizes are $\Delta z = 0.06$ fm, $\Delta r = 0.6$ fm, and $\Delta t = 0.0025$ fm/c; the results are little affected by changing these step sizes. The dependence of the hydrodynamics on the equation of state, the source terms, viscosity, and τ_o was studied in some details in Chapter VI. Here we concentrate on the importance of the transverse degree of freedom.

The maximum energy density reached in collisions of ^{238}U at 15 GeV/A is about 1.3 GeV/fm^3 (see Fig. VII.5a). This should be compared to 1.4 GeV/fm^3,

obtained when only longitudinal expansion is allowed (see Fig. VI.1). Therefore the transverse degree of freedom can be roughly thought of as a few per cent effect on the energy density. The collision does not reach the state of pure QGP ($\epsilon \geq 2$ GeV/fm^3), and even the mixed phase stage (0.8 GeV/fm^3 $\leq \epsilon \leq$ 2 GeV/fm^3) is relatively short-lived in the central rapidity region. In roughly 2 fm/c after the onset of hydrodynamics, the highly excited fragmentation regions will break off from the cooler central region , and the energy density in the central region is turned into a pion fluid. In Fig. VII.5b we show the distribution of net baryon number density. As expected, most of the baryon number resides in the fragmentation regions, whereas the central rapidity region has very low baryon content. We see that baryons are still condensing in the fragmentation regions when the plasma in the central region has already reached the hadronization stage. This is consistent with what we found in the one dimensional case (Ch. VI).

As we decrease the sizes of the heavy ions, we may expect two effects in competition that determine the importance of transverse expansion. First, a smaller transverse size means that the bulk of the plasma will "realize" the transverse degree of freedom sooner. However, collisions of light ions won't produce as high an energy density as in heavy ions. For example, as shown in Fig. VII.6a, the maximum energy density reached in ^{16}O collisions is only about 0.6 GeV/fm^3, less than half of that in uranium collisions. Therefore the pressure in light systems is also smaller than that in heavy-ion collisions, and smaller transverse expansion is expected. In Fig. VII.6c we show the distribution of transverse velocity in the $z-r$ plane. Comparing Fig. VII.6c with Fig. VII.6a, we conclude that transverse

expansion in the bulk of the plasma is insignificant.

We repeated the calculations for ^{16}O collisions at higher energy to probe the dependence of transverse expansion on beam energies. In Fig. VII.7 we show results for collisions at 100 GeV/A. As expected, the maximum energy density achieved is only a slow function (logarithm) of the beam energies (see Fig. VI.7), reaching only about 1.2 GeV/fm^3 in this case. Here again we have two competing factors contributing to the importance of the transverse expansion. The higher energy density in the system means higher pressure and hence more transverse expansion. On the other hand, the longitudinal expansion is also speeded up, diminishing the significance of the transverse degree of freedom. Overall, higher beam energies do not seem to help the transverse expansion much. The baryon number density is still very low in the fragmentation regions when hadronization has begun in the CRR. This can be understood easily as a time dilation effect: the faster the baryon sources travel, the longer it takes them to condense.

iii) Summary and Discussion

We have presented 2+1-dimensional hydrodynamic calculations of central collisions of identical ions at ultra-relativistic energies. We see that in ^{238}U, the transverse expansion decreases the maximum energy density reached in the system by only a few per cent compared to that in purely longitudinal expansion. To good approximation, the hydrodynamics of the system is 1+1-dimensional (longitudinal). We have seen that decreasing the size of the ions does not change the above conclusion; neither does increasing the beam energies.

It is clear from our calculations that the fragmentaion regions are more "inter-

esting" than the central region. Assuming the inside-outside cascade model, it is at the fragmentation regions that higher energy density is reached, and the regions stay excited for a longer period of time compared to CRR. While most authors have focused on the central region so far because of its simplicity (scaling symmetry, low baryon content), we'd like to point out that local thermal equilibrium is a more reliable assumption in the fragmentaion regions. For example, our calculations indicate that in roughly only 2 fm/c hadronization commences in CRR for heavy-ion collisions at tens of GeV/A. The characteristic time associated with the microscopic collisions in the system is not much less than 2 fm/c, and therefore non-equilibrium effects may be important. Hydrodynamics is probably a much "safer" approximation in the longer lived fragmentation regions. Also, while most signature calculations concentrate on the central region (see Ch. VIII), we think we may have better chances at recognizing QGP events in the fragmentation regions.

It may be tempting to compare the results presented in this chapter to experimental data. However, this won't be a fair comparison without implementing the dynamics of the hadronization and the freeze-out stages, where non-equilibrium effects could become important. We need a good hadronization model as well as a kinetic theory code to describe the system at the final stages. While progess in these fronts is being made, a discussion of these would take us too far out of the scope of this thesis.

Figure Captions

FIG. VII.2 Contour plots of the temperature in units of the temperature at the origin when the hydrodynamic expansion starts, T_o, in consecutive time frames since the beginning of the hydrodynamic expansion at $t = 0$ fm/c. The parameter τ_o and the initial length of the plasma region, Z_m, are taken to be a) 1 fm/c and b) 2 fm/c. The contours are drawn in regular intervals of 0.1, from 0.2 to $T_{\max}$, the maximum temperature in units of T_o.

FIG. VII.3 Angular distribution of the energy viewed in the c.m. frame, for the case $\tau_o = 1$ fm/c. θ is the angle between the flow velocity vector and the z axis: $\theta = \tan^{-1}(v_r/v_z)$. The peak at $\theta = 0$ is cut off to show the development of the transverse flow.

FIG. VII.4 Distributions of the energy in a) longitudinal rapidity, $y = \tanh^{-1} v_z$, and b) transverse velocity, v_r, viewed in the c.m. frame, for the case $\tau_o = 1$ fm/c. The peak at $v_r = 0$ in b) is again cut off to show the transverse motion.

FIG. VII.5 Contour plots of a) the energy density (GeV/fm^3), and b) the net baryon number density (fm^{-3}) in $z - r$ plane shown in consecutive time frames, obtained by solving Eq. VII.2. Central collision of ^{238}U at 15 GeV/A in c.m. frame is assumed. τ_o is taken to be 1 fm/c. The contours are labelled in steps of a) 0.2 GeV/fm^3, from 0.2 GeV/fm^3 to $\epsilon_{\max}$, and b) 0.02 fm^{-3}, from 0.02 fm^{-3} to n_{Bmax}.

FIG. VII.6 Contour plots of a) the energy density (GeV/fm^3), b) the net baryon number density (fm^{-3}), and c) transverse velocity (c) in $z - r$ plane shown in consecutive time frames. Central collision of ^{16}O at 15 GeV/A in c.m. frame is assumed. τ_o is taken to be 1 fm/c. The contours are labelled in steps of a) 0.1

GeV/fm^3 from 0.1 GeV/fm^3 to $\epsilon_{\rm max}$, b) 0.01 fm^{-3}, from 0.01 fm^{-3} to $n_{\rm Bmax}$, and c) 0.01 c, from 0.01 c to max v_r.

FIG. VII.7 Contour plots of a) the energy density (GeV/fm^3), and b) the net baryon number density (fm^{-3}) in $z-r$ plane shown in consecutive time frames, obtained by solving Eq. VII.2. Central collision of ^{16}O at 100 GeV/A in c.m. frame is assumed. τ_o is taken to be 1 fm/c. The contours are labelled in steps of a) 0.2 GeV/fm^3, from 0.2 GeV/fm^3 to $\epsilon_{\rm max}$, and b) 0.002 fm^{-3}, from 0.002 fm^{-3} to $n_{\rm Bmax}$.

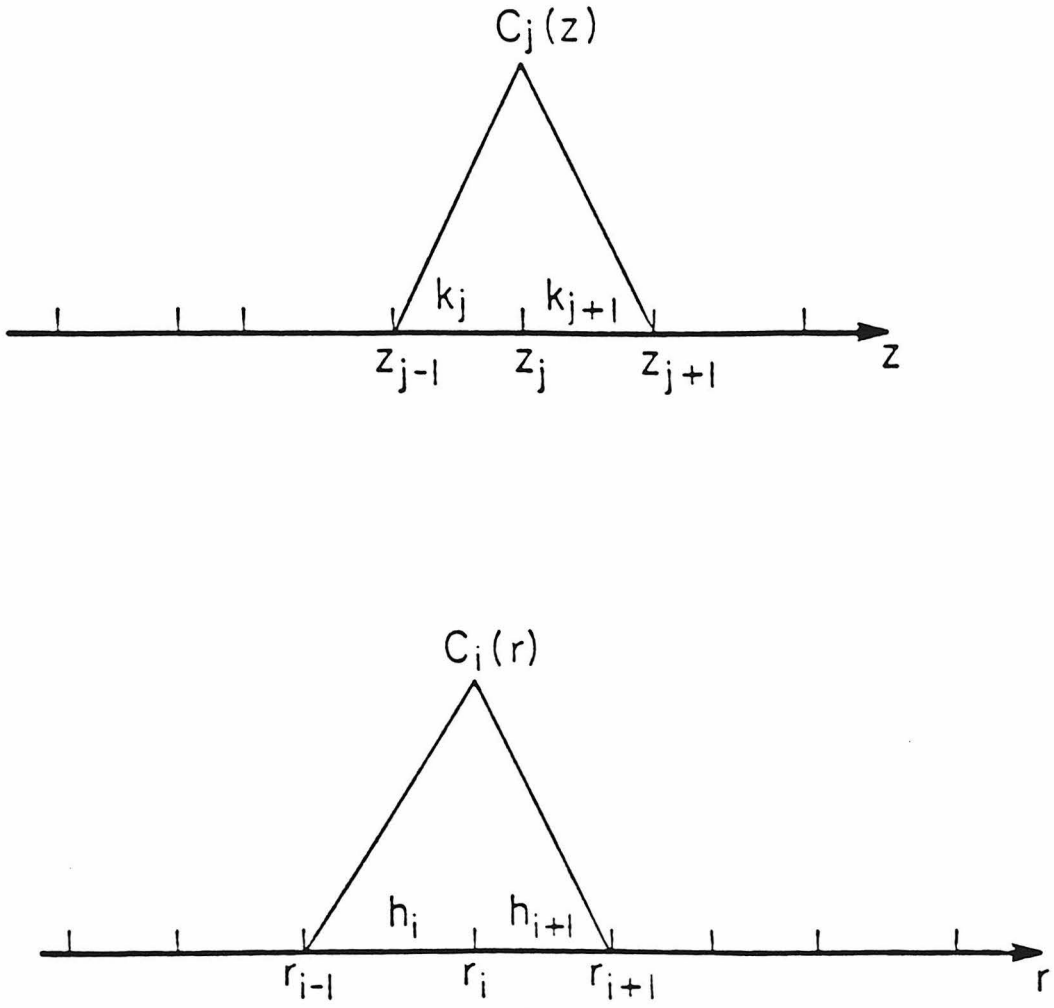

FIG. VII.1 Finite element basis functions. Relevant fields (ϵ, v_z, v_r) are expanded in these functions in method 1 described in Sec. VII.1.

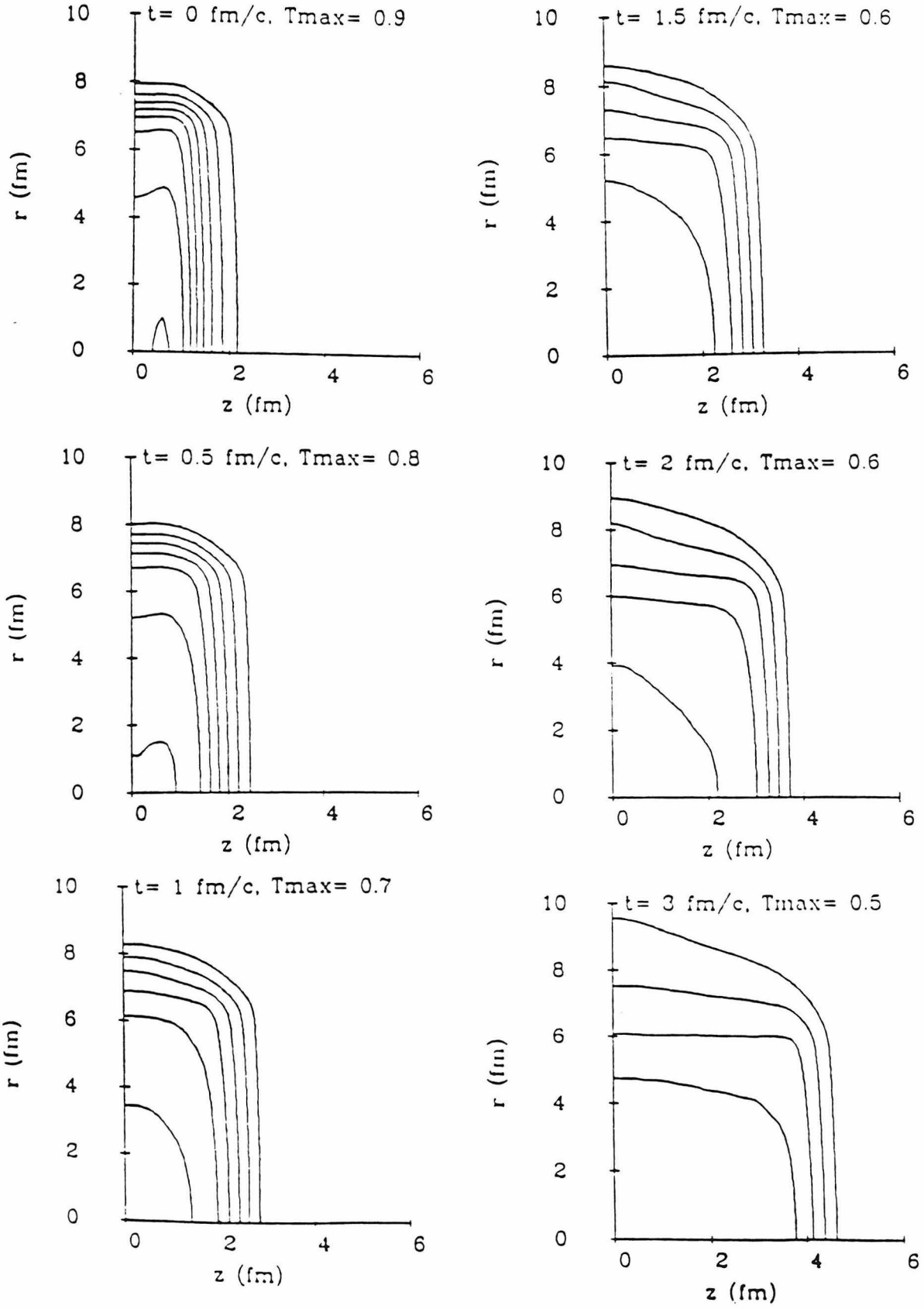
t= 0 fm/c, Tmax= 0.9
t= 1.5 fm/c, Tmax= 0.6
t= 0.5 fm/c, Tmax= 0.8
t= 2 fm/c, Tmax= 0.6
t= 1 fm/c, Tmax= 0.7
t= 3 fm/c, Tmax= 0.5
r (fm)
z (fm)
0
2
4
6
8
10

FIG. VII.2 a

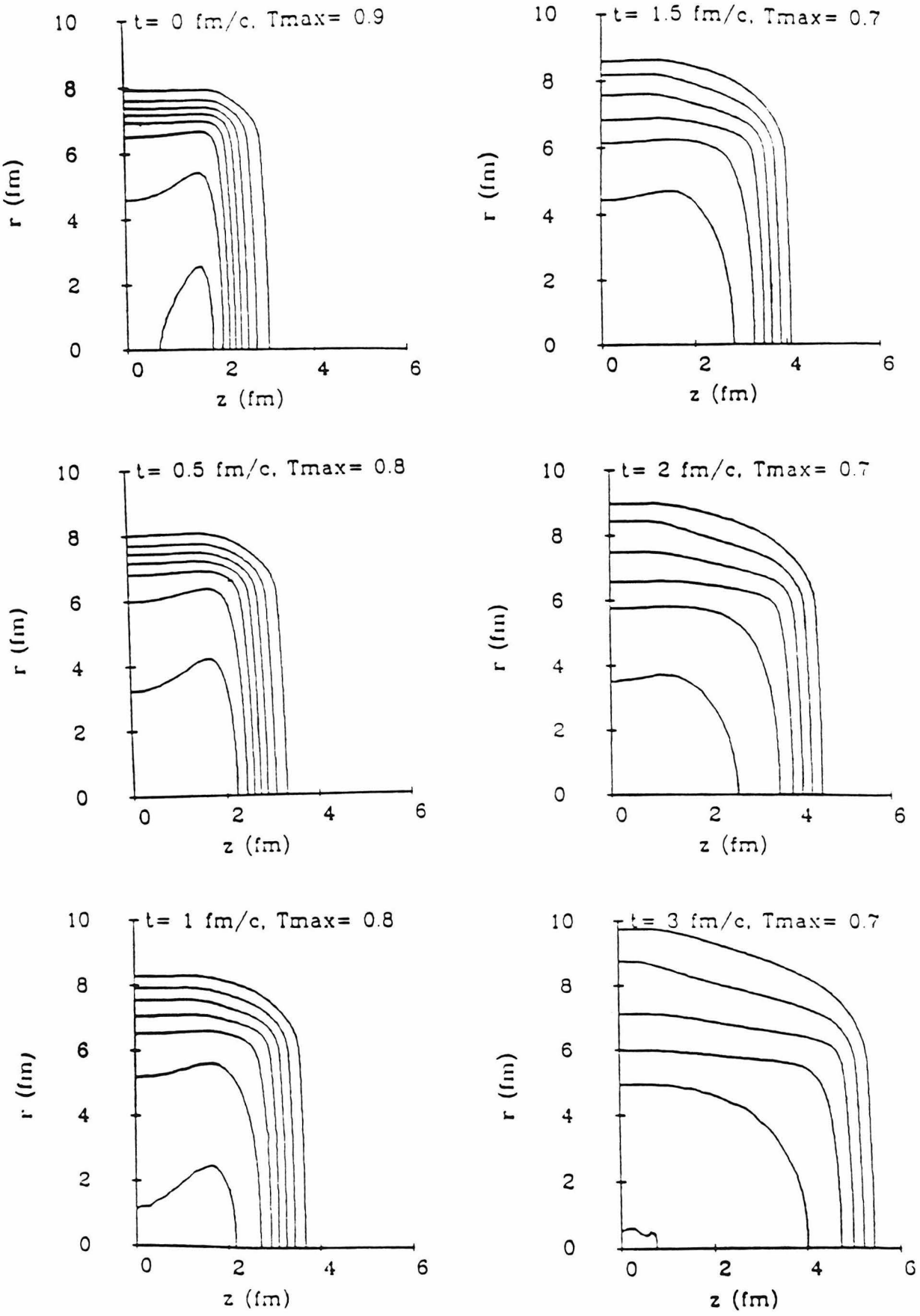
t= 0 fm/c, Tmax= 0.9
t= 1.5 fm/c, Tmax= 0.7
t= 0.5 fm/c, Tmax= 0.8
t= 2 fm/c, Tmax= 0.7
t= 1 fm/c, Tmax= 0.8
t= 3 fm/c, Tmax= 0.7
r (fm)
z (fm)
0
2
4
6
8
10

FIG. VII.2 b

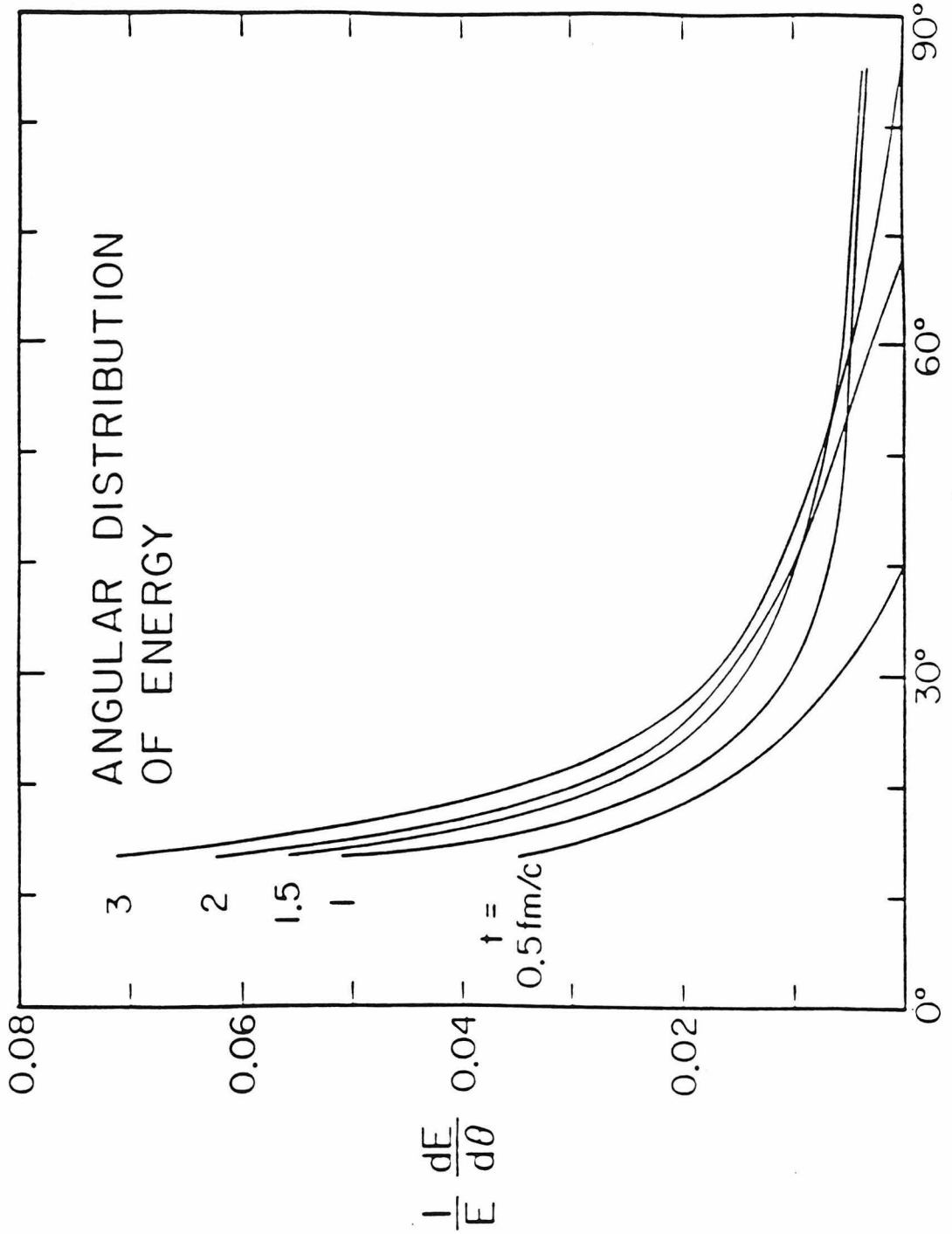
ANGULAR DISTRIBUTION
OF ENERGY
3
2
1.5
1
t =
0.5 fm/c
0.08
0.06
0.04
0.02
0°
30°
60°
90°
θ
1/E dE/dθ

FIG. VII.3

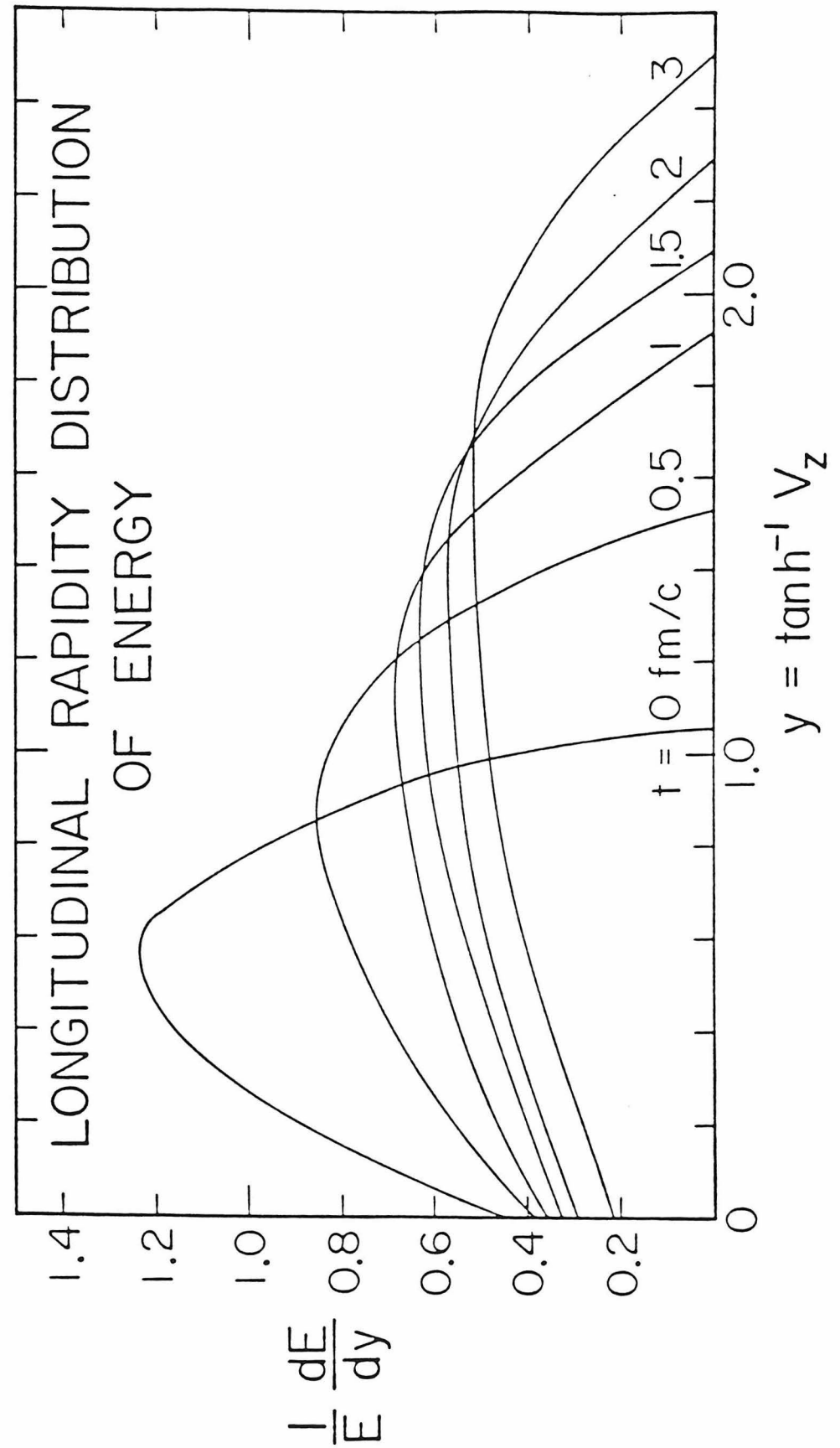
LONGITUDINAL RAPIDITY DISTRIBUTION
OF ENERGY
$\frac{1}{E}\frac{dE}{dy}$
1.4
1.2
1.0
0.8
0.6
0.4
0.2
0
1.0
2.0
$y = \tanh^{-1} V_z$
t = 0 fm/c
0.5
1
1.5
2
3

FIG. VII.4 a

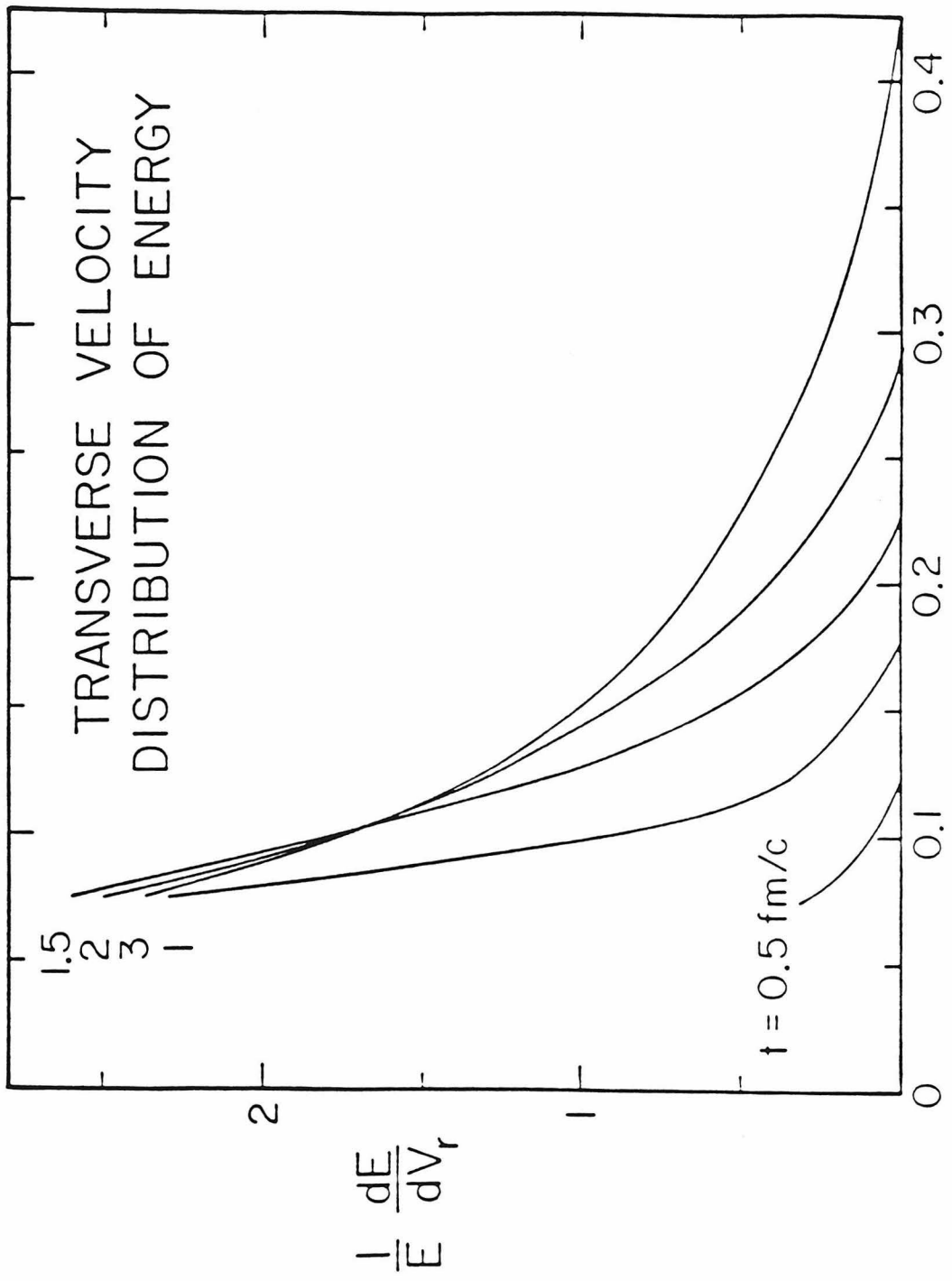
TRANSVERSE VELOCITY
DISTRIBUTION OF ENERGY
1.5
2
3
1
t = 0.5 fm/c
0
0.1
0.2
0.3
0.4
V_r
2
1
$\frac{1}{E}\frac{dE}{dV_r}$

FIG. VII.4 b

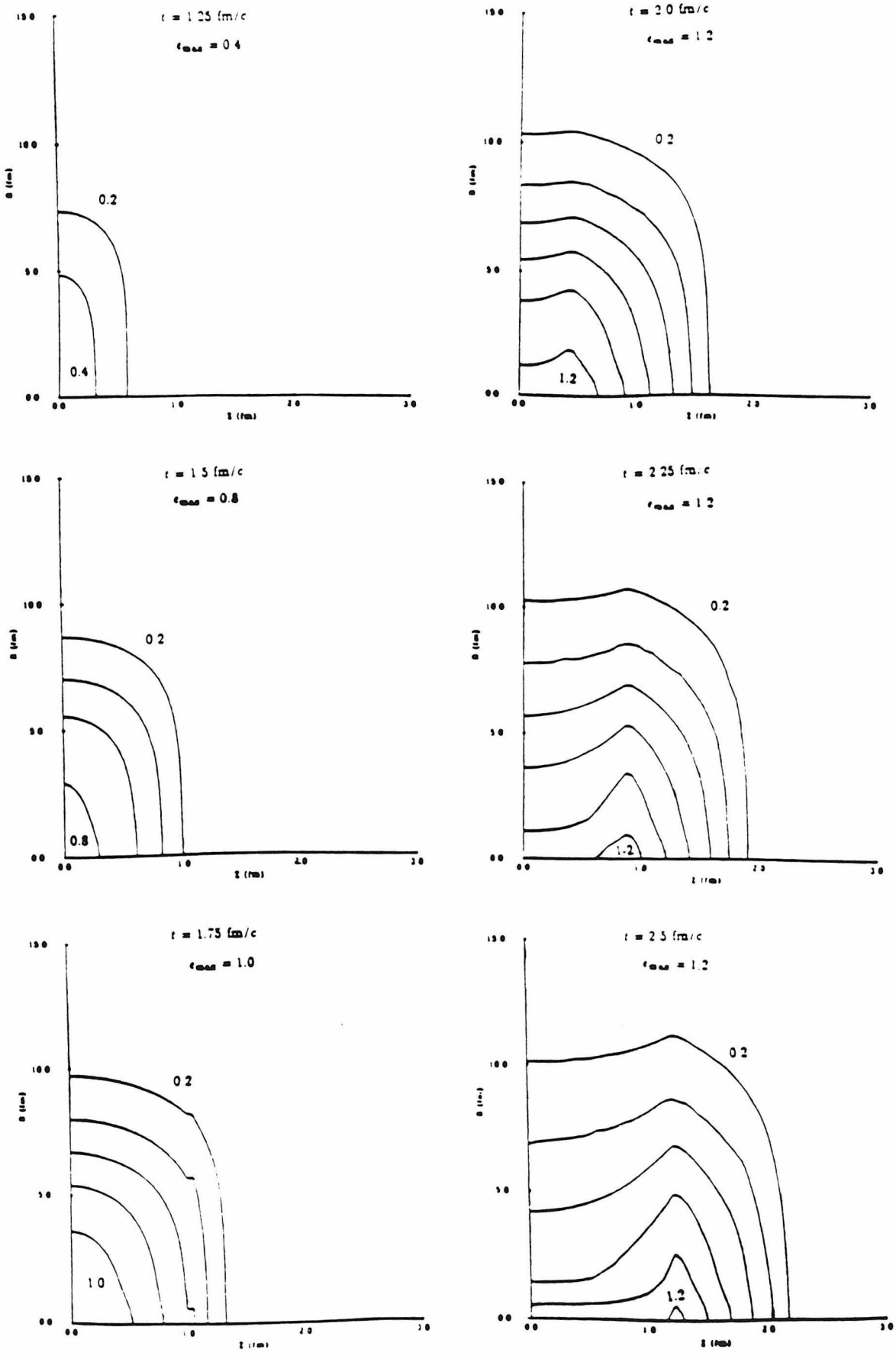

FIG. VII.5a ENERGY DENSITY GeV/fm^3 A=238 $y_o = 3.4$

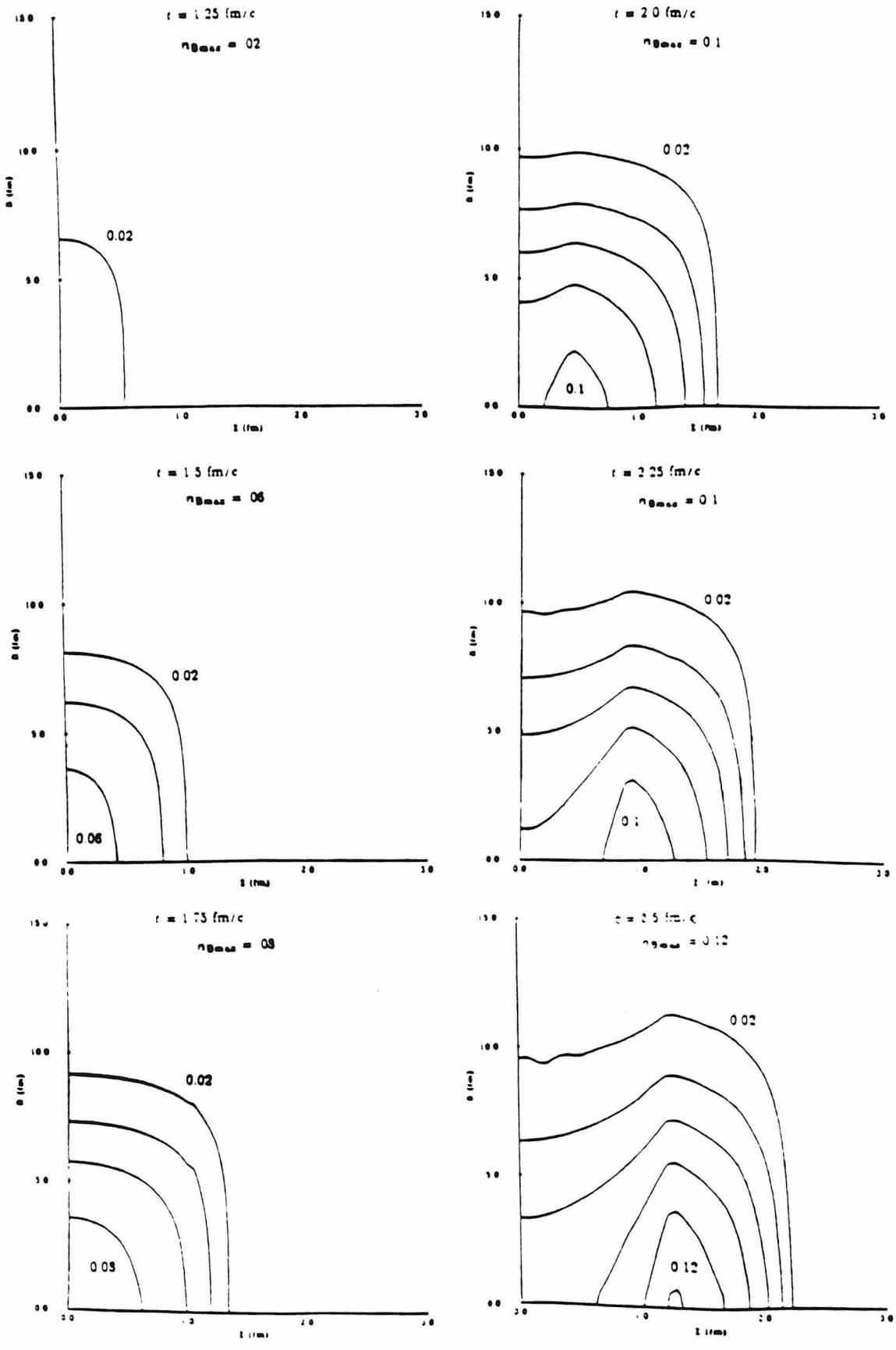

FIG. VII.5b NET BARYON DENSITY fm^{-3} A=238 $y_o = 3.4$

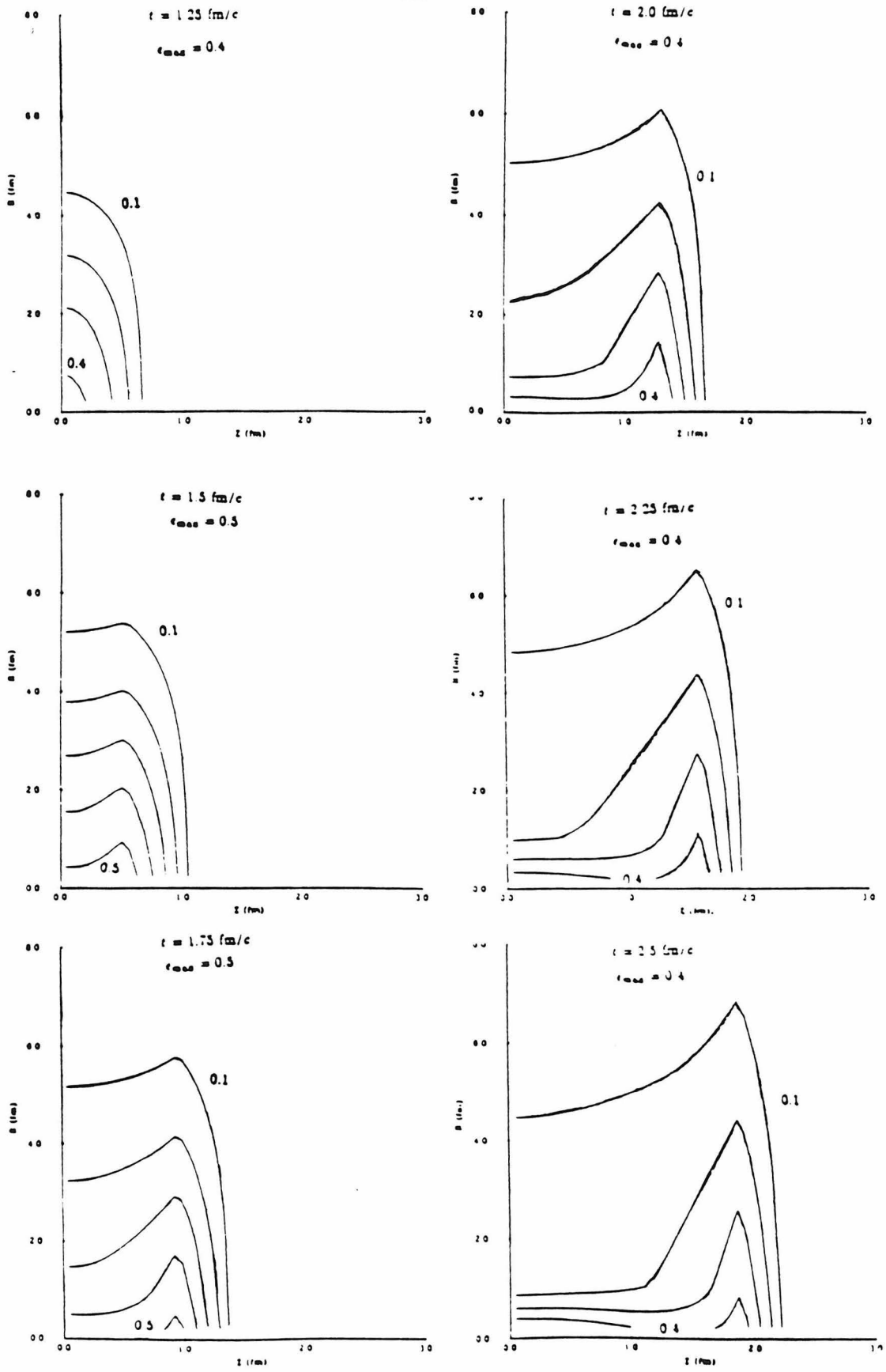

FIG. VII.6a ENERGY DENSITY GeV/fm^3 A=16 $y_o = 3.4$

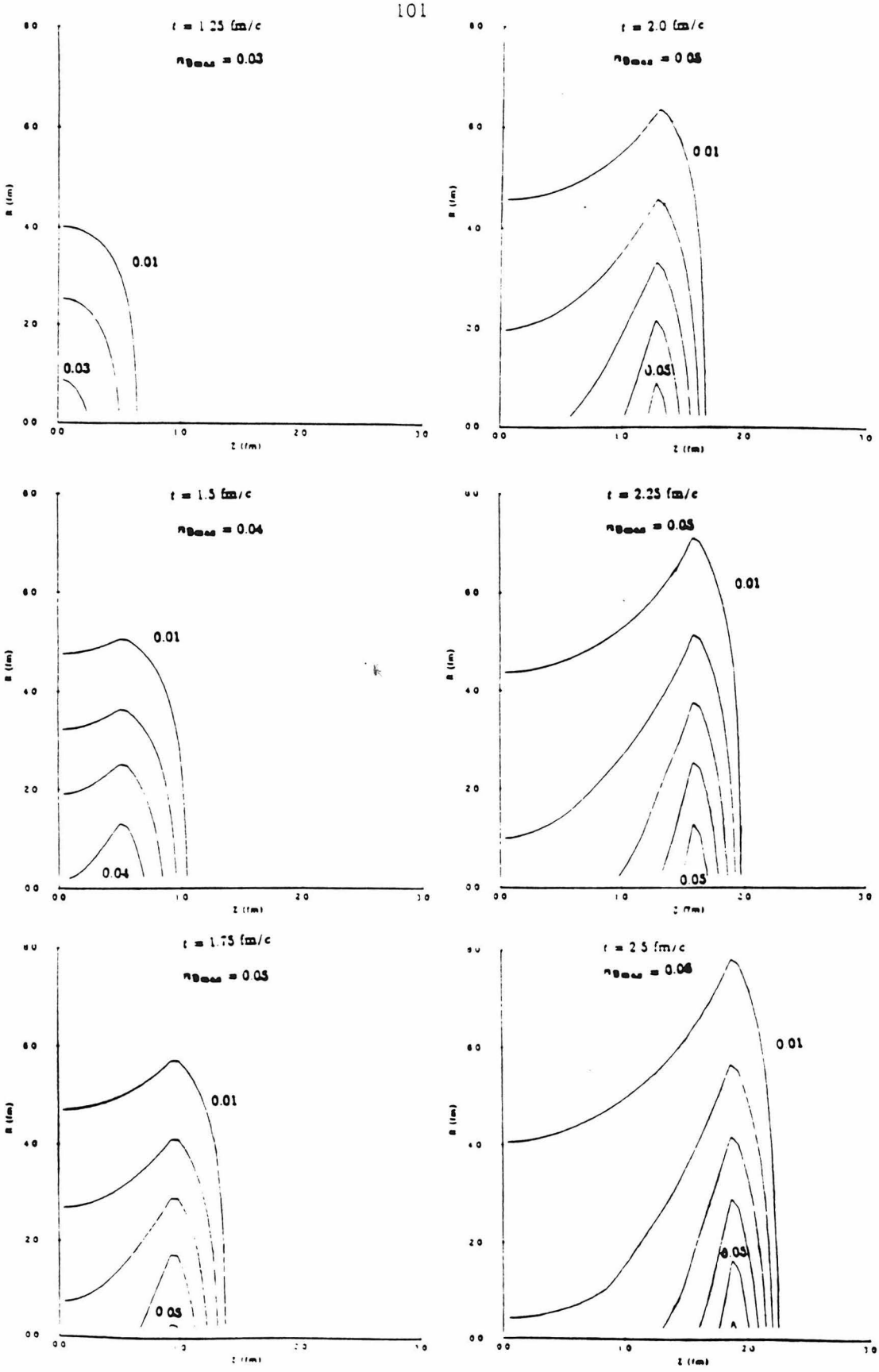

FIG. VII.6b NET BARYON DENSITY fm^{-3} A=16 $y_o = 3.4$

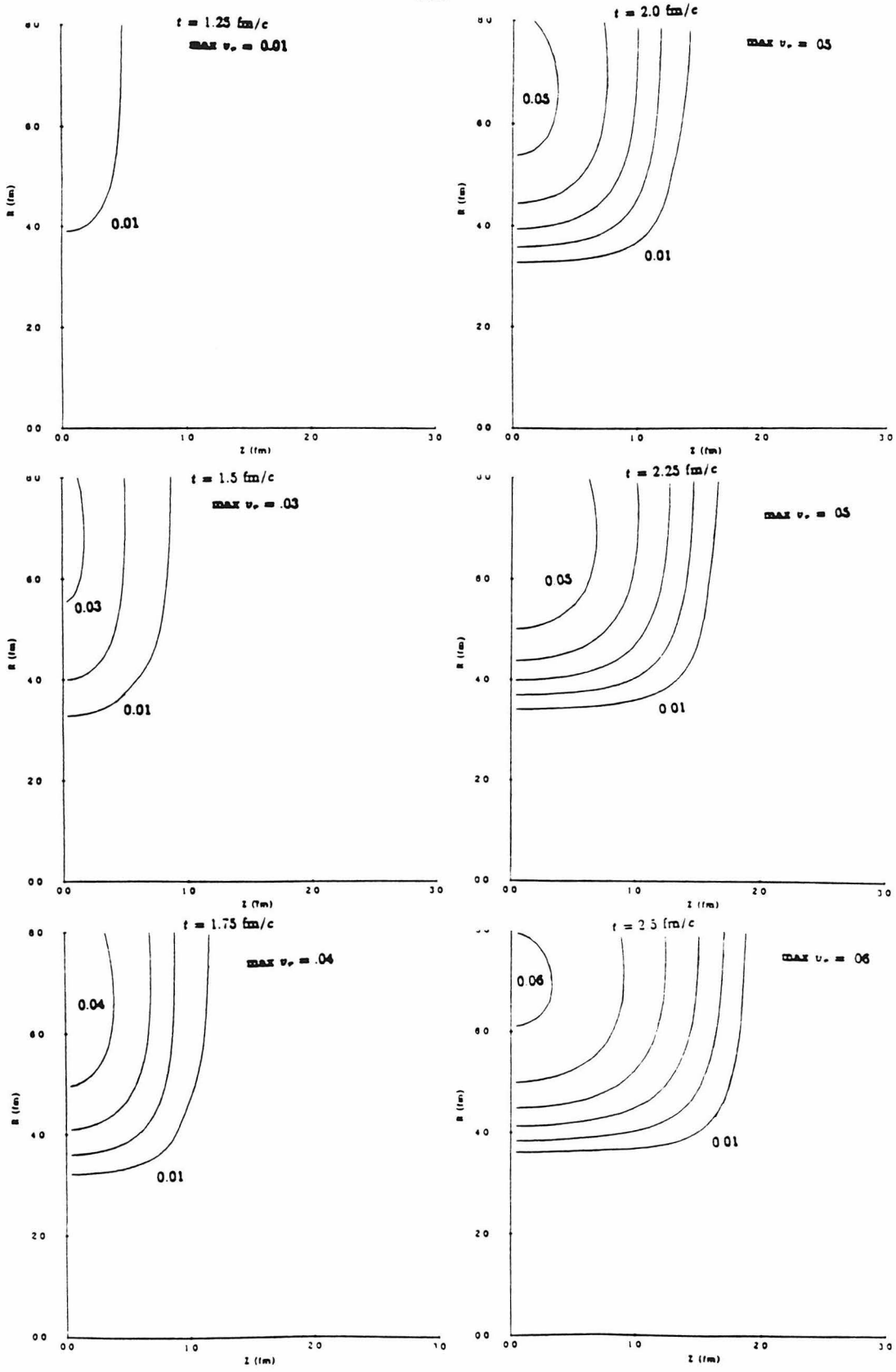

FIG. VII.6c TRANSVERSE VELOCITY A=16 $y_o = 3.4$

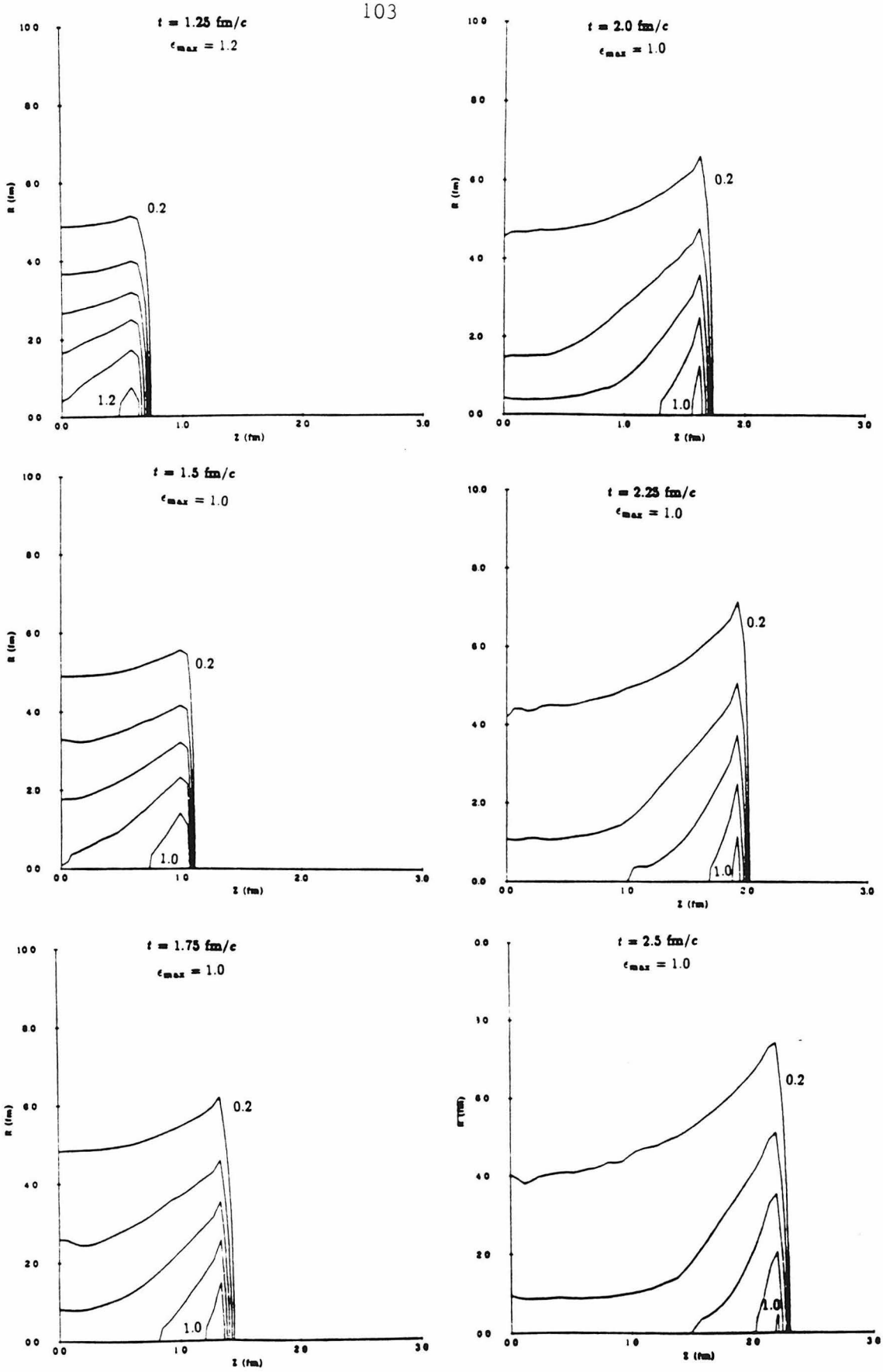

FIG. VII.7a ENERGY DENSITY GeV/fm^3 A=16 p_0 = 5.3

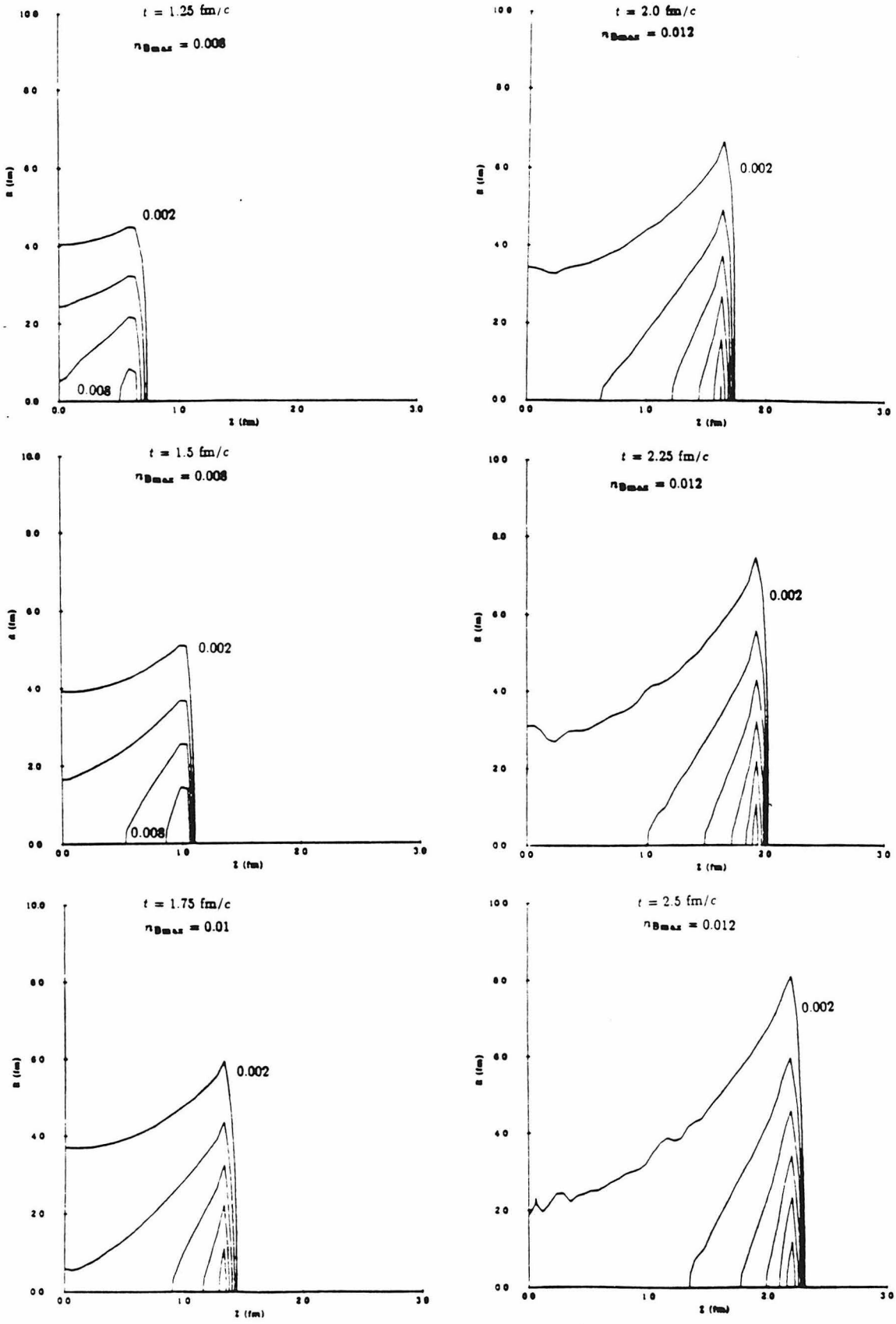

FIG. VII.7b NET BARYON DENSITY fm^{-3} A=16 $y_o = 5.3$

CHAPTER VIII

Signatures of Formation of QGP in URHIC

The most important challenge in the field of ultra-relativistic heavy-ion collisions today is probably to identify signatures of formation of quark-gluon plasma in the process. The answer of this question will not only serve as a guideline to the design of the detectors and the data analyses, but may also even determine the worthiness of these experiments according to some physicists. Over the years, many possible signatures have been proposed. But there seems to be a consensus emerging that there is not one unambiguous signature, and that the identificaton of a QGP event will involve correlation of several independent "signatures". We shall discuss some of these propositions in this chapter, namely, dilepton and photon production, strangeness, and transverse momentum distribution in the first three sections. Then we shall go through a quick survey of a list of other proposed signatures.

The estimation of a possible signature typically involves two ingredients. First, at the microscopic level we have to calculate the production cross section of the particular observable used as signature. So, for example, we need to calculate the dilepton production rate from quarks and gluons (Sec. VIII.1). Then we have to fold this microscopic physics into the macroscopic flow of the system. While pre-equilibrium emission may be important, we shall take the standpoint that emission of these signatures takes place mostly during the hydrodynamic phase, and so the hydrodynamic models we developed in the last few chapters will be natural frameworks for signature calculations.

VIII.1 Dilepton and photon production

Photons and dilepton pairs are produced abundantly throughout the plasma phase, and since they interact with the plasma or the final state hadrons only electromagnetically, information about the early stages of plasma formation may be preserved, as well as that of the later stages. In a QGP, photons are produced mainly by quark-anti-quark annihilation (Fig. VIII.1a) or bremsstrahlung from quark-quark scattering (Fig. VIII.1b), whereas in a hadron gas, the dominant mechanism of photon production is through hadronic decays, such as those of the neutral pions (Fig. VIII.1c). Even in an URHIC event with QGP formed for a short period of time, hadronic decays still contribute significantly to the photon spectrum and constitute a severe background problem. Lepton pairs are produced by quark-anti-quark annihilation in a QGP (Fig. VIII.1d) and by $\pi^+ - \pi^-$ annihilation in a hadron gas (Fig. VIII.1e). Again the latter process will be the background for QGP signal given in the former process. We shall consider in a little more detail dilepton production; photon production is quite similar.

From the structure of the graph in Fig. VIII.1d, we can see that the rate per volume of dilepton emission is given by

$$R = -64\pi^2\alpha^2 \int \frac{d^3\vec{p}_1}{(2\pi)^3 2E_1} \frac{d^3\vec{p}_2}{(2\pi)^3 2E_2} L^{\mu\nu}(\vec{p}_1, \vec{p}_2) \frac{1}{q^4} W_{\mu\nu}(q) \quad . \tag{VIII.1}$$

Here, α is the fine structure constant, and $1/q^4$ comes from the photon propagator. $L^{\mu\nu}$ is the familiar leptonic tensor [Bj64],

$$L^{\mu\nu} = (\vec{p}_1.\vec{p}_2 + m^2)g^{\mu\nu} - p_1^\mu p_2^\nu - p_2^\mu p_1^\nu \quad ,$$

which represents the contribution from the lepton legs of the graph in Fig. VIII.1d in standard perturbative QED. $W^{\mu\nu}$ is the hadronic tensor, and for emission from QGP, it has been shown to be [Mc85]

$$W^{\mu\nu}(q) = \int d^4x \; e^{-iq\cdot x}\langle J^\mu(x)J^\nu(0)\rangle \quad ,$$

where $\langle\rangle$ denotes taking the thermal expectation value:

$$\langle\mathcal{O}\rangle = \mathrm{Tr}\; e^{-\beta H}\mathcal{O}/\mathrm{Tr}\; e^{-\beta H} \quad ,$$

with H being the Hamiltonian of the system and β the inverse of the temperature.

Just from the tensor structure and the fact that $W^{\mu\nu}$ is symmetric with respect to interchange of μ and ν, we see that $W^{\mu\nu}$ can be decomposed into two structure functions A and B:

$$\begin{aligned} W^{\mu\nu}(q) =& (q^2 g^{\mu\nu} - q^\mu q^\nu) A(q^2, u\cdot q, T, \Lambda) \\ &+ \left[g^{\mu\nu}(u\cdot q)^2 - (u^\mu q^\nu + q^\mu u^\nu)\, u\cdot q + u^\mu u^\nu q^2\right] B(q^2, u\cdot q, T, \Lambda) \; , \end{aligned}$$

where u is the four-velocity of the fluid, T the temperature, and Λ the QCD scaling parameter. The calculation of A and B is in general very complicated if perturbative QCD is not assumed. A rigorous computation of these structure functions from QCD probably awaits further advances of lattice gauge calculations.

In first order QCD, the cross section for dilepton emission at coordinates x from a plasma of u and d quarks at zero baryon density is known to be [Fe76, Sh78, Ka81]

$$\left(\frac{dN}{dMd^4x}\right)_{q-\bar{q}} = \frac{5}{9}\left(\frac{\alpha^2}{\pi^3}\right)\left(1+\frac{2m_l^2}{M^2}\right)^{1/2} MT^2 H\left(\frac{M^2}{T^2}\right) \quad , \qquad \text{(VIII.2a)}$$

where

$$H(\xi^2) = \int_0^\infty dy\ (e^y + 1)^{-1} \ln\left[1 + e^{-\xi^2/4y}\right] \quad ,$$

m_l is the lepton mass, and M is the invariant mass of the dilepton pair. The analogous formula for emission from hadron gas is [Do81]

$$\left(\frac{dN}{dMd^4x}\right)_\pi = \frac{1}{12}\frac{\alpha^2}{\pi^3} F_\pi^2(M^2)\left(1 - \frac{4m_\pi^2}{M^2}\right) \left(1 + \frac{2m_l^2}{M^2}\right)\left(1 - \frac{4m_l^2}{M^2}\right)^{1/2} MT^2 G(W,\lambda) \quad . \tag{VIII.2b}$$

Here $W = \left(M^2/2m_\pi^2\right) - 1$, $\lambda = m_\pi/T$, and

$$G(W,\lambda) = \int_\lambda^\infty dy\ (e^y - 1)^{-1} \ln\left(\frac{1 - \exp\left[-Wy - P(y^2 - \lambda^2)^{1/2}\right]}{1 - \exp\left[-Wy + P(y^2 - \lambda^2)^{1/2}\right]}\right) \quad ,$$

with $P = (W^2 - 1)^{1/2}$. $F_\pi^2(M^2)$ is the pion form factor taken from experiment.

Now we have to integrate the dilepton spectrum over the history of the URHIC process. More concretely, we shall take the temperature distribution from hydrodynamics, calculate the dilepton production rate at each space-time point, and integrate over the four-volume of the system. We need to do the calculation first assuming that a QGP is not formed. So in this case, we just use Eq. (VIII.2b) throughout. We then repeat the calculation with a phase transition, using Eq. (VIII.2a) during the quark-gluon phase. If the results of these two calculations differ significantly, we may have a viable signature of the QGP.

The dilepton emission rate spectrum per unit longitudinal rapidity y and transverse momentum $p_\perp$ using scaling hydrodynamics in cylindrical coordinates can be expressed analytically [Ka87],

$$\frac{dN}{dM^2 dy d^2p_\perp} = \frac{\alpha^2}{2\pi^3} \int \tau d\tau r dr I_0(\gamma_r v_r p_\perp/T) K_0(\gamma_r v_r M_\perp/T) \left\{\frac{5}{9}\theta(Q) + \left[\frac{5}{9} f_Q + G_\pi(M^2) f_H\right]\theta(M) + G_\pi(M^2)\theta(H)\right\} \quad , \tag{VIII.3}$$

where the four-velocity of the fluid is

$$u^\mu = \gamma_r \left(\frac{t}{\tau}, v_r \cos\phi, v_r \sin\phi, \frac{z}{\tau} \right) \quad ,$$

and the transverse mass $M_\perp = \sqrt{M^2 + p_\perp^2}$. The theta functions here specify the three regimes in the system: $\theta(Q) = 1$ only in the pure quark-gluon phase ($\epsilon \geq \epsilon_Q$); $\theta(M) = 1$ only during the mixed phase ($\epsilon_H \leq \epsilon \leq \epsilon_Q$), and $\theta(H) = 1$ for the hadron gas ($\epsilon \leq \epsilon_H$). During the mixed phase, the fraction of volume occupied by the quark-gluon phase, $f_Q = (\epsilon - \epsilon_H)/(\epsilon_Q - \epsilon_H)$, and that occupied by the hadron phase, $f_H = 1 - f_Q$, are assumed to radiate dileptons independently. G_π is the additional factor due to the pions,

$$G_\pi(M^2) = \frac{1}{12} \left(1 - \frac{4m_\pi^2}{M^2} \right) F_\pi^2(M^2) G(W, \lambda) \quad ,$$

and I_0 and K_0 are the modified Bessel functions. A plot of this result is shown in Fig. VIII.2. A similar calculation assuming spherical expansion of the plasma was done by Chin [Ch82]; his result is shown in Fig. VIII.3.

Note that because of the Boltzmann factor, $\exp(-E/T)$, lepton pairs of larger masses are emitted earlier in the process, when T is higher. Therefore, there should exist a window of lepton masses where emissions from QGP dominate. This window has been estimated to be $1 \leq M_\perp \leq 3$ GeV. Another possibility of using dilepton spectra to diagnose formation of QGP is based on the observation that dilepton emission from hadronic gas is dominated by the ρ-meson channel (Fig. VIII.1e). Since the hot plasma would emit dileptons with higher total energy than those from the accompanying hadronic gas, the ρ-meson peak in the dilepton mass spectrum should subsize as the transverse energy of the pair increases [Si85].

Clearly much improvement on dilepton and photon spectrum calculation is needed. On the microscopic physics side, we need to improve on the perturbative QCD calculation, whereas on the macroscopic side, we need more realistic hydrodynamics, as well as better understanding of non-equilibrium effects.

VIII.2 Strangeness production

In a hot QGP, temperature is probably high enough that SU(3) flavor symmetry is approximately restored, provided that chemical equilibrium can be reached in a reasonably short period of time. We expect therefore large abundances of strange quarks produced during the plasma phase. And since the characteristic time scale in heavy-ion collisions is very short compared to that of weak interactions, strangeness is to good approximation a conserved quantum number in the process. The only way to destroy these strange quarks is through $s - \bar{s}$ annihilation, which has a relatively small cross section. Naively we would thus expect that the formation of QGP enhances the final abundances of strange and anti-strange baryons and mesons. But for strangeness to be qualified as a signature, we have to show that some experimentally observable strangeness content in a hadron gas is indeed small compared to that in a QGP. We shall briefly discuss some of these calculations [Ka86, Ko86, Ma86, Mc87, Mu87].

The dominant reaction in a QGP creating strange quarks is through pair creation from two gluons (Fig. VIII.4abc) and from two quarks (Fig. VIII.5), while the reverse reactions are the loss channels. We can therefore set up a rate equation for the proper strange quark density, n_s: [Ma86]

$$\partial_\mu n_s^\mu = R_{\text{gain}} - R_{\text{loss}} \quad , \tag{VIII.3}$$

where

$$R_{\rm gain} = \int d\Gamma \tilde{F}_s(p_3,p_4)\Big[F_G(p_1,p_2)\sum_{\rm spin,color}|\mathcal{M}_{gg\to s\bar{s}}|^2 + F_Q(p_1,p_2)\sum|\mathcal{M}_{q\bar{q}\to s\bar{s}}|^2\Big] \ ,$$

and

$$R_{\rm loss} = \int d\Gamma F_s(p_3,p_4)\Big[\tilde{F}_G(p_1,p_2)\sum_{\rm spin,color}|\mathcal{M}_{s\bar{s}\to gg}|^2 + \tilde{F}_Q(p_1,p_2)\sum|\mathcal{M}_{s\bar{s}\to q\bar{q}}|^2\Big] \ .$$

Here, F_G, F_Q and F_s are the phase space factors for the gluons, quarks and strange quarks in the initial states, whereas $\tilde{F}$ are for the final states:

$$F_G = f_g(p_1)f_g(p_2) \ ; \quad F_Q = f_q(p_1)f_{\bar{q}}(p_2) \ ; \quad F_s = f_s(p_3)f_{\bar{s}}(p_4) \ ;$$

$$\tilde{F}_G = [1+f_g(p_1)]\,[1+f_g(p_2)] \ ;$$

$$\tilde{F}_Q = [1-f_q(p_1)]\,[1-f_{\bar{q}}(p_2)] \ ;$$

$$\tilde{F}_s = [1-f_s(p_3)]\,[1-f_{\bar{s}}(p_4)] \ .$$

In equilibrium, f_q (f_g) just takes the Fermi-Dirac (Bose-Einstein) form:

$$f_g(p) = \frac{1}{\exp(p\cdot u/T)-1} \ ;$$

$$f_q = f_{\bar{q}} = \frac{1}{\exp(p\cdot u/T)+1} \ .$$

The matrix elements for the reaction, $\mathcal{M}$, are to be squared and summed over color and spins. These can be computed easily using first order QCD [Ge78, Co79, Ma86]. Using the fact that the matrix elements are the same for the gain and the loss terms for a particular process (eg. $|\mathcal{M}_{gg\to s\bar{s}}|^2 = |\mathcal{M}_{s\bar{s}\to gg}|^2$), we can combine $R_{\rm gain}$ and $R_{\rm loss}$ and rewrite Eq. (VIII.3) as

$$\partial_\mu n_s^\mu = \left(e^{-2\beta\mu}-1\right) I(\mu,T) \ , \qquad \text{(VIII.4)}$$

where $I = I_{\rm gluon} + I_{\rm quark}$, with

$$I_{\rm gluon} = \left(e^{-2\beta\mu} - 1\right)^{-1} \left(R^{gg}_{\rm gain} - R^{gg}_{\rm loss}\right) \quad ,$$

$$I_{\rm quark} = \left(e^{-2\beta\mu} - 1\right)^{-1} \left(R^{q\bar{q}}_{\rm gain} - R^{q\bar{q}}_{\rm loss}\right) \quad .$$

A common factor $[\exp(-2\beta\mu) - 1]$, with μ the strange quark chemical potential and β the inverse temperature, has been factored out in (VIII.4), and we can see explicitly that the flow will just conserve the strange quark density after chemical equilibrium is reached ($\mu = 0$).

When the QGP cools down to the transition temperature, the quarks and gluons recombine to form hadrons, which are eventually detected. At this point we have to invoke some fragmentation models to facilitate calculations of final strange hadron abundances. If we naively recombine a quark and an anti-quark to form a meson and three quarks to form a baryon, we run into the problem of decreasing the entropy of the system. One way to get around this problem is to allow the quarks and the gluons to fragment into more quarks and gluons before recombination [Ko86]:

$$g \rightarrow q\bar{q} \quad , \quad q\bar{q} \rightarrow \pi g \quad .$$

We can calculate the average probability of fragmentation of quarks and gluons by comparing the initial and final entropy of the system. It is found that every gluon and about one third of the quarks must fragment before hadronization.

One fragmentation model that is relatively simple to use is the flux tube model [Sc51, Ca79, Ba83, Ma87], which pictures formation of a meson as the breaking

of the gluon string (Fig. VIII.6). The probability of such a fragmentation can be estimated by a semi-classical tunneling formula:

$$f_i = Ne^{(-m_i^2/\sigma)} \quad ,$$

where m_i is the mass of the quark pair, σ the QCD string tension, and N is a normalization constant. The effective number of quarks participating in recombination is therefore

$$\tilde{N}_q = N_q + f_q \tilde{N}_g \quad , \quad \tilde{N}_{\bar{q}} = N_{\bar{q}} + f_q \tilde{N}_g \quad ,$$

$$\tilde{N}_s = N_s + f_s \tilde{N}_g \quad ,$$

where N_g and N_s are the number of light (u,d) and strange quarks prior to the onset of phase transition, and $\tilde{N}_g$ is the effective number of gluons.

We can now apply a simple hadronization model to calculate abundances of final hadrons from $\tilde{N}_g$, $\tilde{N}_s$. One example is the combinatorial break-up model [Ko86], which just assigns constant probabilities for hadron formation: one for mesons, α_o, and one for baryons, β_o. We therefore have

$$\begin{aligned}
N_\pi &= \alpha_o \tilde{N}_q \tilde{N}_{\bar{q}} \\
N_K &= \alpha_o \tilde{N}_q \tilde{N}_{\bar{s}} \quad N_{\bar{K}} = \alpha_o \tilde{N}_s \tilde{N}_{\bar{q}} \\
N_\phi &= \alpha_o \tilde{N}_s \tilde{N}_{\bar{s}} \\
N_N &= \frac{1}{3!} \beta_o \tilde{N}_q^3 \quad N_{\bar{N}} = \frac{1}{3!} \beta_o \tilde{N}_{\bar{q}}^3 \\
N_Y &= \frac{1}{2!} \beta_o \tilde{N}_q^2 \tilde{N}_s \quad N_{\bar{Y}} = \frac{1}{2!} \beta_o \tilde{N}_{\bar{q}}^2 \tilde{N}_{\bar{s}} \\
&\cdot \\
&\cdot \\
&\text{etc.}
\end{aligned} \tag{VIII.5}$$

The constants α_o and β_o can be determined by invoking the conservation laws for each flavor:

$$\tilde{N}_q = N_\pi + N_K + 3N_N + 2N_Y + ...$$

$$\tilde{N}_{\bar{q}} = N_\pi + N_{\bar{K}} + 3N_{\bar{N}} + 2N_{\bar{Y}} + ...$$

$$\tilde{N}_s = N_{\bar{K}} + N_\phi + N_Y + ...$$

$$\tilde{N}_{\bar{s}} = N_K + N_\phi + N_{\bar{Y}} + ... \quad .$$

After hadronization, the system evolves as a hadron gas, and we have to keep track of the baryo-chemistry in the system. There are three classes of reactions that concern us here: strangeness production, exchange and annihilation. The most important strangeness producing/annihilating reactions are:

$$\begin{aligned} &\pi + N \rightleftharpoons K + Y \quad \pi + \bar{N} \rightleftharpoons \bar{K} + \bar{Y} \quad \pi + \pi \rightleftharpoons K + \bar{K} \\ &\pi + Y \rightleftharpoons \Xi + K \quad \pi + \bar{Y} \rightleftharpoons \bar{K} + \bar{\Xi} \\ &\pi + \Xi \rightleftharpoons \Omega + K \quad \pi + \bar{\Xi} \rightleftharpoons \bar{K} + \bar{\Omega} \quad , \end{aligned} \tag{VIII.6a}$$

whereas those for strangeness exchange are:

$$\begin{aligned} &\bar{K} + N \rightleftharpoons Y + \pi \quad K + \bar{N} \rightleftharpoons \bar{Y} + \pi \\ &\bar{K} + Y \rightleftharpoons \Xi + \pi \quad K + \bar{Y} \rightleftharpoons \bar{\Xi} + \pi \\ &\bar{K} + \Xi \rightleftharpoons \Omega + \pi \quad K + \bar{\Xi} \rightleftharpoons \bar{\Omega} + \pi \quad . \end{aligned} \tag{VIII.6b}$$

Since the quark exchange reactions (which are the dominant channels to produce strange baryons) involve N and $\bar{N}$, we have to also include reactions involving N, $\bar{N}$, which compete with above:

$$\begin{aligned} &N + \bar{N} \rightleftharpoons \pi's \\ &Y + \bar{N} \rightleftharpoons \bar{K} + \pi's \quad \bar{Y} + N \rightleftharpoons K + \pi's \\ &\Xi + \bar{N} \rightleftharpoons 2\bar{K} + \pi's \quad \bar{\Xi} + N \rightleftharpoons 2K + \pi's \\ &\Omega + \bar{N} \rightleftharpoons 3\bar{K} + \pi's \quad \bar{\Omega} + N \rightleftharpoons 3K + \pi's \quad . \end{aligned} \tag{VIII.6c}$$

We can therefore set up a reaction network describing (VIII.6), and the rate equations then look like

$$\partial_\mu \rho_i^\mu = R_i^{\text{gain}} - R_i^{\text{loss}} \quad , \tag{VIII.7}$$

with

$$R_i^{\text{gain}} = \sum_{\text{production}} \langle \sigma v \rangle_{jk \to i} \; \rho_j \rho_k \quad .$$

Here j and k denote the initial particles, which react to give particle i with a thermal average cross section, $\langle \sigma v \rangle_{jk \to i}$, taken from experimental data with extrapolation if necessary. All production channels are to be included. Similarly,

$$R_i^{\text{loss}} = \sum_{\text{loss}} \langle \sigma v \rangle_{i \to jk} \; \rho_j \rho_k \quad .$$

The program is thus clear. Eq. (VIII.4) is solved together with the hydrodynamic equations in the QGP phase, and then Eq. (VIII.5) is used to relate quark densities to hadron densities immediately after the phase transition. Finally, Eq. (VIII.7) is solved together with the hydrodynamic equations to evolve the system until freezeout. The same calculation is repeated for hadron gas using Eq. (VIII.7) throughout. The comparison of these two calculations can then determine whether a signature is possible.

The most natural proposal is to look at K/π ratio [Gl85]. Results of the above calculation using scaling hydrodynamics indicate a K/π ratio three times higher in a QGP than that found in p-p collisions [Ma86]. However, the K/π ratio in a hadron gas turns out to be even higher. This seemingly surprising result can be understood as follows: the formation of QGP generates large entropy increase, and therefore the number of pions goes up, reducing the K/π ratio. We conclude that K/π cannot be used as a signature of QGP.

Other signatures using strangeness have been proposed, such as strange anti-baryon abundances. Results of a calculation assuming uniform expansion of the plasma is shown in Fig. VIII.7, showing that normally rare strange anti-baryons could be significantly enhanced by the formation of a QGP [Mu87]. These results, though promising, are sensitive to the lifetime of the plasma (and hence to the hydrodynamics), and a calculation with more realistic hydrodynamics is needed.

The calculation of strangeness production in URHIC shares many of the difficulties as those encountered in dilepton production calculation. The use of perturbative QCD is again not on firm ground, but seems to be the only thing we can do at this point. Hydrodynamics almost certainly breaks down in the very early and very late stages of the reaction, and we have no handle on non-equilibrium emissions. In addition, there are uncertainties in the hadronization scenarios, as well as in the cross sections needed in Eq. (VIII.7). Again in this case, experimental inputs will be important for the theorists to refine these calculations.

VIII.3 Transverse momentum distribution

Naively we expect that any kinematic information of the early stages in URHIC would be washed out by the interactions among final state hadrons, and therefore kinematic variables cannot be used as signatures of QGP. There may be one exception, however. It has been proposed that a first order phase transition would show up as a flattening of the curve in a plot of the transverse momentum vs. multiplicity [Sh79, Va82]. The reason is quite simple: during a first order phase transition, the pressure remains unchanged while the energy density varies significantly (from ϵ_H to ϵ_Q, say). Now the transverse momentum reflects the pressure in the system, and

the multiplicity is a measure of the energy density. Therefore a plot of the average transverse momentum, $\langle p_\perp \rangle$, vs. multiplicity should give a flat region corresponding to the mixed phase. In fact, such a behavior has been seen in cosmic ray [Bu85] and $p - \bar{p}$ data [Ar82] (Fig. VIII.8).

We can go through a crude estimate of the transverse momentum distribution using the bag model equation of state and assuming spherical expansion [Ka85b]. Ignoring the pion mass, we have

$$\langle p_\perp \rangle = \int d^3p \; p \sin\theta F(p) = \frac{\pi}{4} \frac{E_\pi}{N_\pi} \quad ,$$

where $F(p)$ is the spherical momentum distribution and N_π is the total number of pions. But our ideal gas of massless pion carries entropy proportional to total number of particles: $S_\pi = 3.7 N_\pi$. Therefore $\langle p_\perp \rangle$ is directly related to energy per unit entropy:

$$\langle p_\perp \rangle = 2.9 \left(\frac{E_\pi}{S_\pi} \right) \quad . \tag{VIII.8}$$

The bag model equation of state can be used to relate both the energy and the entropy density to temperature [Vo86,87]:

$$\epsilon = g_Q \frac{\pi^2}{30} T^4 + B \quad ,$$
$$s = g_Q \frac{2\pi^2}{45} T^3 \quad ; \text{ for } T \geq T_u \; .$$

Here T_u is the upper boundary of the deconfinement transition, above which we would have a pure QGP. Similarly,

$$\epsilon = g_H \frac{\pi^2}{30} T^4 \quad ,$$
$$s = g_H \frac{2\pi^2}{45} T^3 \quad ; \text{ for } T \leq T_l \; .$$

T_l is the lower boundary of the phase transition. In above, B is the bag constant, and g_Q and g_H are the degeneracies in the QGP and hadron gas respectively. In the mixed phase, $T_l \leq T \leq T_u$, we just do a linear extrapolation between the two formulae. We have therefore expressed both $\langle p_\perp \rangle$ and ϵ in T:

$$\langle p_\perp \rangle = 2.9\frac{E}{S} = \begin{cases} 2.2T \ , & \text{if } T \leq T_l \ ; \\ 2.2T + 0.67\frac{T-T_l}{T_u-T_l}\frac{T_u^4}{T^3} \ , & \text{if } T_l \leq T \leq T_u \ ; \\ 2.2T + 0.67\frac{T_u^4}{T^3} \ , & \text{if } T \geq T_u \ . \end{cases}$$

A plot is shown in Fig. VIII.9. Experimental data seem to fit surprisingly well onto this curve [Ka85b].

For central heavy-ion collisions, the correct geometry is probably that of a cylinder. To make the above calculation more realistic, we have to run our cylindrical hydrodynamic code until the freezeout stage, and invoking some hadronization model, we need to extract the average transverse momentum of final state particles. Such a calculation using scaling hydrodynamics has been done by von Gersdorff *et al.*, and their result is shown in Fig. VIII.10 [Vo86,87].

VIII.4 Other signatures

We shall very briefly mentioned some other signatures of the QGP proposed. Heinz *et al.* considered the abundances of anti-matter clusters using chemical equilibrium between the different hadronic species in the hadron phase and the quarks in the plasma [He84]. In a calculation similar to that done for strange hadrons, neglecting the global expansion of the plasma during phase transition, the authors conclude that the chance to form an anti-alpha nucleus at phase transition in a baryonless plasma is about two orders of magnitude higher than in a hadron gas.

Gyulassy suggested that a deflagation shock may develop in the plasma at phase transition. These deflagation bubbles may give rise to unusual fluctuations of multiplicity, dN/dy, and enhanced transverse momenta. Also, events with high transverse energy density associating with high circularity would be expected [Gy83,84a,b].

Lopez *et al.* considered the charge anti-correlations of pions of similar momenta [Lo84]. In a normal hadronic jet, Field and Feynman [Fi78] first predicted and Brandelik *et al.* [Br81] later observed that neighboring hadrons' charges are anticorrelated. This can be understood easily using the picture of the flux tube model (Fig. VIII.6). Hadrons freezing out from a QGP would not have similar short range anti-correlations however, because the quarks and gluons come from a large thermal pool, the plasma.

There have also been proposals using the fact that if a plasma is formed, the coefficient of shear viscosity, η, would be very much smaller than in a nuclear medium [Ha82, Ra84] (see Chapter V). The spectators in the nuclear collisions will therefore be affected differently whether a plasma is formed or not. In particular, Raha *et al.* claims that the temperature of spectators would be smaller by a factor of 3-4 had there been a plasma.

Yet another possible signature is the enhancement of ϕ-meson ($s-\bar{s}$) production in a QGP [Sh85]. The idea is that ϕ production is normally suppressed in hadonic reaction because of the Okubo-Zweig-Iizuka rule (disconnected quark diagrams get suppressed) [Li76, Fr77, Ok77]. In a QGP however, the OZI rule is not violated and ϕ can be produced abundantly. It is tempting to predict similar enhancement of J/ψ ($c-\bar{c}$) production in a QGP. But here since the charm quarks are much rarer in abundances, and screening in the plasma makes it actually harder for the

c and $\bar{c}$ to "feel" each other and come into binding, Matsui *et al.* [Ma86a] conclude that there is actually a suppression of J/ψ in a QGP, which may still be used as a signature.

We have surveyed a list of possible signatures for the formation of QGP in URHIC. We have made use of penetrating probes (dilepton and photon), which interact only weakly with the final state hadrons and thus should store information about the early stages of the reaction. We observed the enhancement of strange quarks in a QGP, and tried to utilize that for signature. We also made use of the transverse momenta to probe the pressure in the reaction region, which should carry distinct signal for a first order phase transition. Some other proposals exploit the fact that a QGP relaxes many restrictions in a hadronic system such as charge anti-correlation and the OZI rule. Some rely on extraordinary kinematic conditions associated with the transition from hadronic gas to a QGP (deflagation bubble, decrease of viscosity). Most of these proposals suffer from uncertainties in the theoretical calculations such as non-perturbative and non-equilibrium effects. The hydrodynamic models employed in most calculations are also too crude; a realistic hydrodynamic code is essential for a rigorous evaluation of these signatures.

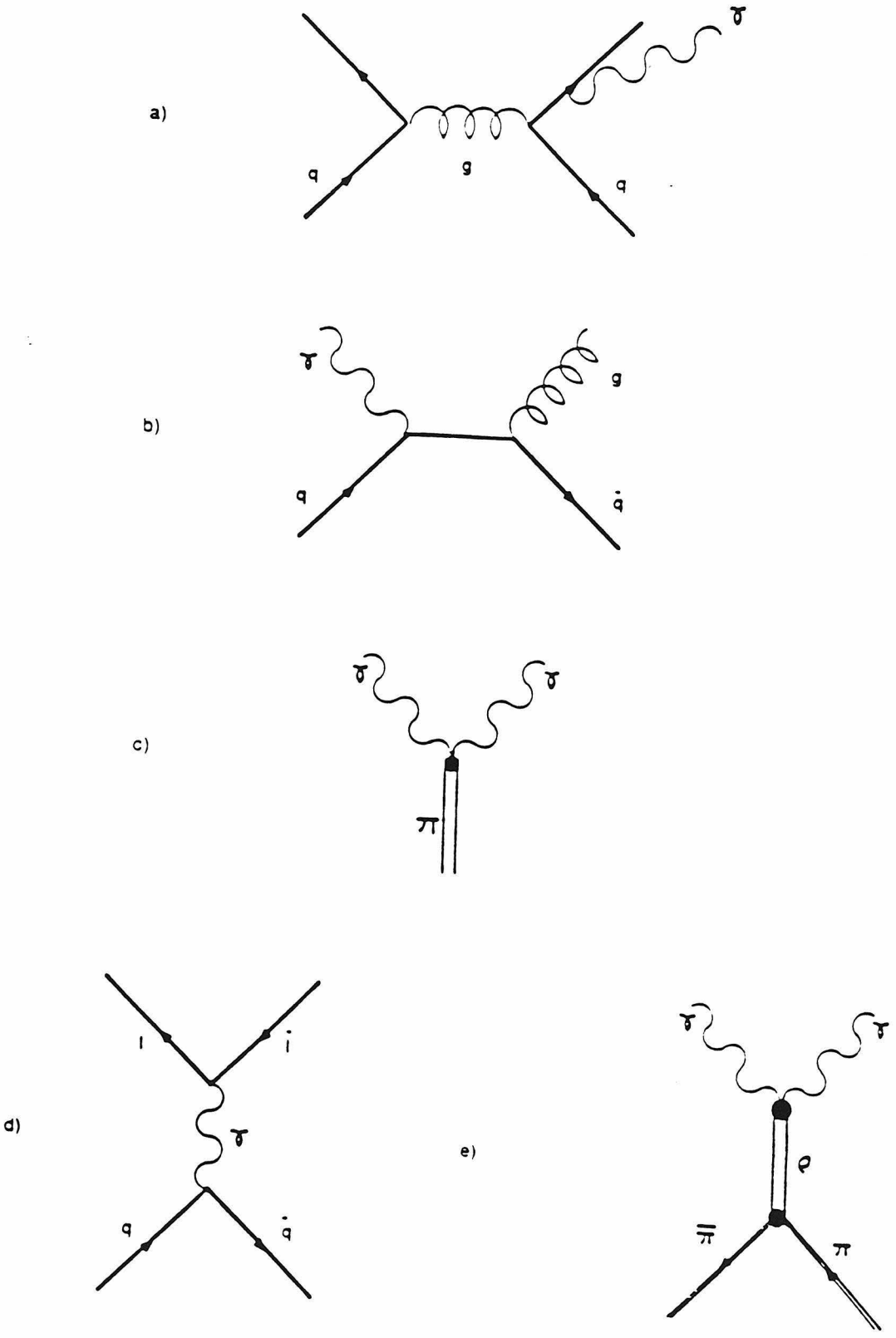

FIG. VIII.1 Emission of photons from a) quark-quark scattering, b) quark-anti-quark annihilation, c) pion decay, e) $\pi - \bar{\pi}$ annihilation. In d) dilepton emission from quark-anti-quark annihilation is shown.

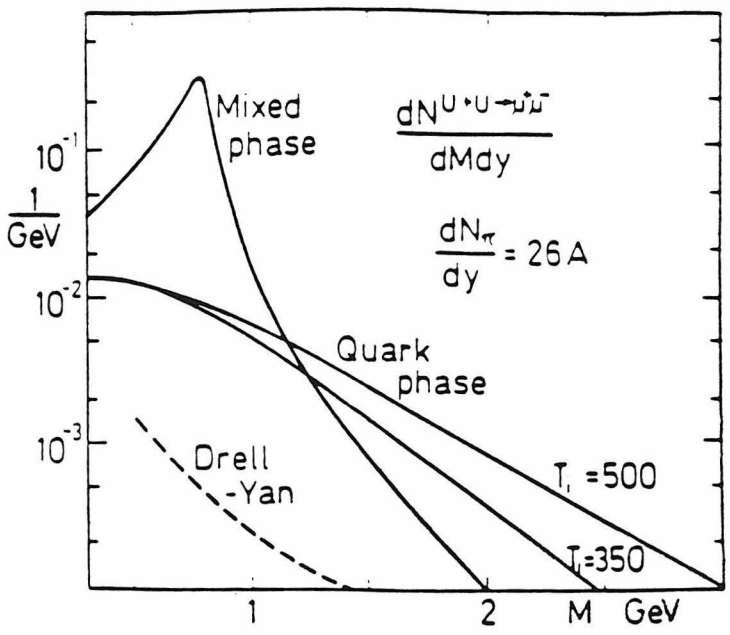

FIG. VIII.2 The mass spectrum at $y = 0$ of dileptons emitted from a scaling cylindrical flow with $T_i = 350$ MeV and $\tau_o = 1.5$ fm/c. The bag-model equation of state, Eq. VI.5, is used [Ka87].

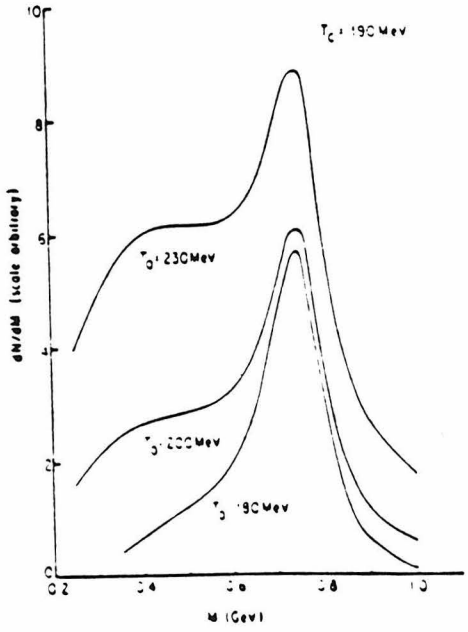

FIG. VIII.3 The mass spectrum of dileptons emitted from spherically expanding fireballs of initial temperature $T_o = 180$, 200, 230 MeV. Critical temperature of deconfinement transition is taken as 190 MeV [ChS2].

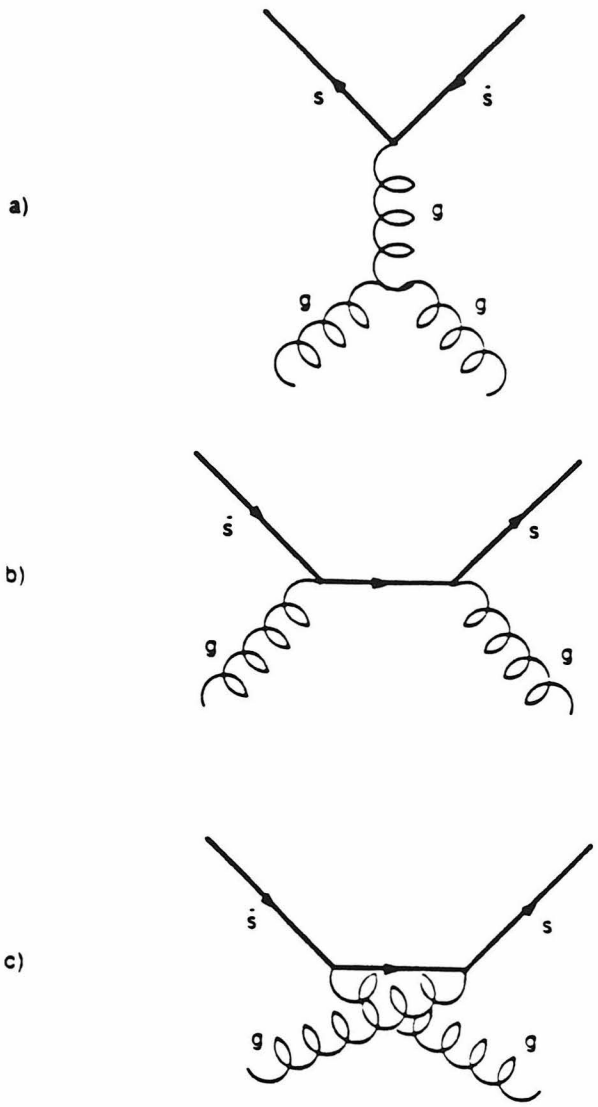

FIG. VIII.4 Dominant channels of strange quarks creation and annihilation from two-gluon processes.

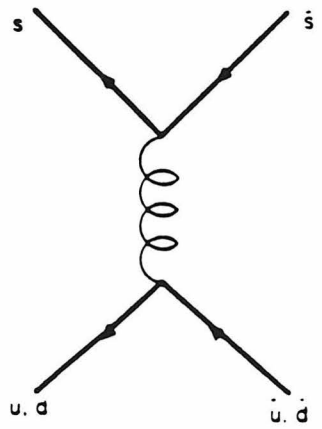

FIG. VIII.5 Strange quarks creation and annihilation from quark-anti-quark annihiliations.

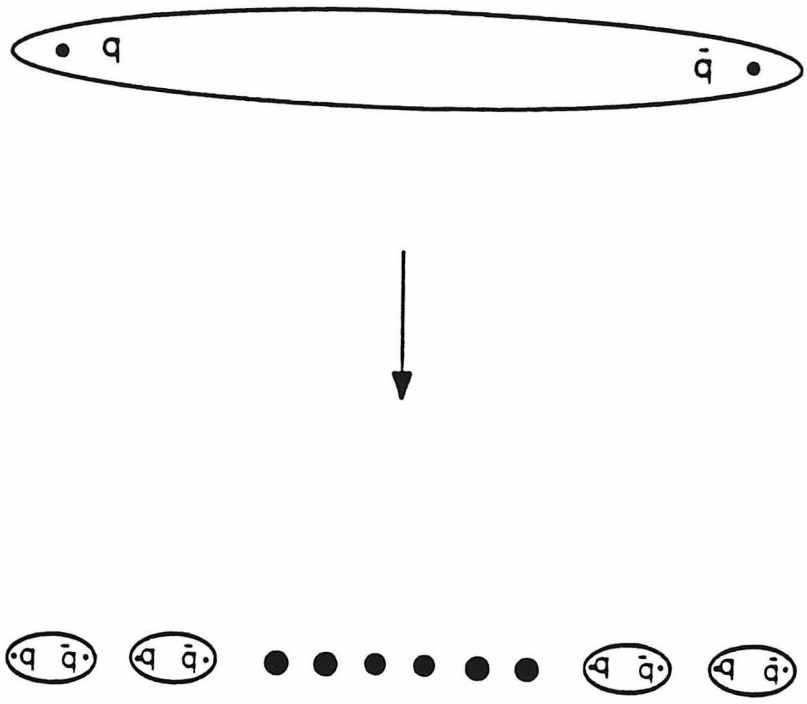

FIG. VIII.6 Fissioning of a flux tube as a model of hadronization into mesons.

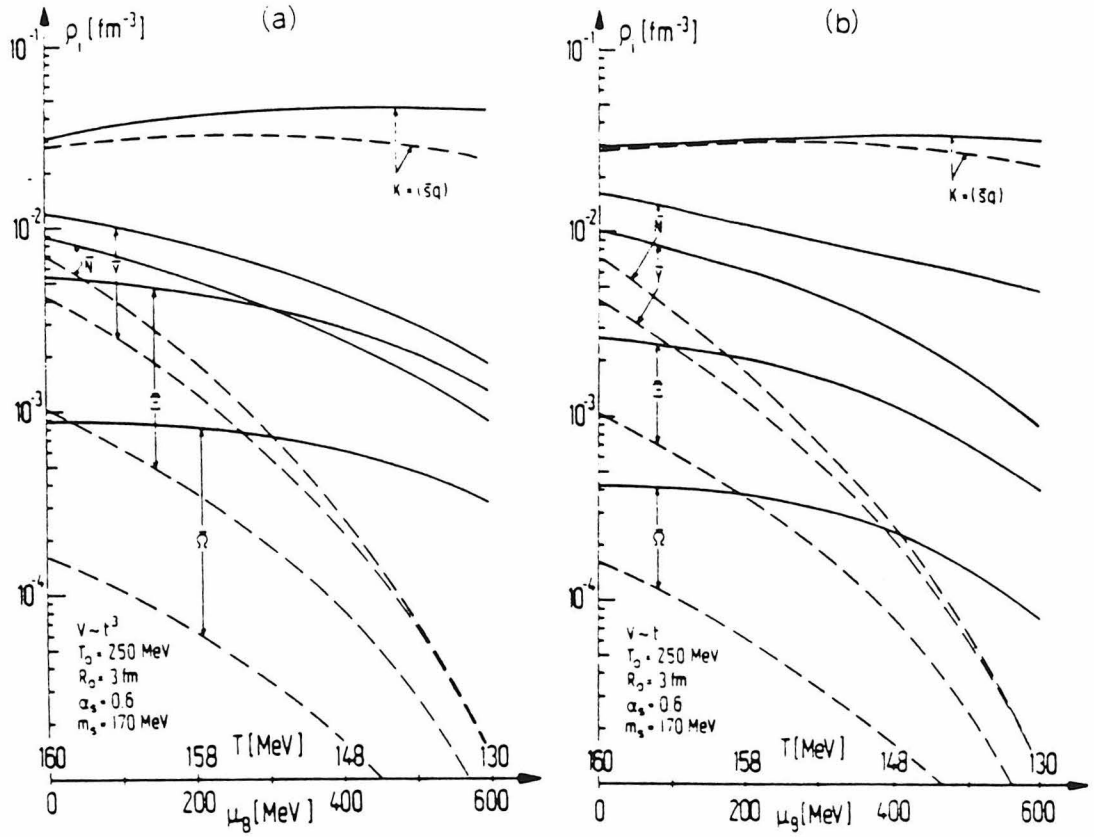

FIG. VIII.7 Calculated strange hadron densities in ultra-relativistic heavy-ion collisions as a function of the critical temperature of deconfinement phase transition.T (MeV) or the baryon chemical potential, μ_B. Solid curves show results for events with plasma formation, while dashed curves indicate hadronic gas abundances at equilibrium. The expansion of the plasma is assumed to be a) spherical, b) longitudinal [MuS7].

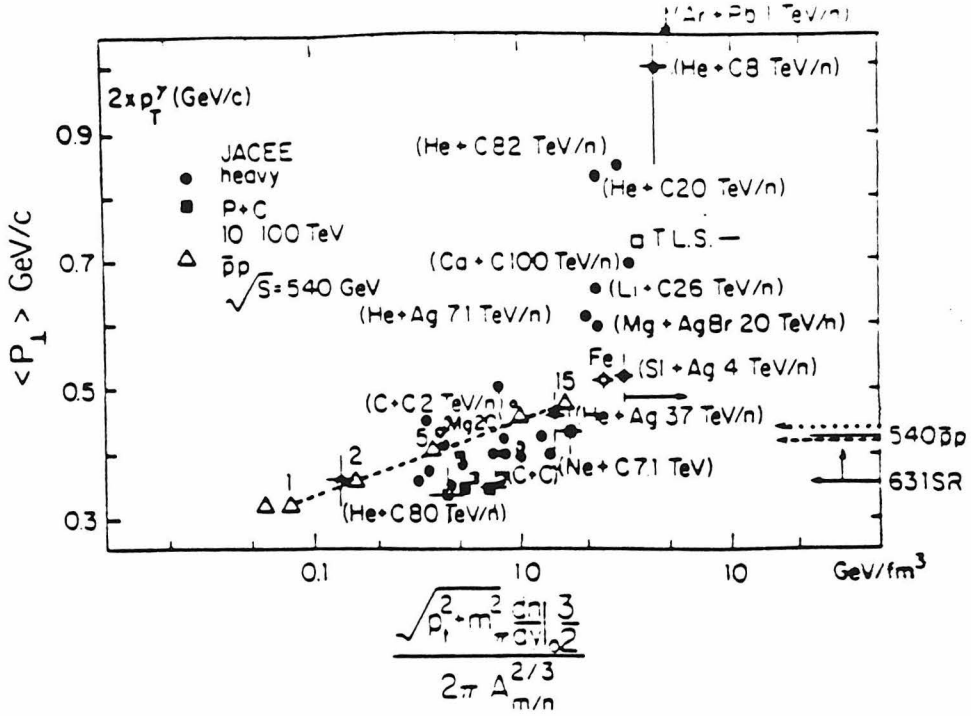

FIG. VIII.8 Average transverse momenta vs. multiplicity compiled from cosmic ray and proton data [Ka85].

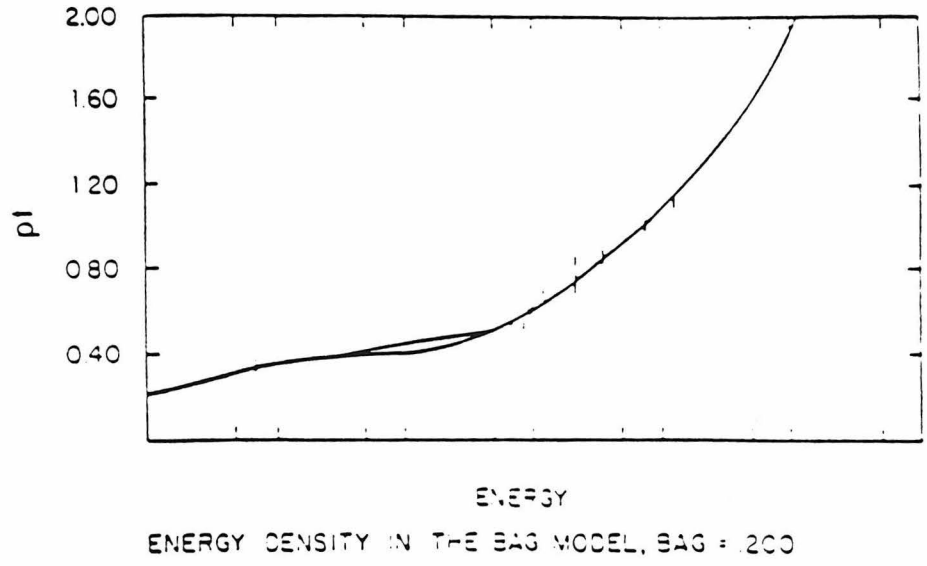

FIG. VIII.9 Plot of transverse momentum $p_\perp = 2.9E/S$ vs. energy density E/V using bag-model equation of state as described in Sec. VIII.3. The flat part of the curve reflects a first order phase transition. Data from FIG. VIII.8 have been inserted assuming the relation $E/V = 4.7p_\perp^4 A_{min}^{2/3} dN/dy$. Spherical expansion is assumed [Ka85].

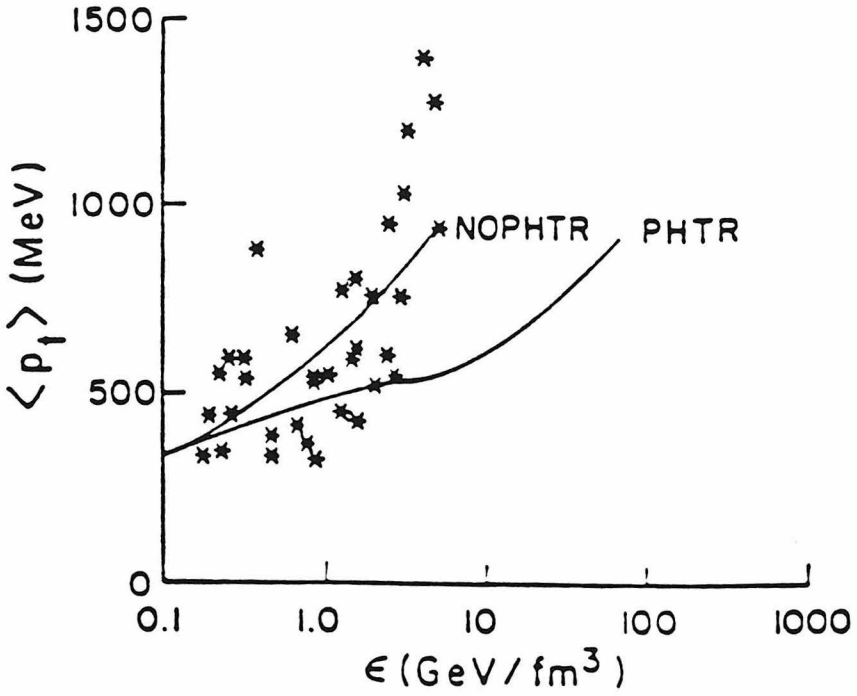

FIG. VIII.10 Same as in FIG. VIII.9, except that cylindrical scaling hydrodynamics with a transverse radius of 4.2 fm assumed [VoS7].

CHAPTER IX

Summary and Conclusion

Ultra-relativistic heavy-ion collisions provide promising opportunities to create an extended region of extremely high energy density. Whether the matter in this extreme condition exists in the form of a deconfined plasma of quarks and gluons, or some highly excited hadron gas, or even some previously undiscussed new form of matter is not certain yet. But we can almost be sure that new physics can be learned, which will have implications for not only nuclear and particle physics, but also astrophysics as well.

A proposal to build a heavy-ion collider at Brookhaven National Laboratory (RHIC), which can accelerate uranium ions to 100 GeV/A in the center-of-mass frame is nearing approved, and we can expect the first such experiments be run in the mid-90's. A series of experiments using light to medium ions at high energies are also being planned and run at CERN in the near future [Ba86a]. Most probably, what the experimentalists will see are just thousands of particles, mostly photons, leptons and pions, going through their detectors. How are we going to analyze these data and extract useful physics? In particular, how can we decipher information about the early stages of the reaction, which contain most of the interesting physics? If a quark-gluon plasma is indeed formed in some of these collision events, how would we know it's there? We have in this thesis presented some of the first theoretical attempts to describe ultra-relativistic heavy-ion collisions.

The standard scenario was outlined by Bjorken, Kajantie, McLerran among others using the inside-outside cascade model and scaling hydrodynamics. The

produced particles in the reaction go through subsequent stages of free-streaming, thermalization, hydrodynamics, hadronization, and freezeout. We have discussed this picture in a little bit more detail in Chapter II.

The system probably spends the major part of its lifetime in the hydrodynamic phase, and therefore a realistic hydrodynamic model is essential to describe the dynamics of the system. We have pointed out some weaknesses of Bjorken's scaling hydrodynamics. While scaling should be a good approximation near the center of the system, it almost certainly breaks down towards the fragmentation regions. We therefore proposed to lift the restriction to scaling symmetry and include source terms in the hydrodynamic equations so as to incorporate the fragmentation regions in the hydrodynamics. The addition of source terms in the hydrodynamic equations also has the advantage of allowing us to model the production mechanism in URHIC. In Chapter IV we have considered two "benchmark" models of the source terms: the inside-outside cascade and the multiple-collision model.

The assumption of local thermal equilibrium is not strictly justified throughout the hydrodynamic phase. One way to include non-equilibrium effect in first order is to put in viscosities. The transport coefficients have been estimated by Gavin using a relaxation time approximation for the semi-classical kinetic theory of a QGP, and by Danielewicz and Gyulassy using QCD phenomenology. We have summarized their results in Chapter V.

We then presented our hydrodynamic models in Chapter VI (1+1-dimensional) and Chapter VII (2+1-dimensional). We indeed observed large scaling violations near the fragmentation regions and strong sensitivity of the hydrodynamics on the source terms and the materialization time τ_o. However, we found very little effects

of the viscosities or the existence of a first order phase transition. For the range of energy we are considering here, the transverse degree of freedom is not significant prior to hadronization, and the hydrodynamics of the system is to good approximation one-dimensional (longitudinal). Transverse expansion contributes to only a few per cent decrease in the maximum energy density achieved in URHIC compared to the longitudinal expansion.

Hydrodynamics is not sensitive to the underlying degrees of freedom in the system (maybe except when there is a phase transition). Therefore, to look for a signature of the QGP, we have to consider observables that depend on the microscopic physics. We devoted Chapter VIII to a survey of different proposals of QGP signatures. Most of these signature calculations involve two steps: first calculate the elementary cross section of a particular observable, then the abundances of this observable are evaluated according to this cross section and the hydrodynamic evolution of the system. We see that most of the current calculations have uncertainties in both steps; while the applicability of perturbative QCD is questionable, the hydrodynamics used are also very often unrealistic. Much more work is needed to improve these calculations. So far, there seems to be no one unambiguous signature of the formation of QGP in URHIC.

Further advances in the theory of ultra-relativistic heavy-ion collisions probably await more experimental inputs such as nuclear stopping power, dilepton emission spectra, etc. These would guide the theorists in modeling the reaction mechanism. A good 3+1-dimensional hydrodynamic code will eventually be needed, as well as understanding of non-equilibrium effects. If non-equilibrium effects prove to be

much more important than we currently think, we may have to abandon hydrodynamics altogether and work on the kinetic theory level. Finally we hope lattice gauge calculations will provide us with more insights into non-perturbative QCD, especially the confinement problem.

APPENDIX A

Difference Equations for Longitudinal Hydrodynamics

To solve Eqs. VI.3, we first locate the (u, v) grid points on the (y, s) plane by discretizing Eq. VI.2:

$$\frac{y_i^{j+1} - y_i^j}{s_i^{j+1} - s_i^j} = \tanh\left(\theta_i^j - y_i^j\right) , \tag{A.1}$$

and

$$\frac{s_i^{j+1} - s_{i-1}^{j+1}}{y_i^{j+1} - y_{i-1}^{j+1}} + \frac{s_{i-1}^{j+1} - s_{i-2}^{j+1}}{y_{i-1}^{j+1} - y_{i-2}^{j+1}} = 2 \tanh\left(\theta_{i-1}^{j+1} - y_{i-1}^{j+1}\right) , \tag{A.2}$$

where the lower (upper) index labels positions on $\hat{\mathbf{u}}$ ($\hat{\mathbf{v}}$). These equations represent the curves along $\hat{\mathbf{v}}, \hat{\mathbf{u}}$ directions, and their intersections are the grid points.

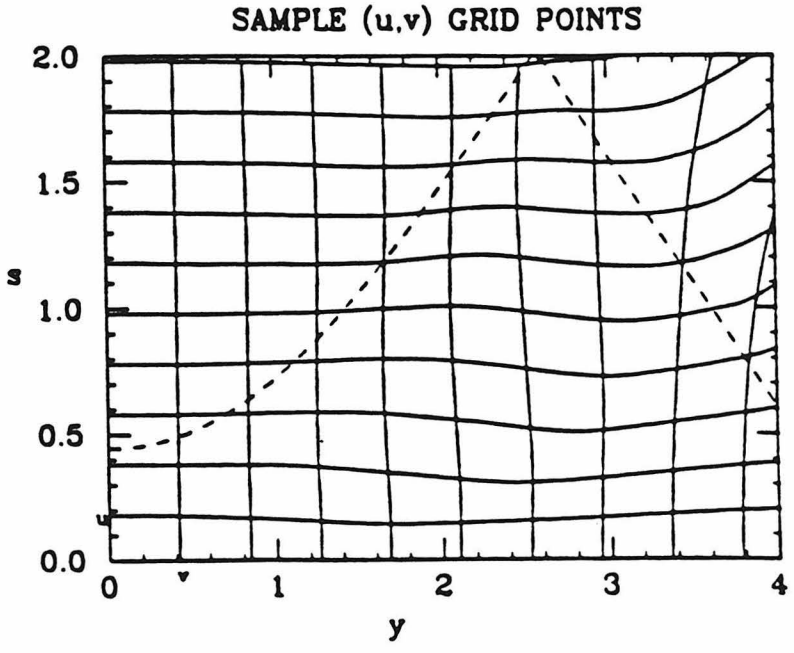

FIG. A1.1 Sample (u, v) grid points on the $y - s$ plane. The dashed lines mark the boundaries of the source region.

Examples of these curves on the $y-s$ plane are shown in Fig. A.1. Notice that the curves in the $\hat{\mathbf{u}}$ direction start out from $y=0$ axis initially perpendicular to the s-axis. The viscosity slows down the flow resulting in a slight diving of the u-curves towards the y-axis, but the huge pressure gradient at the end of the source region accelerates the plasma causing the curves to bend up after passing through the source region. If perfect scaling holds, these curves just form rectangular grids.

We then solve the difference equations corresponding to Eqs. VI.3 on the grid points generated with Eq. A.1 and Eq. A.2:

$$\epsilon_i^{j+1} = \epsilon_i^j + \Delta v_i^j \left\{ \left[\frac{\chi_i^j}{t_{d_i}^j} \theta'^{j+1}_i - (\epsilon_i^j + P_i^j) \right] \theta'^{j+1}_i + t_{d_i}^j S_{1_i}^j \right\} \quad , \tag{A.3a}$$

$$\theta_i^{j+1} = \theta_i^j + \left[(\epsilon_i^j + P_i^j) - \frac{\chi_i^j}{t_{d_i}^j} \right]^{-1} \Delta v_i^j \left\{ \frac{1}{t_{d_i}^j} \left[\chi_i^j [a_{1_i}^j \theta'^j_i - a_{2_i}^j] \theta'^j_i + \chi_i^j \theta''^j_i + \chi'^j_i \right] + t_{d_i}^j S_{2_i}^j - P'^j_i \right\} \quad , \tag{A.3b}$$

and

$$n_{B_i}^{j+1} = n_{B_i}^j + \Delta v_i^j \left[t_{d_i}^j \sigma_{B_i}^j - n_{B_i}^j \theta'^{j+1}_i \right] \quad . \tag{A.3c}$$

We have used the following notations:

$$A'^j_i = \frac{A_{i+1}^j - A_{i-1}^j}{2\Delta u_i^j} \quad ,$$

$$A''^j_i = \frac{1}{2} \left[\frac{A_{i+1}^j - A_i^j}{\Delta u_i^j} + \frac{A_i^j - A_{i-1}^j}{\Delta u_{i-1}^j} \right] \quad ,$$

and

$$a_1 \equiv \frac{2\alpha\beta}{a^2} \quad ,$$

$$a_2 \equiv \frac{\alpha}{a} \left(2\frac{\beta^2}{a^2} + 1 \right) \quad .$$

For stability reasons, in the second terms of both Eq. VI.3a and Eq. VI.3c, $\partial_u \theta$ is evaluated at $\hat{\mathbf{v}} = (j+1)\Delta v$, while $(\epsilon + P)$ in (VI.3a) and n_B in (VI.3c) are calculated at $\hat{\mathbf{v}} = j\Delta v$. Without the viscosity term, this scheme is stable as long as the rapidity gradient does not become negative, which typically happens at a shock front. We expect that the viscosity term will improve the numerical stability even if a shock front is developed.

APPENDIX B

Difference Equations for Cylindrical Hydrodynamics

We use the two-step Lax-Wendroff Method [La60, Ri67] to solve Eq. VII.2. A conservation-law form equation

$$\partial_t U + \partial_z F(U) + \partial_r G(U) = 0 \tag{B.1}$$

can be solved by the following difference scheme:

$$\begin{aligned} U_{j,l}^{n+\frac{1}{2}} =& \frac{1}{4}\left(U_{j+1,l}^{n} + U_{j-1,l}^{n} + U_{j,l+1}^{n} + U_{j,l-1}^{n}\right) \\ & - \frac{\Delta t}{2\Delta z}\left(F_{j+1,l}^{n} - F_{j-1,l}^{n}\right) - \frac{\Delta t}{2\Delta r}\left(G_{j,l+1}^{n} - G_{j,l-1}^{n}\right) \quad , \end{aligned} \tag{B.2a}$$

and then

$$U_{j,l}^{n+1} = U_{j,l}^{n} - \frac{\Delta t}{\Delta z}\left(F_{j+1,l}^{n+\frac{1}{2}} - F_{j-1,l}^{n+\frac{1}{2}}\right) - \frac{\Delta t}{\Delta r}\left(G_{j,l+1}^{n+\frac{1}{2}} - G_{j,l-1}^{n+\frac{1}{2}}\right) \quad . \tag{B.2b}$$

Here, $U_{j,l}^{n}$ indicates the value of U at the n^{th} time step, j^{th} z-step, and l^{th} r-step. Values of U at roughly half a time step are first calculated with Eq. (B.2a), and then Eq. (B.2b) is used to carry the fields from time step n to $n+1$ using

$$F_{j,l}^{n+\frac{1}{2}} = F\left(U_{j,l}^{n+\frac{1}{2}}\right) \quad ,$$

and

$$G_{j,l}^{n+\frac{1}{2}} = G\left(U_{j,l}^{n+\frac{1}{2}}\right) \quad .$$

This scheme is known to be stable even in the presence of shock fronts for a linear system [Ri67]. Relativistic hydrodynamics, however, are highly non-linear, and

it turns out that the scheme becomes unstable even without shock formation. We cure the instabilities by the method of pseudo-viscosity [Ri67]. Here we introduce the artificial viscosity term:

$$D^n_{j,l} = \frac{1}{2}a\left[|U^n_{j+1,l} - U^n_{j,l}|\left(U^n_{j+1,l} - U^n_{j,l}\right) - |U^n_{j,l} - U^n_{j-1,l}|\left(U^n_{j,l} - U^n_{j-1,l}\right)\right] \quad , \quad \text{(B.3)}$$

where a is the coefficient of artificial viscosity, typically chosen to be of order 1. Then we modify (B.2b) to:

$$U^{n+1}_{j,l} = U^n_{j,l} - \frac{\Delta t}{\Delta z}\left(F^{n+\frac{1}{2}}_{j+1,l} - F^{n+\frac{1}{2}}_{j-1,l} - D^n_{j,l}\right) - \frac{\Delta t}{\Delta r}\left(G^{n+\frac{1}{2}}_{j,l+1} - G^{n+\frac{1}{2}}_{j,l-1}\right) \quad . \quad \text{(B.2b')}$$

We have checked that the results are not sensitive to the values of a, as long as $a > 0$.

We handle the boundaries at $z = 0$ and $r = 0$ by starting the grid points half a step away from the origin:

$$r_1 = -0.5\Delta r \ , \quad r_2 = 0.5\Delta r \ , \quad r_3 = 1.5\Delta r \ , \ ...$$

$$z_1 = -0.5\Delta z \ , \quad z_2 = 0.5\Delta z \ , \quad z_3 = 1.5\Delta z \ , \ ... \ ,$$

where Δr and Δz are the grid sizes in r and z directions respectively. Here the first grid points are put in there just to ensure the symmetry properties of the fields. For example,

$$U^n_{1,l} = U^n_{2,l} \quad , \quad F^n_{1,l} = -F^n_{2,l} \quad , \quad G^n_{1,l} = G^n_{2,l} \quad ,$$

for the 1^{st}, 3^{rd}, and 4^{th} components, and

$$U^n_{1,l} = -U^n_{2,l} \quad , \quad F^n_{1,l} = F^n_{2,l} \quad , \quad G^n_{1,l} = -G^n_{2,l} \quad ,$$

for the 2^{nd} components.

References

Ab65 M. Abramowitz and I. E. Stegun, *Handbook of Mathematical Functions* (Dover, New York, 1965), p. 586.

Al81 K. Alpgård *et al.*, Phys. Lett. **107B**, 315(1981).

Ar82 UA1 Collab., G. Arnison *et al.*, Phys. Lett. **89B**, 253(1979).

Ba83 G. Baym *et al.*, Nucl. Phys. **A407**, 541(1983).

Ba83a B. Banerjee, N. K. Glendenning, and T. Matsui, Phys. Lett **127B**,453 (1983).

Ba84 Gordon Baym, Phys. Lett. **138B**, 18(1984).

Ba84a H. W. Barz, B. Kämpfer, L. P. Csernai, and B. Lukács, Phys. Lett. **143B**, 334(1984).

Ba85 H. W. Barz, B. Kämpfer, L. P. Csernai, and B. Lukács, Phys. Rev. C**31**, 268(1985).

Ba86 H. W. Bartz, B. Kämpfer, L. P. Csernai, and B. Lukács, Michigan State University preprint MSUCL-577, 1986.

Ba86a A. Bamberger *et al.*, CERN preprint EP 86-194, 1986.

Bj64 J. D. Bjorken and S. D. Drell, *Relativistic Quantum Mechanics* (McGraw-Hill, New York, 1964), p.114.

Bj75 J. D. Bjorken, *Lecture Notes on Current-Induced Reactions*, eds. J. Kor̈ner, G. Kramer, and D. Schildknecht (Springer-Verlag, New York, 1975).

Bj83 J. D. Bjorken, Phys. Rev. D**27**, 140(1983).

Bl81 R. Blankenbecler *et al.*, Phys. Lett. **107B**, 106(1981).

Bl87 J. -P. Blaizot and J. -Y. Ollitrault, Saclay preprint PhT/87-06, submitted to Phys. Lett. B, 1987.

Br81 R. Brandelik *et al.*, (TASSO Collaboration), Phys. Lett. **100B**, 357(1981).

Bu84 W. Busza and A. S. Goldhaber, Phys. Lett. **139B**, 235(1984); W. Busza, Nucl. Phys. **A418**, 635c(1984).

Bu85 T. H. Burnett *et al.*, Nucl. Phys. **A447**, 189(1985).

Ca79 A. Casher, H. Neuberger, and S. Nussinov, Phys. Rev. D**20**, 179 (1979).

Ch74 A. Chodos, R. L. Jaffe, C. B. Thorn, and V. Weisskopf, Phys. Rev. D**9**, 3471(1974); A. Chodos, R. L. Jaffe, K. Johnson, and C. B. Thorn, Phys. Rev. D**10**, 2599(1974).

Ch82 S. A. Chin, Phys. Letts **119B**, 51(1982).

Ch85 M. -C. Chu, Phys. Rev. C**31**, 1739(1985).

Ch86 M. -C. Chu, Phys. Rev. D**34**, 2764(1986).

Co76 R. Courant and K. Friedrichs, *Supersonic Flow and Shock Waves* (Springer-Verlag, New York, 1976).

Co79 B. L. Combridge, Nucl. Phys. **B151**, 429(1979).

Cl85 R. B. Clare and D. Strottman, Los Alamos National Laboratory report (1985).

Da85 P. Danielewicz and M. Gyulassy, Phys. Rev. D**31**, 53(1985).

De75 T. DeGrand, R. L. Jaffe, K. Johnson, and J. Kiskis, Phys. Rev. D**12**, 2060 (1975).

Do81 G. Domokos and J. I. Goldman, Phys. Rev. D**23**, 203(1981).

Ec40 C. Eckart, Phys. Rev. **58**, 919(1940).

El86 H. Elze, M. Gyulassy, and D. Vasak, Nucl. Phys. **B276**, 706 (1986).

En82 J. Engels *et al.*, Nucl. Phys. **B205**, 545(1982).

Fe76 E. L. Feinberg, Nuovo Cimento **34A**, 391(1976).

Fi78 R. D. Field and R. P. Feynman, Nucl. Phys. **B136**, 1(1978).

Fr77 S. C. Frautschi *et al.*, Nucl. Phys. **B121**, 141(1977).

Ga85 Sean Gavin, Nucl. Phys. **A435**, 826(1985).

Ga87 G. Gatoff, A. K. Kerman and T. Matsui, MIT preprint CTP#1338-REV, submitted to Phys. Rev. D, 1987.

Ge78 H. M. Georgi, S. L. Glashow, M. E. Machacek, and D. V. Nanopoulos, Ann. Phys. **114**, 273(1978).

Gl59 R. J. Glauber, in *Lectures in Theoretical Physics*, eds. W. E. Brittin and L. G. Dunham, Vol. 1, 315(Interscience, New York, 1959).

Gl85 Norman K. Glendenning and Johann Rafelski, Phys. Rev. C**31**, 823(1985).

Gy83 M. Gyulassy, K. Kajantie, H. Kurki-Suonio, and L. McLerran, Nucl. Phys. **B237**, 477(1984).

Gy84 M. Gyulassy and T. Matsui, Phys. Rev. D**29**, 419(1984).

Gy84a M. Gyulassy, K. Kajantie, H. Kurki-Suonio, and L. McLerran, Nucl. Phys. **B237**, 477(1984).

Gy84b M. Gyulassy, Nucl. Phys. **A418**, 59c(1984).

Gy87 M. Gyulassy and L. P. Csernai, Lawrence Berkeley Laboratory preprint LBL-20610, 1986.

Ha82 F. Halzen and H. -C. Liu, Phys. Rev. D**25**, 1842(1982).

He84 U. Heinz, P. R. Subramanian, and W. Greiner, Z. Phys. **A318**, 247 (1984).

He85 U. Heinz, Ann. Phys. **161**, 48(1985).

He87 U. Heinz, Nucl. Phys. **A461**, 49c(1987).

Ho83 A. Hosoya and K. Kajantie, Nucl. Phys. **B250**, 666(1985).

Ho84 A. Hosoya, M. Sakagami, and M. Takao, Ann. Phys. (N.Y.) **154**, 229(1984).

Ja82 *Quark Matter Formation and Heavy Ion Collisions*, eds. M. Jacob and H. Satz (World Scientific, Singapore, 1982).

Ka81 K. Kajantie and H. I. Miettinen, Z. Phys. **C9**, 341(1981).

Ka82 K. Kajantie and L. McLerran, Phys. Lett. **119B**, 203(1982).

Ka83 K. Kajantie, R. Raitio, and P. V. Ruuskanen, Nucl. Phys. **B222**, 152(1983); K. Kajantie and L. McLerran, Nucl. Phys. **B214**, 261(1983); K. Kajantie and R. Raitio, Phys. Lett. **121B**, 415(1983).

Ka83a J. Kapusta, Phys. Rev. C**27**, 2037(1983).

Ka85 *Quark Matter '84*, ed. K. Kajantie, Lecture Notes in Physics, Vol. **221** (Springer, Heidelberg, 1985).

Ka85a K. Kajantie and T. Matsui, Phys. Lett. **164B**, 373(1985).

Ka85b J. Kapusta, S. Pratt, L. McLerran, H. von Gersdorff, Phys. Lett. **163B**, 253(1985).

Ka86 J. Kapusta and A. Mekjian, Phys. Rev. D**33**, 1304(1986).

Ka87 K. Kajantie, Nucl. Phys. **A416**, 225c(1987).

Ko86 P. Koch, B. Müller, and J. Rafelski, Phys. Rep. **142**, 167(1986).

La59 L. D. Landau and E. M. Lifshitz, *Fluid Mechanics* (Pergamon Press, London, 1959).

La60 P. D. Lax and B. Wendroff, Comm. Pure Appl. Math. **13**, 217(1960).

Li76 H. Lipkin, Phys. Lett. **60B**, 371(1976).

Lo84 Jorge A. Lopez, Jitendra C. Parikh, and Philip J. Siemens, Phys. Rev. Lett. **53**, 1216(1984).

Lu84 *Quark Matter '83*, eds. T. W. Ludlam and H. E. Wegner, Nucl. Phys. **A418** (1984).

Ma86 T. Matsui, L. McLerran and B. Svetitsky, Phys. Rev. D**34**, 783(1986); **D34**, 2047(1986).

Ma86a T. Matsui and H. Satz, Phys. Lett. **B178**, 416(1986).

Mc85 L. McLerran and T. Toimela, Phys. Rev. D**31**, 545(1985).

Mc87 L. McLerran, Nucl. Phys. **A461**, 249c(1987).

Mi70 Charles W. Misner, Kip S. Thorne, John Archibald Wheeler, *Gravitation* (W. H. Freeman, San Francisco, 1970), p. 130.

Mo82 I. Montvay and E. Pietarinen, Phys. Lett. **110B**, 148(1982).

Mu85 B. Müller, *The Physics of the Quark-Gluon Plasma*, Lecture Notes in Physics, Vol. 225 (Springer, Heidelberg, 1985).

Mu87 B. Müller, Nucl. Phys. **A461**, 213c(1987).

Na83 S. Nadkarni, Phys. Rev. D**27**, 917(1983).

Ok77 S. Okubo, Phys. Rev. D**16**, 2336(1977).

Pl85 M. Ploszajczak and M. J. Rhoades-Brown, Phys. Rev. Lett. **55**, 147(1985).

Po75 H. D. Politzer, Phys. Rep. **14C**, 129(1974).

Po87 J. Polonyi, Nucl. Phys. **A461**, 279c(1987).

Ra84 S. Raha, R. M. Weiner, and J. W. Wheeler, Phys. Rev. Lett. **53**, 138(1984).

Re65 F. Reif, *Fundamentals of Statistical and Thermal Physics* (McGraw-Hill, New York, 1965).

Ri67 Robert D. Richtmyer and K. W. Morton, *Difference Methods for Initial-Value Problems* (Interscience, New York, 1967).

Sa81 *Statistical Mechanics of Quarks and Hadrons*, ed. H. Satz (North-Holland, Amsterdam, 1981).

Sc51 J. Schwinger, Phys. Rev. **82**, 664(1951).

Sh78 E. Shuryak, Sov. J. Nucl. Phys. **28**, 408(1978).

Sh79 E. Shuryak and O. V. Zhirov, Phys. Lett. **89B**, 253(1979).

Sh80 E. V. Shuryak, Phys. Rep. **61**, 71(1980).

Sh85 Asher Shor, Phys. Rev. Lett. **54**, 1122(1985).

Si85 P. J. Siemens and S. A. Chin, Phys. Rev. Lett. **55**, 1266(1985).

Ta76 F. E. Taylor *et al.*, Phys. Rev. D**14**, 1217(1976).

Th77 W. Thomé *et al.*, Nucl. Phys. **B129**, 365(1977).

Va62 R. Varga, *Matrix Iterative Analysis* (Prentice-Hall, Englewood Cliffs, 1962), p. 273.

Va82 L. van Hove, Phys. Lett. **118B**, 138(1982).

Vo86 H. von Gersdorff, L. McLerran, M. Kataja and P. V. Ruuskanen, Phys. Rev. D**34**, 794(1986).

Vo87 H. von Gersdorff, Nucl. Phys. **A461**, 251c(1987).

We85 K. Wehrberger and R. M. Weiner, Phys. Rev. D**31**, 222(1985).

Wo84 C. Y. Wong, Phys. Rev. D**30**, 961(1984).

Wo84a C. Y. Wong, Phys. Rev. Lett. **52**, 1393(1984); Phys. Rev. D**30**, 972(1984).

Wo85 C. Y. Wong, Phys. Rev. D**32**, 94(1985).